Institute of Space and Aeronautical Science, University of Tokyo
Report No. 525, May 1975

Characteristic of the Contaminated Langmuir Probe and Countermoves for its Application to the Space Observations

By

Koh-ichiro OYAMA

CONTENTS

Acknowledgements

A number of acknowledgements are called for. First of all the author would like to express his sincere and hearty thanks to Prof. K. Hirao for his continuous guidance and encouragement during the course of this work. Prof. K. Takayanagi, Dr. T. Itoh, Dr. A. Nishida and Dr. N. Kawashima also gave encouragements to him. He is also indebted to Dr. T. Dote of the Institute of Physical and Chemical Research for his stimulating discussions and continuous leadership of our field, Langmuir probe measurement.

The most part of the experiments were carried out by using the space plasma simulation chamber of the Institute of Space and Aeronautical Science, University of Tokyo (I.S.A.S.) operated by Mr. S. Kojima under supervision of Space Plasma Investigation Committee. A part of the experiments reported in this thesis was done by Mr. S. Mitome to fullfill author's investigation. The instruments used for rocket experiment were designed and manufactured by the members of Shoei Electric Company in Yokohama. Especially successful rocket experiments are due to Mr. H. Tamura of the Shoei Electric Company, Messrs. A. Hasebe and K. Kajiya of the electronics shop of the I.S.A.S. for making electron temperature probe and to Mr. Takeguchi who made a glass sealed Langmuir probe which was first tested on a S-210-6 rocket.

Thanks are also due to instructive discussions with colleagues in Space Science and Engineering Divisions of I.S.A.S. Many helpful suggestions on electron temperature probe were given by Prof. T. Hayashi.

The rocket launching was successfully carried out under the cooperation of the members of the Space Engineering Division of the I.S.A.S.

Managements of the complicated rocket experiments were done by Prof. T. Obayashi, Prof. M. Oda, Dr. S. Miyamoto and others.

The author must express his sincere acknowledgement to Prof. S. Yamashita, T. Thaira, Y. Yamashita and K. Kawabata of Kagoshima University for their continuous encouragements.

Finally the author expresses his gratitude to Miss. T. Okamoto for her typewriting of this thesis and to Ryoko, the author's wife, for her continuous encouragement.

PREFACE

The first attempt on direct measurement of electron temperature in the ionosphere was made in 1947 by Reifman and Dow. Subsequently, a large number of results become available from rocket, satellite and ground-based observations and it is found that the charged particle temperatures generally exceed, often by a considerable factor, those of the neutral particles. There are three main reasons why these results are of interest. The charged particle temperatures are important parameters for the distribution of ionization in the topside ionosphere where diffusive equilibrium prevails, and influence the rate of recombination at lower altitudes. The redistribution of ionization following temperature changes may contribute to the diurnal changes of the layer peak, and changes in recombination rate during ionospheric storms may also be important. The major source of energy which maintains the temperature excess of charged particles from the neutral gas, with which the charged particles are in thermal contact through collisions, is the solar EUV radiation, but the possibility exists of revealing the existence of other sources at night, at high latitudes or during ionospheric storms. Finally, the close relationship between the magnetosphere and ionosphere has been recognized to a considerable degree as a result of the study of charged particle temperatures and the diurnal interchange of energy between these regions.

After the pioneering but unsuccessful attempt of Reifman and Dow to apply the laboratory technique of Langmuir probe to measurements in the ionosphere, continuous development was made in several laboratories resulting in successful observations both from rockets and satellites since 1959. During the same period the increasing number of electron density profiles of the topside ionosphere, obtained from topside sounding or by other techniques, led to many analyses of these profiles using diffusive equilibrium theory and the deduction of plasma temperature from them. Soon after, the suggestion originally made by W. E. Gordon in 1958 that electron temperature might be measured by observing the Thomson scatter of a radio wave from the ionosphere led to a rapid development of the incoherent scatter technique and the establishment at several locations in Europe and America of observing stations. These Thomson radars have given a great contribution to ionosphere study by observing electron and ion temperatures, plasma density, ion composition and drift velocities over each station. Especially basic parameters of ionosphere, electron and ion temperatures have been routinely observed from various angles. Diurnal variation including conjugate point effect, seasonal and annual variations have been studied over the station accomodated. Sometimes Thomson scatter radar supports rocket and satellite experiments by doing a simultaneous measurement. However, in the collaboration with satellite and rocket probes, a comparison study of the data gives one serious but curious inconsistency. The electron and ion temperatures obtained with radar technique are lower than satellite data. Because the existence of such discrepancy gives some possibility that data obtained from such techniques may sometimes give false conclusion, many probe physicists have tried to solve the problem by suggesting that the

discrepancy comes from in-stiu satellite probes, such as Langmuir probe and retarding potential trap. In spite of their efforts, the problem still remains. As for Langmuir probe, they can't find any reason to cause such contradiction, while for retarding potential trap, one attributes the inconsistency to the effective decrease of potential applied to an electrode, other puts the blame to energy distribution of ambient plasma.

In this thesis, I will discuss the topic described above under the assumption that such confusion is caused by the use of a contaminated Langmuir probe. The word "contaminated" is quite ambiguous and the contamination itself doesn't seem worthwhile to be studied. But because of that reason, I believe, the contamination effect has been overlooked in space plasma and most of the probe physicists are indifferent to this problem. In spite of such indifference of scientists, results reported by several authors concerning the problem seem to support my idea but not explicitly. Here I will study the contamination effect as systematically as possible and apply my idea to space plasma measurements for the purpose of solving the above problem.

Somewhere in the world, some probe physicists are trying to solve the inconsistency or writing the paper concerning this. Therefore it seems quite timely for me to present this thesis which investigate the above problem and it is my pleasure to make myself understand "How serious the contamination is".

I hope and believe that this study will contribute more or less to space plasma observation which is most popularily carried out by means of Langmuir probe and retarding potential trap.

Chapter I General Introduction

1. Introduction

Direct evidence for the existence of ionized layers in the earth's upper atmosphere has existed since the pioneering experiments of Appleton and Barnett [*1*] in England in 1925 and those of Breit and Tuve [*2*] in America in 1926. The basic theory governing the function of solar ultraviolet radiation in forming an ionized layer in the atmosphere was given by Chapman [*3*] in 1931 and intensive studies of ionospheric electron density were made during and after the second world war. However, major advances in understanding the physics of the ionosphere have been made since the late 1950's, largely as a result of new technique, viz, in-situ measurement with rockets and satellites and earth-based radar observations of Thomson (incoherent) scatter. Direct rocket sounding initiated by Reifman and Dow [*4*] with the use of V-2 rocket presented the first stage for much informations about the ionosphere. Reifman and Dow were the first who used the rocket for the study of the ionosphere and applied Langmuir probe to the space plasma observation, although data obtained was not absolutely correct and the observation altitude was limited below 120 Km.

Bogges, Brace and Spencer [*5*] following Reifman and Dow gave the first com-

plete electron temperature profile up to around 300 Km of Langmuir probe and first showed that electrons are not in thermal equilibrium with the neutral gases. Since then, electron temperature which is one of the most essential parameters for the ionospheric study has been continuously observed mainly by means of Langmuir probe.

On the other hand, Thomson scatter radar technique appeared in 1962 as a powerful device for the ionosphere study [*6, 7*]. Thomson scatter technique, which gives electron and ion temperatures by sending a gigantic r.f. pulse and detecting the very weak echo scattered by the free electrons, has become the most useful one during a last few years. However when the comparison study became available between backscatter and Langmuir probe techniques, the results from two techniques presented a serious problem. Temperature obtained with two methods did not agree; electron temperature observed with Langmuir probe was about 1.4 times higher than the backscatter value. Ion temperature measured with an electrostatic analyzer also conflicts with the value from incoherent scatter technique. These discrepancies were successively reported and discussed by many scientists. However in spite of the immense efforts of many scientists, the problem still remains without any definite solution. The purpose of this thesis is to discuss the above problem and try to solve the discrepancy. Before entering into the principal, I will summarize the ionosphere from the aspect of thermal balance in this chapter and get the preliminary information about the electron temperature and ion temperature.

2. Energetics of the Ionosphere (theoretical study)

The thermal balance for the electrons in the ionosphere has been discussed by a number of authors. Figure 1 gives an idealized diagram of the processes important in the present discussion. Solar ultraviolet radiation gives rises to photoelectron production chiefly at the altitude below 300 Km. This process and the subsequent cooling of the fast photoelectrons has been discussed by Hanson [*8*], Dalgarno et al. [*9*] and McElroy [*10*]. Below about 200 Km fast photoelectrons travel only a short distance before being reduced to thermal electrons, principally by the inelastic collision with neutral particles. A small fraction of the excess energy of these photoelectrons is given to the ambient electrons via Coulomb encounters. The electron gas is thereby heated, but loses energy through collisions with the neutrals and Coulomb encounters with the ions. Above 300 Km a fast photoelectron may travel some distance from the place where it is created, before it is brought to thermal speeds. Further, since the number of neutrals is decreasing rapidly with height, an increasing fraction of the energy is given to the ambient electrons. Thus, fast photoelectrons traveling upwards from the level where they are created serve to raise the heat input at all altitudes above 500 Km to a value considerably in excess of that deposited by the locally produced photoelectrons.

A significant fraction of the fast photoelectrons created at altitudes of order of 300 Km and higher has sufficient energy to escape the local ionosphere completely

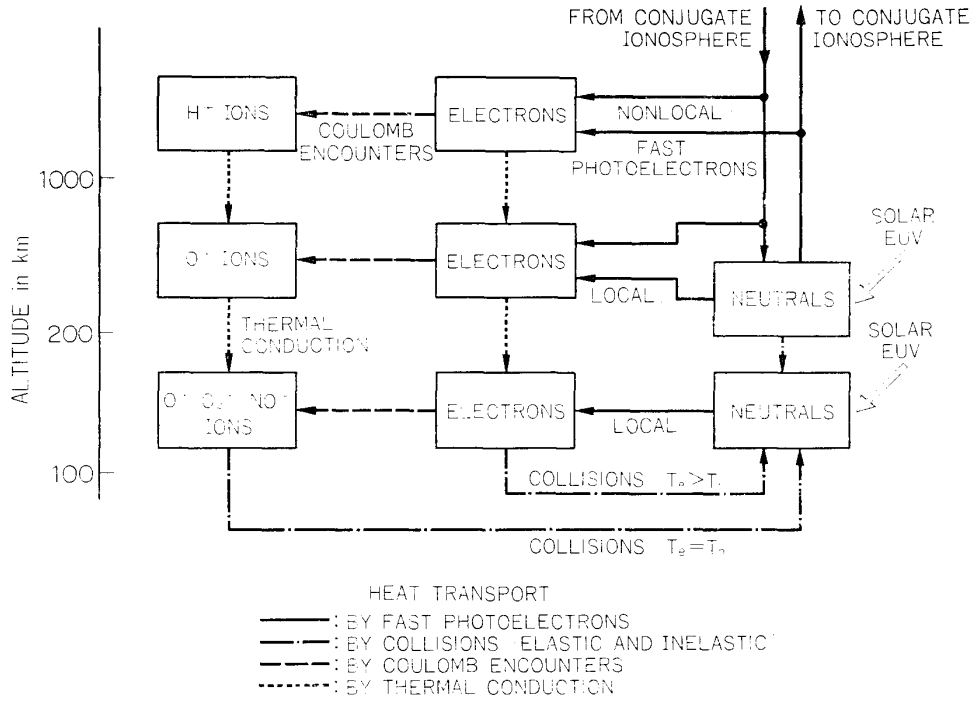

FIG. 1. A block diagram representing in an idealized manner the various heat transfer processes between the electrons, ions and neutral constituents of the ionosphere.

and traverses the protonosphere to the conjugate ionosphere travelling along the lines of force of earth's magnetic field. Hanson, who first drew attention to these electrons, estimated their number as 10^9 electrons per 1 cm^{-2} sec at 1000 Km altitude.

More recently, direct experimental evidence for such a flux has been obtained by Carlson [*11*], Carru [*12*] et al. and Evans [*13*].

The equation which describes the thermal balance is expressed as follows

$$N_e k C_v \partial T_e/\partial t - \nabla(K_e \nabla T_e) = Q_e - L_e \qquad (1)$$

If the main heat flow is along the earth's magnetic field lines and if the flat earth approximation is used, the electron temperature profile $T_e(Z)$ is given as follows in terms of the altitude Z, the time t, and the magnetic dip angle I (Geisler and Bowhill, 1965 [*14*]).

$$N_e k C_v \partial T_e/\partial t - \sin^2 I \frac{\partial}{\partial Z}\left(K_e \frac{\partial T_e}{\partial Z}\right) = Q_e - L_e \qquad (2)$$

where K_e the electron thermal conductivity, N_e the electron density (cm^{-3}), k Boltzmann's constant (1.38×10^{-16} ergs/°K), C_v the specific heat of the electron gas at a constant volume, Q_e the electron heat production rate, L_e the losses by collisions with ions L_{ei} or neutral particles L_{en}, $\sin^2 I \frac{\partial}{\partial Z}\left(K_e \frac{\partial T_e}{\partial Z}\right)$ the losses by thermal con-

duction. Under daytime or even sunrise conditions, $N_e k C_v \partial T_e/\partial t$ is negligible compared to L_e. The commonly observed values of the temperature increase rate are about $12°K$ per min. i.e., $0.2°K$ per sec, and the equivalent $N_e k C_v \partial T_e/\partial t$ value is $2\ eV\ \mathrm{cm}^{-3}s^{-1}$ for an electron density $N_e = 10^5\ \mathrm{cm}^{-3}$; L_{ei} reaches the same value as soon as the difference between electron and ion temperature $(T_e - T_i)$ is $10°K$. Therefore the steady state equation between loss and production is valid even during periods of rapid change (Da Rosa [*15*]).

The energy input Q_e is proportional to the local electron density;

$$Q_e = qN_e = Q_U + Q_D + Q_L \tag{3}$$

where q is the energy input from the photoelectron to the ambient electron gas per thermal electron. The quantity q depends only on the intensity and energy distribution of the streaming photoelectron flux at the place where the energy deposition is considered. In the daytime upper ionosphere, the energy input is devided into three corresponding to the photoelectrons of three different origins; firstly due to the upward flux of photoelectrons created below, Q_U, secondly due to the downward flux of photoelectrons created in the conjugate region and travelling along the magnetic field lines, Q_D, and thirdly due to locally created photoelectrons, Q_L, the relative importance of which decreases rapidly when altitude increases above 300 Km. During winter predawn period, after sunrise in the conjugate area, photoelectrons of the second type are major components. This effect was actually reported as the conjugate point effect of the electron temperature which is not described in detail further. The photoelectron of the first type was first suggested by Hanson [*8*] as described before and taken into the calculation by Geisler and Bowhill [*14*].

The upward flux of the photoelectrons created below can travel to the other place and heat the ambient plasma (non-local heating). The non-local heating becomes effective above about 300 Km, as is shown in Fig. 2. The loss rate L_e is described in the followings.

Losses from electrons to neutral particles are

$$L_{en} = \frac{4kN_eN_n}{\sqrt{\pi}} \cdot \frac{M_eM_n}{M_e+M_n}\left[2k\left(\frac{T_e}{M_e}+\frac{T_n}{M_n}\right)\right]^{1/2}(T_e - T_n) \times \left[\sum_n A_n \Omega^{-n/2}\Gamma\left(\frac{n+6}{2}\right) + 2\sum_n \sigma_n v_{on}^{5/2} \exp(-\Omega v_{on})\right] \tag{4}$$

Losses from electrons to ions via Coulomb collisions are

$$L_{ei} = 4\sqrt{2\pi}\frac{N_eN_ie^4}{M_eM_i}k\frac{1n\Lambda}{\left[k\left(\frac{T_e}{M_e}+\frac{T_i}{M_i}\right)\right]^{3/2}}(T_e - T_i) \tag{5}$$

The definition of the terms in Equations (4) and (5) and their numerical values are exactly the same as in the paper of Herman et al. [*20*].

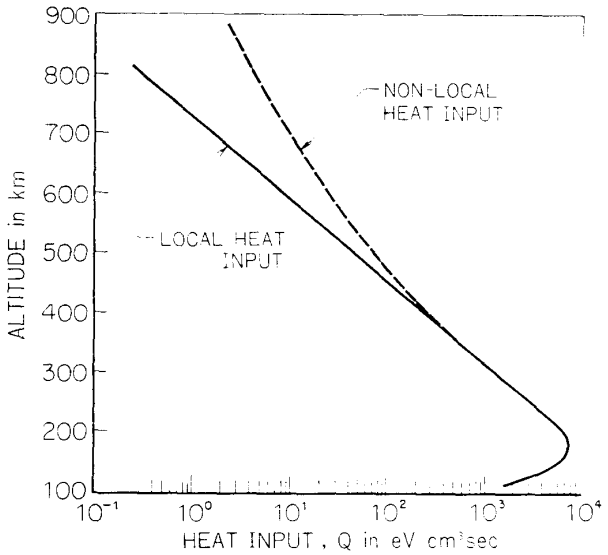

FIG. 2. Variation with altitude of the heat input Q showing both the local heating and also the additional non-local heating which results from including the contribution from photoelectrons originating below 300 Km (Geisler et al. [*14*]).

Equation (4) can be expressed rather simply in the following form

$$\begin{aligned} L_{en} = 1.60\times10^{-12}\, N_e\{&2.47\times10^{-18}N_O(T_e-T_n)T_e^{1/2}+1.71\times10^{-19}N_{N_2}\\ &\times(1-2.1\times10^{-4}T_e)(T_e-T_n)T_e+1.21\times10^{-18}N_{O_2}(1+3.6\times10^{-2}T_e^{1/2})\\ &\times(T_e-T_n)T_e^{1/2}+3.1\times10^{-14}N_{N_2}(T_e-T_n)T_e^{-1/2}+10^{-13}N_{O_2}\\ &\times(T_e-T_n)T_e^{-1/2}+2.46\times10^{-7}N_{H_e}T_e^{1/2}(T_e-T_n)+9.63\times10^{-16}N_H\\ &\times(1-1.35\times10^{-4}T_e)(T_e-T_n)T_e^{1/2}\}(\text{ergs cm}^{-3}\text{ sec}^{-1}) \end{aligned} \qquad (6)$$

where N_n is the density of the neutral constituent, n.

In the above eqquation, the first, second and third terms express the loss rate by elastic scattering by O, N_2 and O_2 respectively, fourth and fifth terms, rotational excitation by N_2 and O_2 respectively. Vibrational energy loss by N_2 and O_2 which are not described in the equation become important when the electron temperature is so high as 3000°K. For the elastic collision with positive ions in Equation (5), we can get rather familiar form in the following way.

$$\begin{aligned} L_{ei} = 7.68\times10^{-19}N_e(T_e-T_i)T_e^{-3/2}&[N_{O_+}+4N_{He_+}+16N_{H_+}+0.50N_{O_2}\\ &+0.53N_{NO_+}](\text{ergs cm}^{-3}\text{ sec}^{-1}) \end{aligned} \qquad (7)$$

where N_{n_+} is the density of the ion constituent, n.

In addition to the above losses, Dalgarno and Degges [*16*] reported that loss rate of the electron energy by the fine structure level of the atomic oxygen is quite large compared with other loss rates, which is expressed as [*21*]

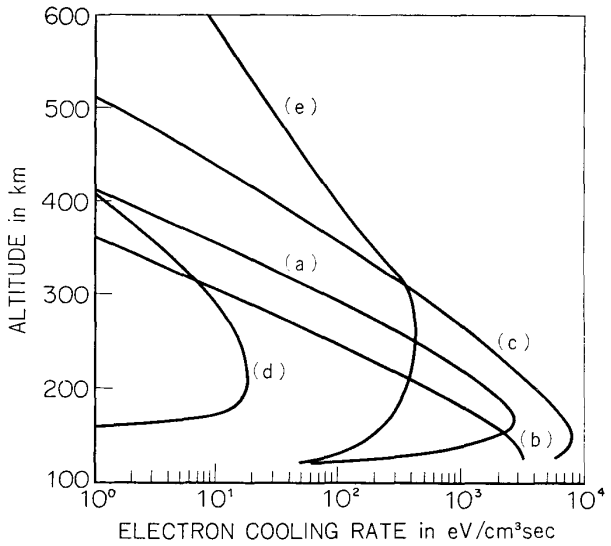

FIG. 3. Calculated electron cooling rates by various collision processes for 1963 July at noon. The curves refer to excitation of (a) vibrational levels of N_2, (b) rotational levels of N_2, (c) fine-structure levels of O, (d) metastable levels of O, (e) elastic collisions with positive ions. The cooling due to elastic collisions with neutrals and from rotational excitation of O_2 are negligible (Dalgarno et al. [16]).

$$L_{eo}^{*}=\frac{2N_eN_O}{\sqrt{\pi}D(kT_e)^{3/2}}\sqrt{\left(\frac{2}{M_e}\right)}\sum_j\sum_{j'\neq j}(E_j-E_{j'})g_{j'}\exp\left(-\frac{E_j}{kT_n}-\frac{I_{jj'}}{kT_e}\right)$$
$$\times\left[1-\exp\left(-\frac{I_{jj'}}{kT_eT_n}(T_e-T_n)\right)\right]\int_0^\infty E'\sigma_{eo}(j'\to j,E')e^{-E'/kT_e}dE' \qquad (8)$$

where N_e the electron density, N_O the atomic oxygen density, M_e the electron mass, T_e, T_i and T_n the electron, ion and neutral temperature, k Boltzmann's constant, E_j the j-th fine structure energy level of atomic oxygen corresponding to the angular momentum quantum number $j, I_{jj'}=E_{j'}-E'_j, g_{j'}=2j+1, \sigma_{eo}(j'\to j,E')$ cross section for downward transition from j' to $j, D=\sum_{j'} g(-E_{j'}/kT_n)$. For the convenience, the following simple numerical approximation to the above equation is obtained.

$$L_{eo}^{*}=(5.92-4.68\times10^{-4}T_e)(9.04+6.57\times10^{-4}T_n)$$
$$\times10^{-25}N_eN_O(T_e-T_n)/T_n(\text{ergs cm}^{-3}\text{ sec}^{-1}) \qquad (9)$$

In Fig. 3, electron cooling rates by various processes described above are calculated, from which we can see the general dominance of each cooling process in various altitudes. Especially it should be noted that below 250 Km, thermal balance is mainly decided by loss rate due to the fine structure level of atomic oxygen.

By the use of equation (1), one can evaluate theoretical profiles of electron temperature. Dalgarno et al. [17] made this sort of calculations to compare with incoherent scatter results at Millstone Hill and at the same time discussed the effect

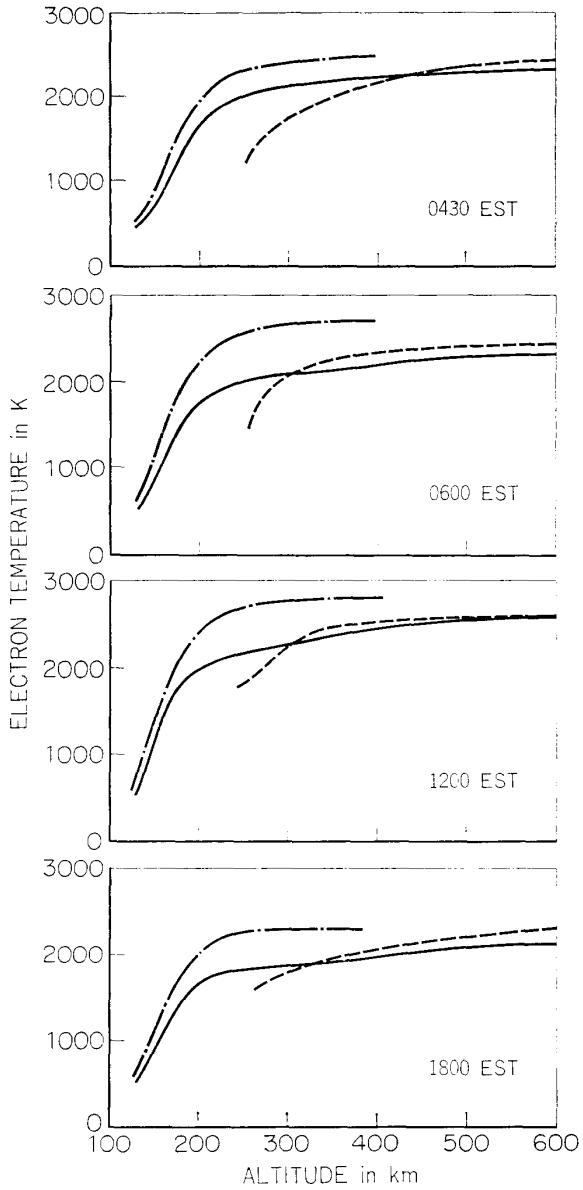

FIG. 4. Electron temperature profiles in July, 1968, at various times throughout the day. The solid lines are the theoretical predictions. Dash-dot curves exclude electron cooling to atomic oxygen, while the dashed curves are the experimental Thomson scatter data of J. V. Evans at Millstone Hill (Dalgarno et al. [*16*]).

of L_{eo}^{*}. When L_{eo}^{*} is included in the calculation, the agreement is generally good as shown in Fig. 4 except that the heat input must be reduced by about 60% at 200 Km where the calculated temperature are too high. Nagy et al. [*18*] also made calculations for Millstone Hill data and obtained temperature which were rather too low at around 200 Km suggesting that the discrepancy may be quite sensitive to the calculation such as the assumed solar spectrum and photoionization cross sections. Lejeune and Petit [*19*] calculated Q_e values (in which non-local heating was not

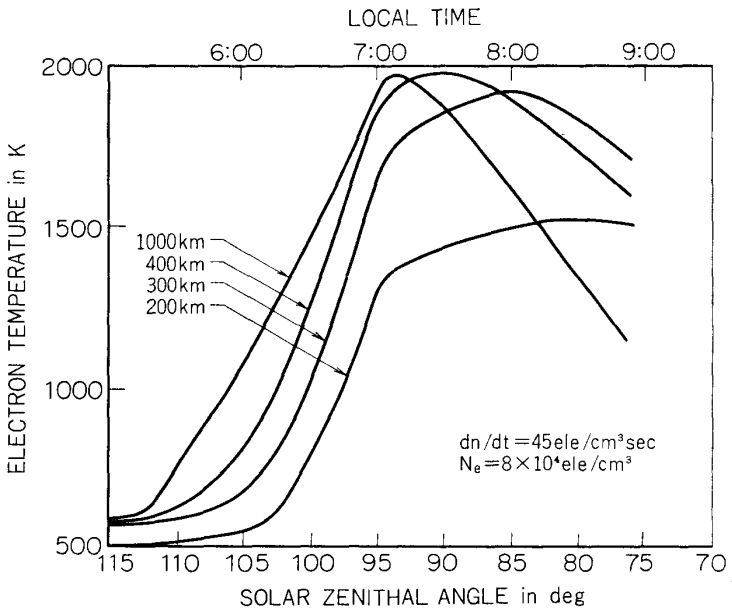

(a)

FIG. 5a. The theoretical behavior of electron temperature during sunrise, for solar cycle minimum, winter (N_e and dn/dt refer to the $F2$ peak) (Da Rosa [*14*]).

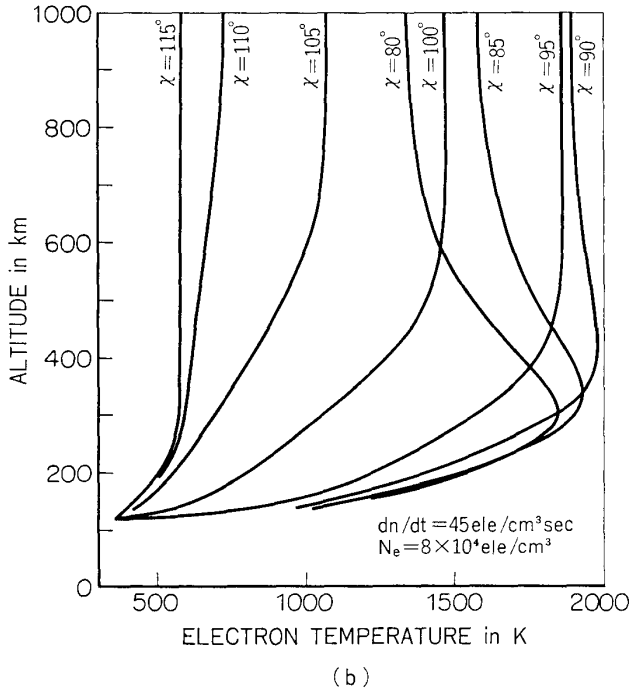

(b)

FIG. 5b. Profile of electron temperature at various times after sunrise (N_e and dn/dt refer to the F_2 peak).

considered) for St. Santin profiles of T_e and T_i from 120–150 Km, and found the observed values to be less than the calculated. They thought that the inconsistency may be attributed to the effect of non-local heating which they believed to be im-

portant down to 200 Km. Despite these relatively small discrepancies, there is little doubt that the solar radiation provides the majority of the energy input to the ionosphere.

Herman and Chandra [*20*] solved simultaneously the continuity equation of electron and the heat conduction equations for electrons, ions and neutral species. They mainly discussed the solar flux dependence of the electron temperature and the effect of the loss due to fine structure of the atomic oxygen. [*21*]. The paper shows that height of the electron temperature maximum decreases as the increase of solar flux intensity, which does conflict with our experimental results as will be discussed in the later chapter.

Concerning the dominance of L_{eo}^{*}, their result also shows that calculated electron temperature at around 200 Km is more than 1000°K higher when the loss due to fine structure of atomic oxygen is neglected. Although Herman et al. solved the time dependent equations, there are quite few who discussed the time variation of electron temperature profile in detail. Da Rosa [*15*] treated the transition of electron temperature during sunrise by including $N_e k C_v \partial T_e / \partial t$. One remarkable result drawn from his theoretical study is the prediction of the appearance of temperature peak sometimes after sunrise but much before the production reaches its maximum, what we call, morning overshoot. In Fig. 5a, one example of the thermal histories shows an obvious peak caused as the result of the competing influence of the increasing heat production and the increasing heat capacity of the electron gas accompanied by the growing concentration. In Fig. 5b are shown the changing behavior of electron temperature profile during sunrise. This sorts of profiles were really observed by Farley et al. as described later.

Concerning the electron temperature of magnetosphere, P. Bauer [*22*], G. Lejeune and M. Petit [*19*] discussed the photoelectron flux streaming into the magnetosphere and calculated the magnetospheric temperature.

3. General structure of the ionospheric electron temperature

Electron temperature profile is calculated with Equation (1) to some extent, whilst it is quite difficult to calculate a global structure of electron temperature and no theory has been reported. Therefore we will discuss data obtained by satellites.

Electron temperature is controlled by geomagnetic field. The principal geographical features of the daytime electron temperature is an increase from equator to latitude 50° of about 600°K, after which the temperature slightly decreases (Fig. 6) (Bowen et al. [*23*], Brace et al. [*24*]). The distribution shows marked geomagnetic control, being symmetrical about the geomagnetic not the geographic equator. Dalgarno suggested that this did not indicate an additional high latitude heat source but arose only from the decrease in electron density and so of the collisional cooling rate. To this effect, at high altitudes, must be added that of the suppression of non-local heating near the magnetic equator. From an analysis of Arial 1 data, Willmore [*25*] showed this explanation to be correct. Superimposed on the latitude effect are smaller scale variations of 200°K. Since such small scale

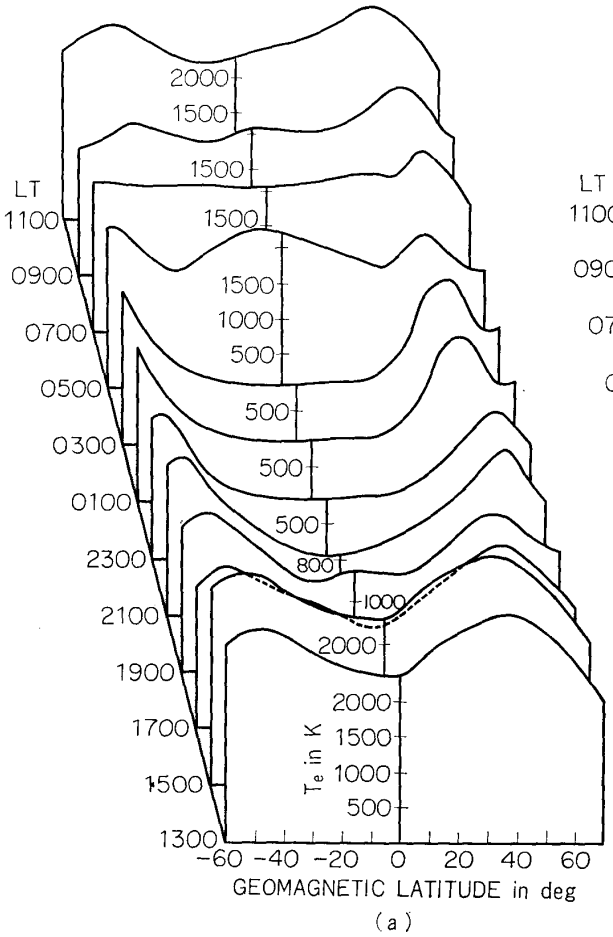

FIG. 6a. Average latitudinal and local time behavior of the electron temperature at 1000 Km altitude as measured by Explorer XXII in the winter soltice period. The night time cooling of the electron gas proceeds rapidly at low geomagnetic latitudes due to the low heat capacity of the low latitude protonosphere magnetic field tubes (Brace et al. [24]).

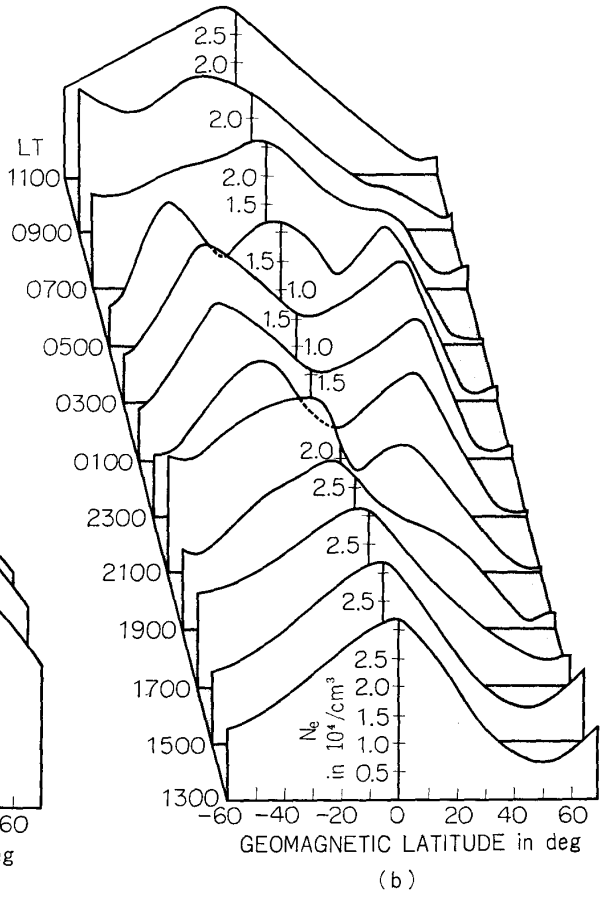

FIG. 6b. Averaged variation of N_e at the 1000 Km level corresponding to T_e data of Figure 6a.

variations are always negatively correlated with N_e variations, they appear to arise merely from local anomalies in N_e, which produce variations in the collisional cooling rate. Thus all the geographical features in the T_e can be explained by variations in electron number density.

Next we summarize the behaviour of electron temperature in each latitude in more detail. At low latitude, the geomagnetic field lines are horizontal and thermal conduction and non-local heating are suppressed. Fig. 7 shows the electron temperature profiles taken at Jicamarca (dip angle; 1°) by Farley et al. [26]. Electron temperature rises to a maximum near 230 Km, then it decreases asympto-

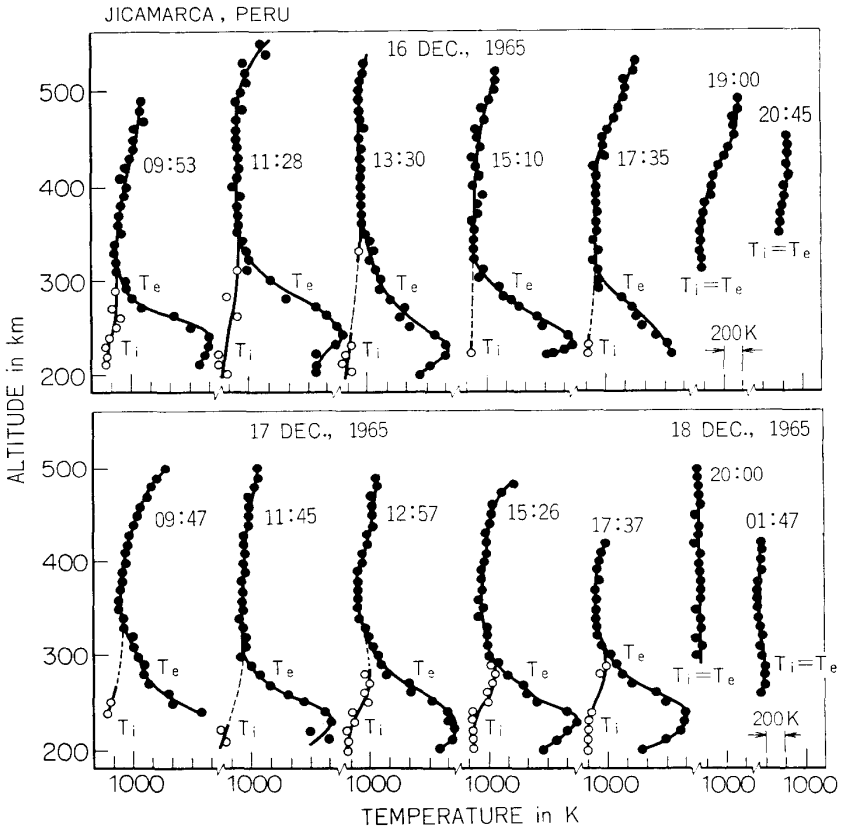

FIG. 7. Electron and ion temperature profiles at equatorial region (Farley et al. [26]).

tically to T_i at greater heights as predicted originally by Hanson who neglected non-local heating.

At middle latitude, electron temperature profiles similar to those of Figure 7 can be observed for several hours of a day. Figure 8 shows the general electron temperature profiles obtained at Uchinoura since 1970 [27]. The profile which has temperature maximum appears around 16 hours in the afternoon. Such a behaviour could be seen in the profiles obtained on some rocket flights. Results obtained at Arecibo and St. Santin show that when electron density at the F peak exceeds $(5\text{–}6)\times10^5 cc^{-1}$, a minimum in T_e develops at near 250–350 Km as a result of the increasing collisional cooling. On the other hand, on days when electron density is lower than the above-described amount $(5\text{–}6)\times10^5 cc^{-1}$, monotonous increase in T_e is observed. [28] At high latitude, electron temperature continues increasing as the increase of the height, as shown in Fig. 9 [29]. Monotonous increase of T_e can be caused by two mechanisms at high latitude. One is the increase of non-local heating in high latitude, the other is the decrease of collisional cooling which is caused by the low density plasma. By comparing Fig. 7 with Fig. 8, one can clearly see the effect of the two mechanisms described above.

The indicated above are the most representative features of electron temperature profile in various latitudes. Sometimes we can get some curious profiles apart

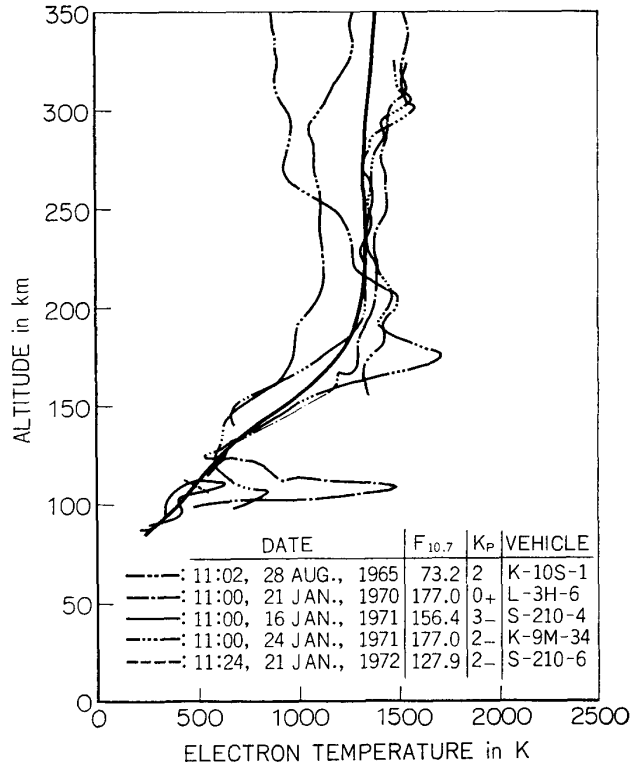

(a)

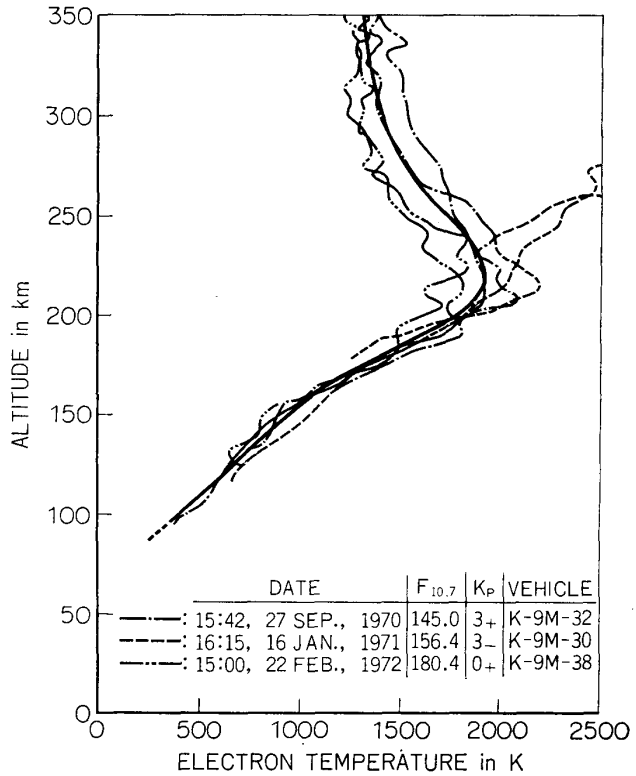

(b)

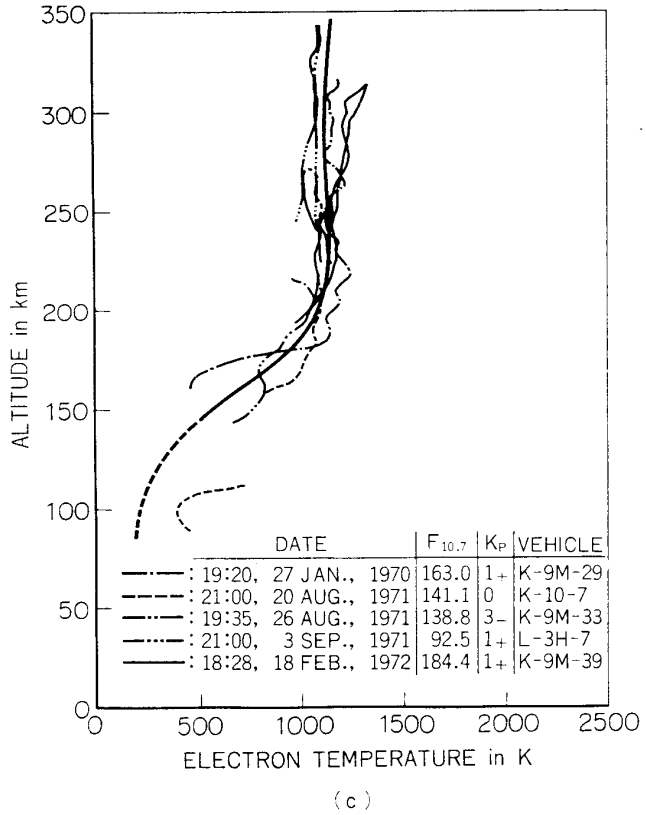

FIG. 8. Electron temperature profiles at middle latitude obtained in Japan, (a) morningtime, (b) afternoon, (c) nighttime. The full lines are the mean values.

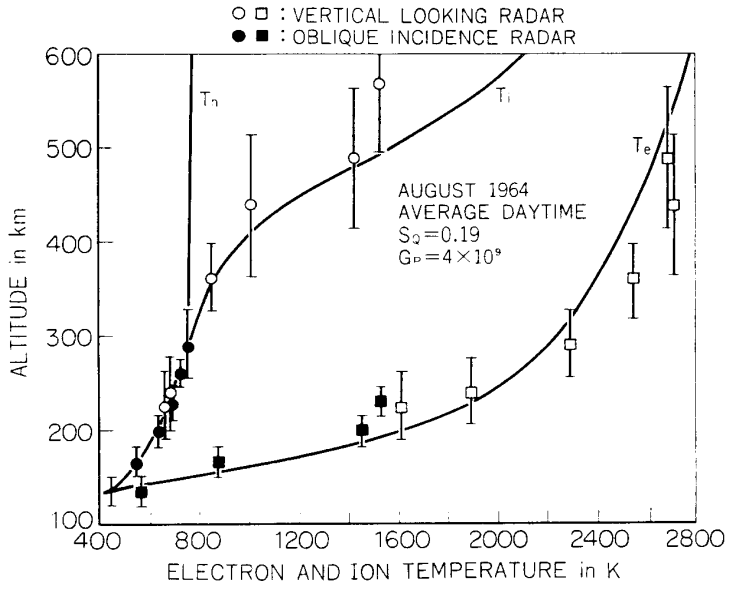

FIG. 9. Electron temperature profile at high latitude. The average daytime (0900–1500 EST) variation of electron and ion temperatures with altitude for August 1964 at Millstone Hill. The bars denote the height of the exploring pulse and the full lines are theoretical predictions. (Evans [*13*]).

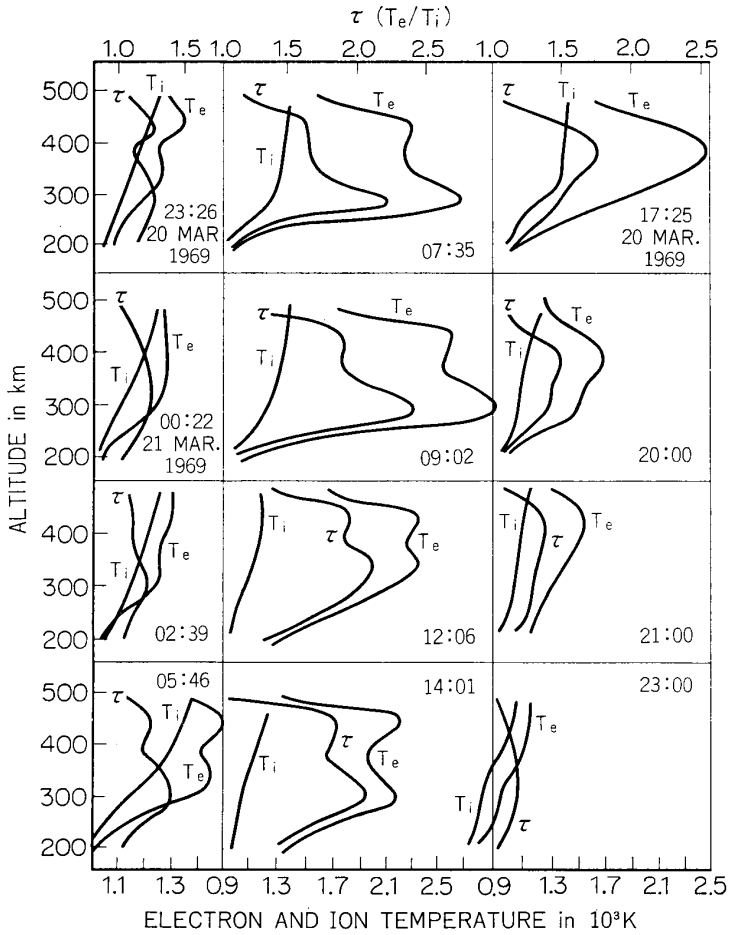

FIG. 10. Another example of the electron and ion temperature profiles at middle latitude for the spring equinox period (20, 21, March, 1969) (Misyura et al. [30]).

from the general structure described above. Midlatitude electron temperature profile observed in U.S.S.R. under the condition of high solar activity in 1968 had two peaks. These two peaks were always observed during the day as shown in Fig. 10.

As described above, electron temperature shows quite variety of profiles depending on the time, place and solar activity. In order to get the complete understanding, further observations are strongly required in many places.

4. SPECIAL FEATURES OF THE ELECTRON TEMPERATURE

4.1 Morning overshoot [24, 31–37]

A striking feature, shown in all reported observations in the topside ionosphere, is that generally temperature maximum does not occur near or after noon, but in the morning. This kind of phenomenon was first predicted by Dalgarno et al. [*36*] and was systematically studied and confirmed by Da Rosa as described in section 2 of this chapter. According to the theory by Da Rosa, the peak is more pronounced in the higher altitude. The result obtained from an isothermal map presented by

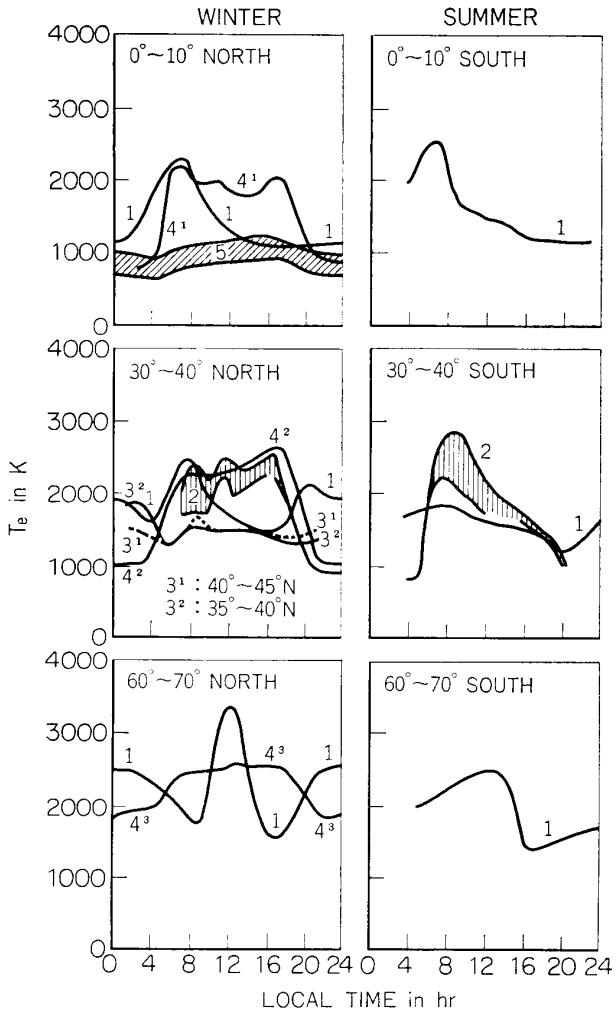

FIG. 11. Diurnal variation of the electron temperature depending on the geomagnetic latitude. Morning overshoot clearly appears in low and midlatitude regions.

TABLE 1. List of observers of diurnal variation of electron temperature.

Date No.	Observer	Date of observation	Place or carrier	Instrument	Height	Ref.
1	Clark et al.	1968 Oct. -1969 Apr.	ESRO-IA	Langmuir probe	600 Km	31
2	Doupnik	1965 Dec. -1966 Aug.	Arecibo	Back-scatter	475 Km	32
$3^{1,2}$	Bourdeau	1962 Oct. -1962 Dec.	Alouette-1	Scale height	500 Km	33
$4^{1,2,3}$	Brace	1965 Eeb. -1965 Apr.	Explorer	Langmuir probe	1,000 Km	24
5	McClure	1965 Nov.	Jicamarca	Back-scatter	700 Km	34

Evans [*37*] seems to support the theory. Sometimes the peak value is the highest between 300–600 Km [*11*]. In order to see this phenomenon more systematically, we summarized all the data which have been reported up to now. The results are illustrated in Fig. 11. These experimental curves are obtained either by incoherent backscatter radar or by direct measurements by means of plasma probes mounted on satellites, or sometimes from the scale height of electron density. The observers of the individual profiles are summarized in Table 1.

In Fig. 11 diurnal variations of the electron temperature are grouped, depending on a geomagnetic latitude. From the figure, we can find two interesting features on diurnal variation of electron temperature. Firstly the magnitude of the overshoot in the early morning varies from 100–2000°K. The effect is greatest near the magnetic equator where the overshoot is between 700° and 2000°K, decreasing at magnetic latitude of 30°–50° to 200°–600°K. At high latitude of 60°–70°, morning overshoot seems to be confined to the summer months [*37*]. Secondly, the time of the dawn maximum seems to have a latitude dependence, that is, the electron temperature maximum occurs around 07 hrs in equator, 08 hrs in midlatitude and near noon at high latitude. Especially this tendency seems much clear in summer hemisphere than in winter zone.

The two facts described above can be considered to be general features of morning overshoot. However Brace's result shows that morning overshoot does not always occur. In his result, temperature maximum occurs near 16 hrs in winter hemisphere, which is contrary to the theory of Dalgarno and Da Rosa. Therefore their theory does not seems to be satisfactory, that is, the theory is not yet unified to explain all the diurnal variation observed. In order to get unified expression of diurnal variation of electron temperature, further satellite experiment is required as well as theoretical study.

Concerning the morning overshoot itself, as described previously, this dawn maximum appears to be the result of a more rapid build up of neutral gas density (and so of heat input) than that of collisional cooling during the early morning, so that the cooling rate lags relative to the heating rate.

4.2 Observation in lower ionosphere

Electron temperature in the ionosphere ranging from 90 Km to 130 Km has been measured almost mainly with Langmuir probe because Thomson technique are subject to the effect of collisions in the neutral gas and this necessitates a correction to the result of incoherent scatter below 120 Km. Therefore the observation is not made with sufficient accuracy. In fact, there are quite few data that have been obtained with back scatter technique.

In Langmuir probe measurement, though a number of electron density profiles have been observed [38], not so many electron temperature profiles have been reported and the values are not so reliable possibly because the correct electron temperature can't be obtained with a contaminated Langmuir probe and even if a clean probe could be used, the measurement of the electron temperature of 200–300°K requires the telemeter channel of high frequency response.

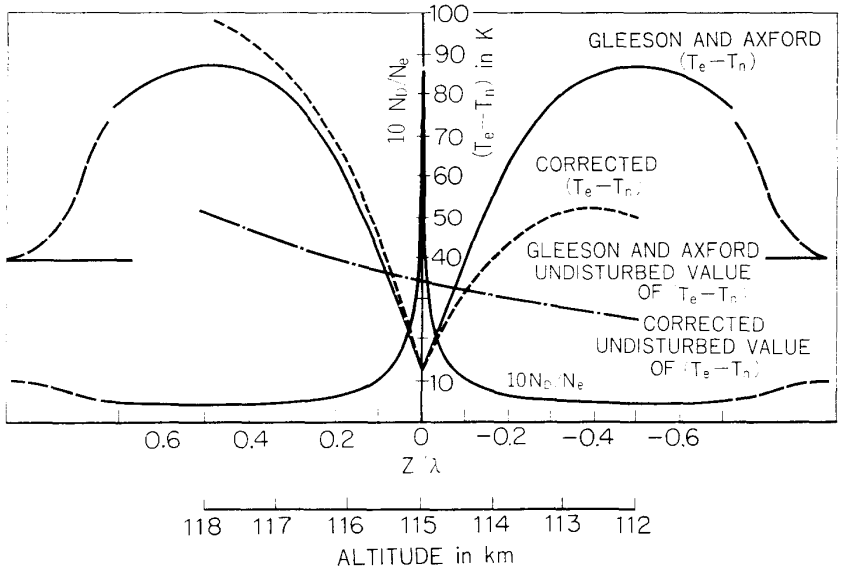

FIG. 12. Predicted (T_e-T_n) profiles in an E_s-layer. The temperature profile applies at an altitude of about 115 Km, with $\alpha N_e=3\times10^{-2}$ sec. The N_D/N_e distribution is from Axford and Cunnold with $\lambda=6$ Km. The solid (T_e-T_n) curves are the Gleeson and Axford [*41*] predicted profiles. The dashed curves are the corrected profiles. Where N_e undisturbed electron density, α recombination coefficient, N_D disturbed density (Hooke [*42*]).

Below 90 Km, even electron density measurement becomes less reliable because no fully adequate theory of probe on supersonic spacecraft has been published and the alternative empirical or semiempirical approach also has been little studied. [*39, 40*]

The following two sections summarize two interesting features in the lower ionosphere which are not still completely understood. One is the electron temperature in an E_s layer which has been observed quite few times, the other is the high electron temperature around dynamo region which was first studied by us and for which no satisfactory explanation has been done yet.

4.3 Electron temperature in the E_s layer

The effect of wind motion in the E region was studied by Gleeson and Axford [*41*], who found that a wind shear pattern which produced a strong E_s layer with a peak density of 8.5 times of the ambient value would lead to a depression of about 70°K in T_e at the center of the layer, a slight enhancement occuring above and below the center of the layer. Hooke [*42*] pointed out that the variations in neutral gas temperature that accompany tidal and gravity wave motions of the neutral gas play a major role in determining the height variations in the electron and ion temperatures through E_s layers of gravity wave and tidal origin. One example of predicted (T_e-T_n) profiles in a sporadic E layer is shown in Fig. 12 where result by Gleeson and Axford is also shown for comparison. Hooke suggested that distinguishing between wind shears caused by prevailing winds (where presumably the temperature profile is something like that given by the standard atmospheres) and wind shears

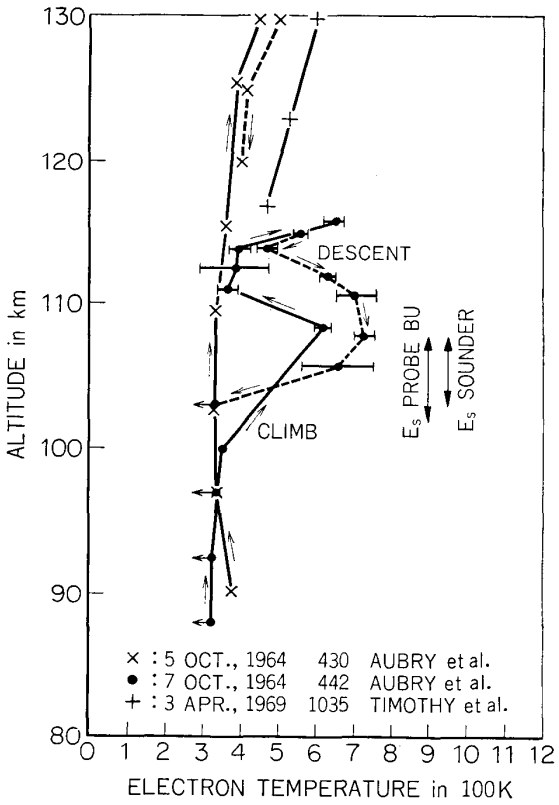

FIG. 13. Electron temperature profiles observed by Aubry et al. [*44*] and Timothy et al. [*45*] Value by Aubry et al. coincides with the neutral temperature of Jacchia 71 and also with the observation of neutral temperature by Golomb et al. [*46*].

of wave origin (where there is an oscillating component of T_n associated with the oscillations in the wind shear profile), may be possible by doing simultaneous observation of electron and neutral temperatures in E_s layer.

From experimental point of view, E_s layer has been studied mainly by the use of electron density data which was obtained from fixed bias probe [*43*]. Observation of the electron temperature in the E_s layer is quite few and was reported only by Aubry et al. as well as by us. The results of Aubry et al. [*44*] are shown in Fig. 13 together with Timothy's result [*45*] which was obtained with the same type as the ac mode Langmuir probe. Data obtained with the ac mode Langmuir probe which is free from contamination effect of a probe surface seems reasonable. Aubry et al. observed electron temperature in the E_s layer in Oct. 7, 1964. At that time Langmuir probe and ionosonde also caught E_s layer around 102–108 Km. It appears that the electron temperature maximum is located at the upper side of the E_s layer, which seems to support the theory presented by Hooke and Gleeson et al. Fig. 14 shows the electron temperature profiles observed at Uchinoura, which may be compared with the above results. In the figure, electron temperature profile observed by the rocket K-10-7 is also shown. When the rocket K-10-7 was launched, ionosonde at Uchinoura recorded E_s layer at the height of 107 Km.

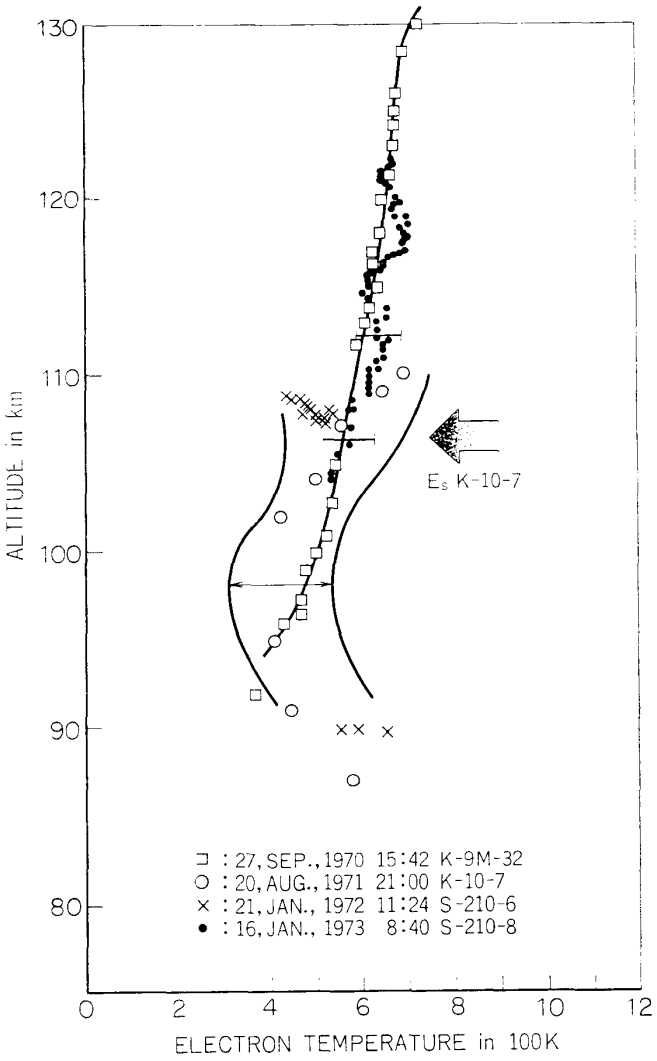

FIG. 14. Electron temperature obtained by Hirao et al. by means of electron temperature probe. Electron temperature observed by K-10-7 is almost equal to the day time value observed with S-210-8 and K-9M-32, the value is 200°K higher than the night time value.

Although the data quality and height resolution are not satisfactory as illustrated in the figure, the electron temperature observed with K-10-7 is nearly the same as that of the daytime profiles observed by S-210-8 and K-9M-30 which are simultaneously illustrated in the figure. Considering that the rocket K-10-7 was launched at 9 hrs in the evening, we will be able to conclude that the electron temperature in or around the E_s layer is certainly higher than that of the ambient plasma.

As described above, it seems quite certain that some heating occurs around E_s region, but it is not clear whether heating occurs in the E_s layer or near the layer. In order to get some precise information, observations by means of a glass sealed Langmuir probe could be considered (see chapters II and III). In summary the rocket data used for the above discussion are listed in the following.

TABLE 2. List of the electron temperature profiles observed with ac Langmuir probe.

Rocket	Date	Time ($L-T$)	Place	Latitude	Observer
SL-502	1969 Apr. 03	10 : 33	Woomera	31° S	Timothy et al.
C 62	1964 Oct. 05	16 : 30	Hummaguir	30°8N	Aubry et al.
C 63	1964 Oct. 07	19 : 42	Hummaguir	30°8N	Aubry et al.
S-210-6	1972 Jan. 21	11 : 24	Kagoshima	31°3N	Hirao et al.
K-10-7	1971 Aug. 20	21 : 00	Kagoshima	31°3N	Hirao et al.
S-210-8	1973 Jan. 16	8 : 40	Kagoshima	31°3N	Hirao et al.
K-9M-32	1970 Sep. 27	15 : 42	Kagoshima	31°3N	Hirao et al.

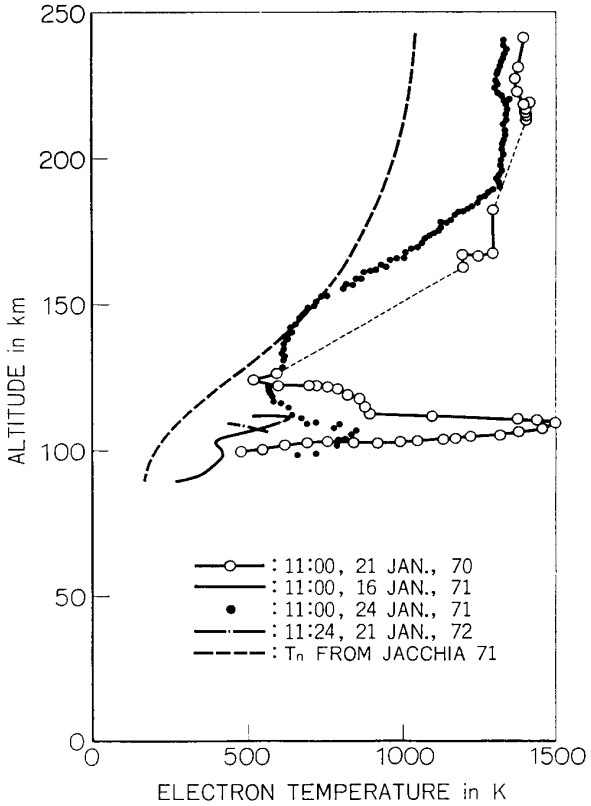

FIG. 15. High electron temperature layer observed at around 105 Km. The layer appears at 11 hrs in local time without exception. [47]

4.4 *Electron temperature around dynamo region*

An interesting layer which has unexpectedly higher temperature than the ambient plasma temperature was found by us. As is shown in Fig. 15, the layer appears around at the height of 100 Km [47]. The deviation of the electron temperature from model neutral temperature seems proportional to the square of the diurnal variation of the horizontal component of the magnetic field which is considered to be induced purely from overhead current. But we have no idea why such layer appears [48]. The profiles obtained by rockets S-210-8 and K-9M-40 launched in 1973, Jan. 16 at 8:40 and in 1972, Sep. 20 at 14:00 respectively did

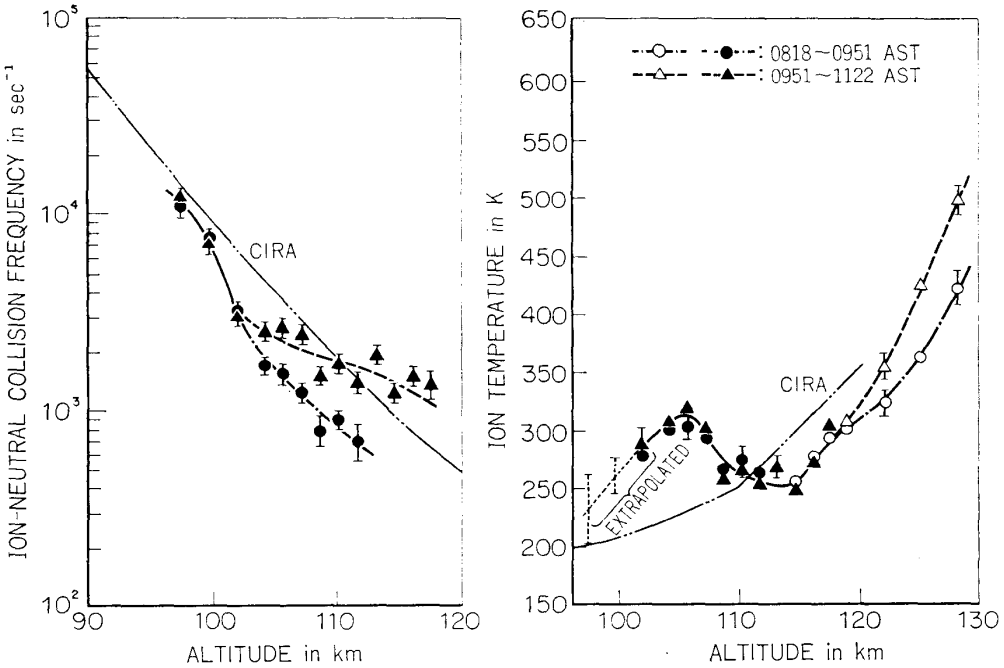

FIG. 16. Values of ion temperature Ti and ion-neutral collision frequency obtained at Arecibo with backscatter technique [*89*] and compared with the CIRA 1965 model atmosphere (Wand [*49*]).

not show such temperature maximum. This fact seems to show that the appearance of high temperature layer is limited just around 11 hours in the morning. The similar phenomena were observed at around 10 hours in the morning by Wand et al. [*49*] by means of Thomson scatter technique. Fig. 16 shows the ion temperature behaviour deduced under the assumption $T_e = T_i$. The profiles show general agreement with CIRA model atmosphere above 110 Km. But the result gives a clear indication of ion temperature maximum around 105 Km. Hooke [*50*] suggested that these phenomena may be explained as due to the reversible heating of parcels of gas as they are compressed adiabatically in the course of the wave motion. Although we have no idea whether the results obtained at K.S.C. and Arecibo come from the same cause, it is quite obvious that the behaviour of this region is more complicated than implied by the model. Further experiments are required to get a complete conclusion.

5. CONCLUDING REMARKS

We briefly summarized the energetics of the ionosphere confining to the electron temperature from theoretical and experimental points of view and picked up some current topics.

The original theory of electron temperature by Hanson and Johnson in 1961 underwent substantial development by the hands of several other authors and it is now clear that the theory can explain the major features of the quiet F region

during the day and, surprisingly, is even able to account for a departure from thermal equilibrium which occurs at night when solar radiation is absent. Our interest is now being directed to the complicated changes which occur in ionospheric storm and effects which may be observed over the auroral zone.

In the D- and E-regions, the situation is unclear and complicated. Several direct comparisons of temperature measured by different methods have been made, in particular, between Langmuir probe and incoherent back scatter technique above 130 Km. Although the agreement between two methods has been sometimes reported, general conclusion derived from the comparison study is that the discrepancy exists in electron temperatures evaluated from Langmuir probe and back scatter technique.

Below 130 Km no such simultaneous comparison has been made, but indirect comparison shows inconsistency between the results obtained by the two methods. The electron temperature obtained from Langmuir probe is higher than the radar value and the radar value is very close to the neutral temperature suggested from model atmosphere. Therefore it is not clear whether a departure from thermal equilibrium in charged and neutral particles really occurs in the E region or the other region. If thermal non-equilibrium does truely exist, it can not be sustained by the same collision processes as in the F region. As will be described in the present thesis, Langmuir probe itself has some ambiguities due to the contamination effect and the backscatter technique is applicable only under some assumptions in the lower ionosphere. Because of these problems in measurement methods the situation of this region is obliged to be much more complicated. Therefore before the study of energetics of the lower ionosphere, we must first identify the cause of the inconsistency between two methods.

Chapter II Analysis of a Contaminated Electrode

1. Introduction

Since Langmuir established the probe method in 1923 [*51*] for the study of plasma, the probe has been used in various fields from laboratory plasma to space one and it achieved a especially great contribution to space observation.

Langmuir has showed that if the plot of the logarithm of probe current (I_p) versus probe voltage (V_p) is straight line for V_p which is negative with respect to the ambient plasma, energy of electrons has a distribution of the maxwellian law and can be described by an electron temperature T_e. T_e is obtained from the slope (e/kT_e) of the straight line. Experimental data, however, often give plots that are nonlinear, or that consist of two or more straight lines. The nonlinearity of the semilogarithmic curve is due to the non-maxwellian distribution of electron velocities, to the superposition of two or more maxwellian distributions. Sometimes the nonlinearity may be caused by some defects in probe technique. In this paper, the problem of the non-linearity due to the non-maxwellian distribution is left as it is

and we will confine our discussion to the probe technique itself, because there is a serious defect in the conventional probe technique as described later.

Most of the earlier publications which report deviations from the maxwellian velocity distribution do not mention above the surface condition of the probe. The probe whose surface is covered with contaminants gives the non-linear semilog. plotted curve that leads to an erroneous electron temperature. There exists a serious difference between two probe curves which are obtained when the bias voltage of Langmuir probe is increased from negative to positive and is decreased from positive to negative with respect to the ambient plasma potential. Electron temperature evaluated from those semilogarithmic curves are always overestimated in both the increasing and decreasing biases.

Since difference of the shape of the probe curves appear as a form we call this the hysteresis phenomenon of the probe. The study of the hysteresis phenomenon of the Langmuir probe seems to have been initiated by Van Berkel [*52*] (1938). She called attention to the fact that a change of work function may influence the reliability of probe measurements.

Anderson [*53*] (1947) studied these changes experimentally by taking oscillographic picture of the probe characteristic with varied frequency of the sweep voltage. In a rare gas discharge with tungsten cathode no changes appeared with varied frequency. However in an oxygen discharge the recording frequency had to be raised to several hundred cycles in order to eliminate the hysteresis effect during one cycle.

Easley [*54*] (1951) made probe measurements in Hg-Ar and Hg-Kr discharges with the oxide cathode. When she eliminated the influence of the changing work function of the probe by measuring each point of the probe characteristic immediately after the probe was cleaned, and when no oscillations, striations or impurities were present in plasma, no deviations from the maxwellian velocity distribution were found. However, when the probe was not properly cleaned, deviations from the straight line in the semilogarithmic plotting appeared in a direction which could be explained by a higher work function of the probe at low probe temperature. She ascribed these results to an increase of the work function of a pure tungsten surface by contamination with mercury.

Wehner and Medicus [*55*] (1952) summarized the reliability of probe measurements and concluded that Langmuir probe measurements can give quite erroneous results by the change of work function of the probe, insulating layers on the probe surface or different work function at different places of the probe surface. In addition to these, there are some papers which discussed the contamination of a probe surface. As described above, they have always attributed the cause of hysteresis curve to the variation of work function of the probe. However, there are some experimental results that can not be explained only by the change of work function. For example "Electron density dependence" could not be explained by changing work function.

Instead of the above mentioned model, we [*56*] presented a contamination layer model, which is given by means of an equivalent circuit and tried to explain

the experimental results with a good success.

The purpose of the chapter is to investigate the contaminated probe quite systematically by the use of laboratory plasma as the application of the present new model. The first part of the chapter is devoted to show some experimental results which verify the present model. The model is finally applied to also the discussion of the measurements by a retarding potential trap.

2. Theoretical study of the contamination layer

2.1 *Contamination of the probe surface*

As we mentioned in the above section, Langmuir probe gives a seriously distorted v-i curve if the probe is not clean or contaminated.

Though a contaminated Langmuir probe is chemically washed, the probe surface is usually not completely cleaned. Various contaminations are absorbed on probe surface and they form a thin film on a metal surface. The contamination substance is mainly water as is shown in later, of which dielectric constant is 80 or so. Therefore it will give a seriously large capacitance. In addition to the water, various substances are also absorbed. These substances are easily considered to have high resistance. Therefore contamination layers thus formed will be electrically expressed in the form of an equivalent circuit which consists of capacitor C_c and resistor R_c connected in parallel as is shown in Fig. 17. The magnitudes of C_c and R_c depend

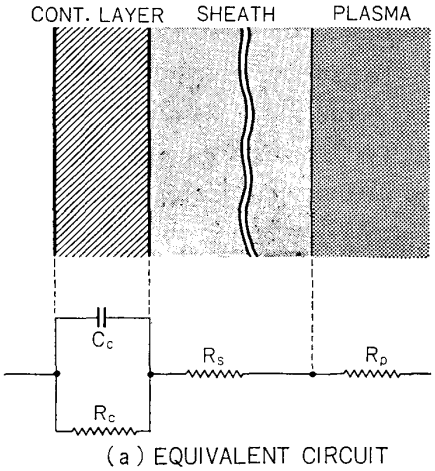

Fig. 17a. Contamination layer and the equivalent circuit for a contaminated Langmuir probe.

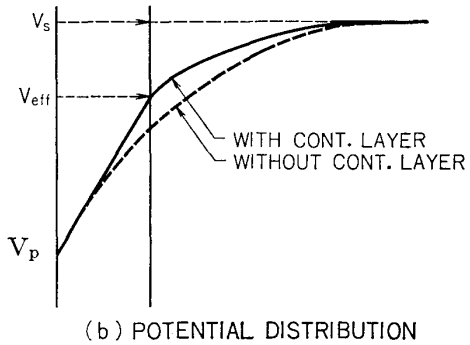

Fig. 17b. Potential distribution near sheath-electrode boundary. V_s are V_p are the space potential and probe voltage respectively.

on the kinds of contamination matters and the degree of the contamination.

Usually C_c and R_c are a few micro-farad and several hundreds kilo-ohm respectively. Fig. 17a shows that if the sweep voltage is applied to the probe, the current flowing into or out from the probe will be affected by the capacitor C_c, in other words, probe current will have various values depending on the sweep frequency of the probe bias. If the probe bias is slowly changed, the capacitance C_c will not influence the probe current because the current flows through the contamination resistor only. The voltage which is actually applied to the contaminated probe surface is not V_p but V_{eff} which is expressed as

$$V_{eff}=\frac{V_p(R_s+R_p)}{R_s+R_c+R_p} \tag{10}$$

Therefore the voltage of the contaminated probe surface, V_{eff}, is always smaller than that actually applied voltage from outside, V_p. Consequently, the decrease of the probe voltage leads to an overestimation of electron temperature. The potential distribution in front of the contaminated electrode is schematically illustrated in Fig. 17b.

V-i characteristic curves in the higher frequency range where C_c is effective will take the different paths depending on the increasing and decreasing biases, because the C_c is charged or discharged within one sweep cycle. As the phenomenon that v-i characteristic takes the different paths may be called "hysteresis", we can say that the increase of the sweep frequency causes an increase of hysteresis. Finally, as the frequency of the sweep voltage becomes again higher, a decrease of the hysteresis will be again experienced, because the charge stored in C_c can't discharge through the circuit within one sweep cycle and C_c behaves like a battery, in other words, the impedance due to C_c becomes negligibly small.

2.2 Frequency and density dependences of the hysteresis curve

The above-described discussion deals with the contamination effect quite qualitatively. Here we would like to discuss it in more detail from another point.

As described above, v-i characteristic curve takes different paths depending on the direction of the sweep of bias. The cause of the different paths is in other words attributed to a phase difference between voltage applied to the probe and the current flowing into or out from the probe; if the probe current changes without time delay corresponding to the applied voltage, hysteresis will not appear. Therefore the increase of the phase difference is physically equal to the increase of the hysteresis. From that reason we can discuss hysteresis phenomena from the point of the phase difference. Our discussion starts from Fig. 17. To make easy the argument the sheath resistance R_s is assumed constant. Although the sheath resistance is not constant during one sweep in real plasma, the discussion will not lose the generality by assuming the constant sheath resistance for the understanding of the various effects accompanied with contaminated electrode. The probe voltage $\vec{V}$ is swept sinusoidally with angular frequency ω instead of triangular wave usually

used, which also leads to a simple calculation. Consequently, the relation between voltage applied to the probe, $\vec{V}$, and the current flowing the circuit, $\vec{I}$, is expressed as follows, which is simply evaluated from the equivalent circuit shown in Fig. 17.

$$V=\left(\frac{1}{\left(\frac{1}{R_c}+j\omega C_c\right)}+R_s+R_p\right)\cdot\vec{I}=|\vec{Z}|\,e^{-j\Psi}\vec{I} \tag{11}$$

$$\Psi=\tan^{-1}\left[\frac{\omega C_c R_c}{R_s+(R_s+R_p)(1+\omega^2C_c^2R_c^2)}\right] \tag{12}$$

$$|\vec{Z}|=\frac{[\{(R_s+R_p)(1+\omega^2C_c^2R_c^2)+R_c\}^2+\omega^2C_c^2R_c^4]^{1/2}}{1+\omega^2C_c^2R_c^2} \tag{13}$$

Where Ψ is the phase difference between the voltage applied to the probe and the current flowing through the circuit. $|\vec{Z}|$ is the absolute value of sheath plasma impedance including the insulation layer. In the above equation, when the frequency of the applied signal increases, impedance of the circuit system, $|\vec{Z}|$, decreases and then gradually approaches to the sheath resistance, R_s+R_p, whilst phase difference, Ψ, starts from zero value, gradually increases, takes the maximum value

$$\Psi_{\max}=\tan^{-1}\left[0.5\left(\frac{(R_s+R_p)}{R_c}+\frac{(R_s+R_p)^2}{R_c^2}\right)\right]^{1/2} \tag{14}$$

at

$$\omega_{\max}=\frac{1}{C_cR_c}\left(1+\frac{R_s+R_p}{R_c}\right)^{1/2} \tag{15}$$

and finally decreases toward zero value. These situations are shown in Figs. 18a and b. Although the equation (12) and the related Figure 18a show a small phase difference (small hysteresis) in lower frequency region, such lower sweep of the bias voltage will never give the correct v-i characteristic curve because in this region the circuit impedance is dominated by $R_p+R_s+R_c$ but not the pure sheath plasma resistance R_s+R_p as was described in the previous section. It is strongly noted that in higher frequency range where total circuit impedance is nearly close to the sheath resistance, v-i characteristic curve will express a behaviour of sheath-plasma impedance. Therefore in this frequency region, we can expect a correct electron temperature from the v-i curve. We will study this prediction in more detail in the later section. The characteristic relating to the sweep frequency of the voltage will be called "Frequency dependence of the hysteresis curve".

Fig. 19a shows that the phase difference decreases monotonously as the sheath resistance R_s increases, whilst the impedance of the circuit takes the value of $R_c/(1+\omega^2C_c^2R_c^2)^{1/2}$ at $R_s=0$ and gradually increases toward the sheath resistance as the sheath resistance R_s increases, which means that the probe characteristic curve is almost controlled by the sheath resistance only. In other words, the probe curve

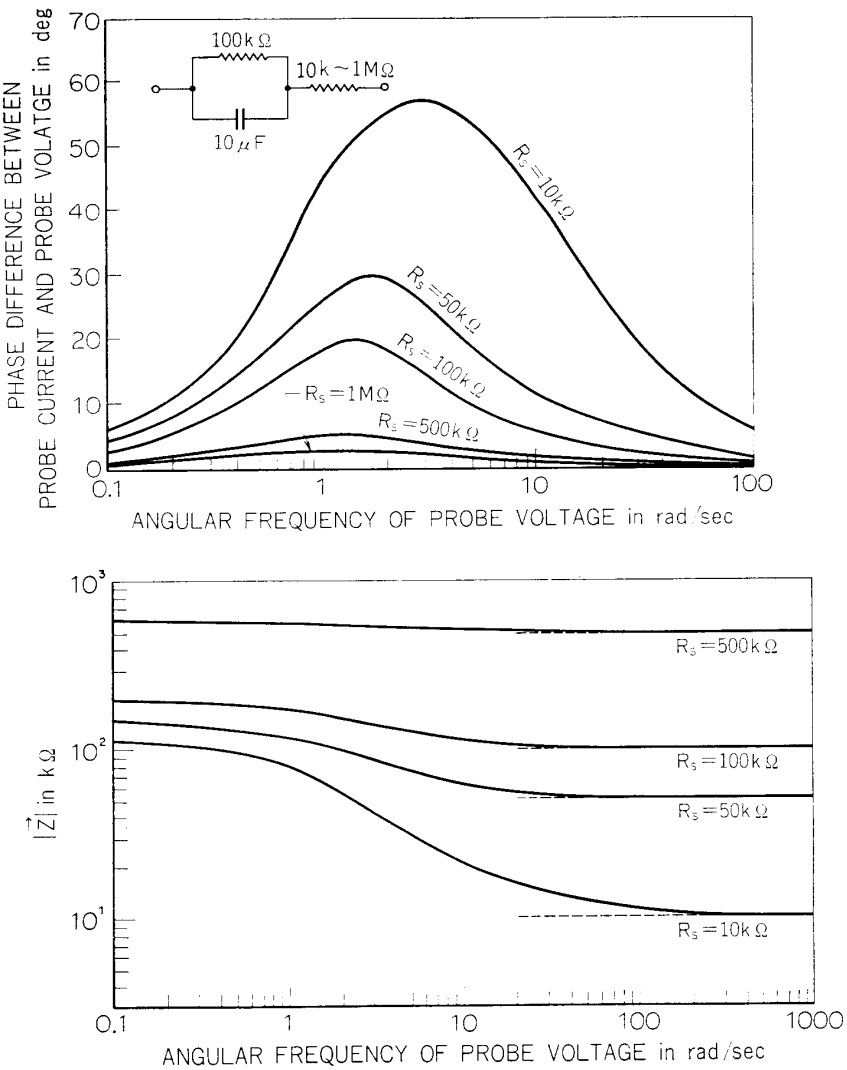

FIG. 18. Phase difference (a) and impedance (b) of the equivalent circuit corresponding to the frequency dependence. Angular frequency ω is charged from 0.1 to 1000 rad./sec. Here R_p is assumed 0.

reaches the correct characteristic as the density of the ambient plasma decreases. The above prediction that the probe curve becomes less influenced as the increasing sheath resistance (which corresponds to the decreasing electron density of the ambient plasma)) will be called "Density dependence of the hysteresis curve" as compared with the former characteristic "Frequency dependence". These situations are illustrated in Figs. 19a and 19b.

As described above, we have discussed the phase difference Ψ and the absolute value of the vector impedance $|\vec{Z}|$ independently, which leads to more or less confusion. Therefore we combine these two factors and summarize the results.

Vector impedance of equation (11) is written as $\vec{V}=(X-iY)\vec{I}$, where

$$X=R_s+R_p+\frac{R_c}{1+\omega^2C_c^2R_c^2} \quad \text{(Real part)} \tag{16}$$

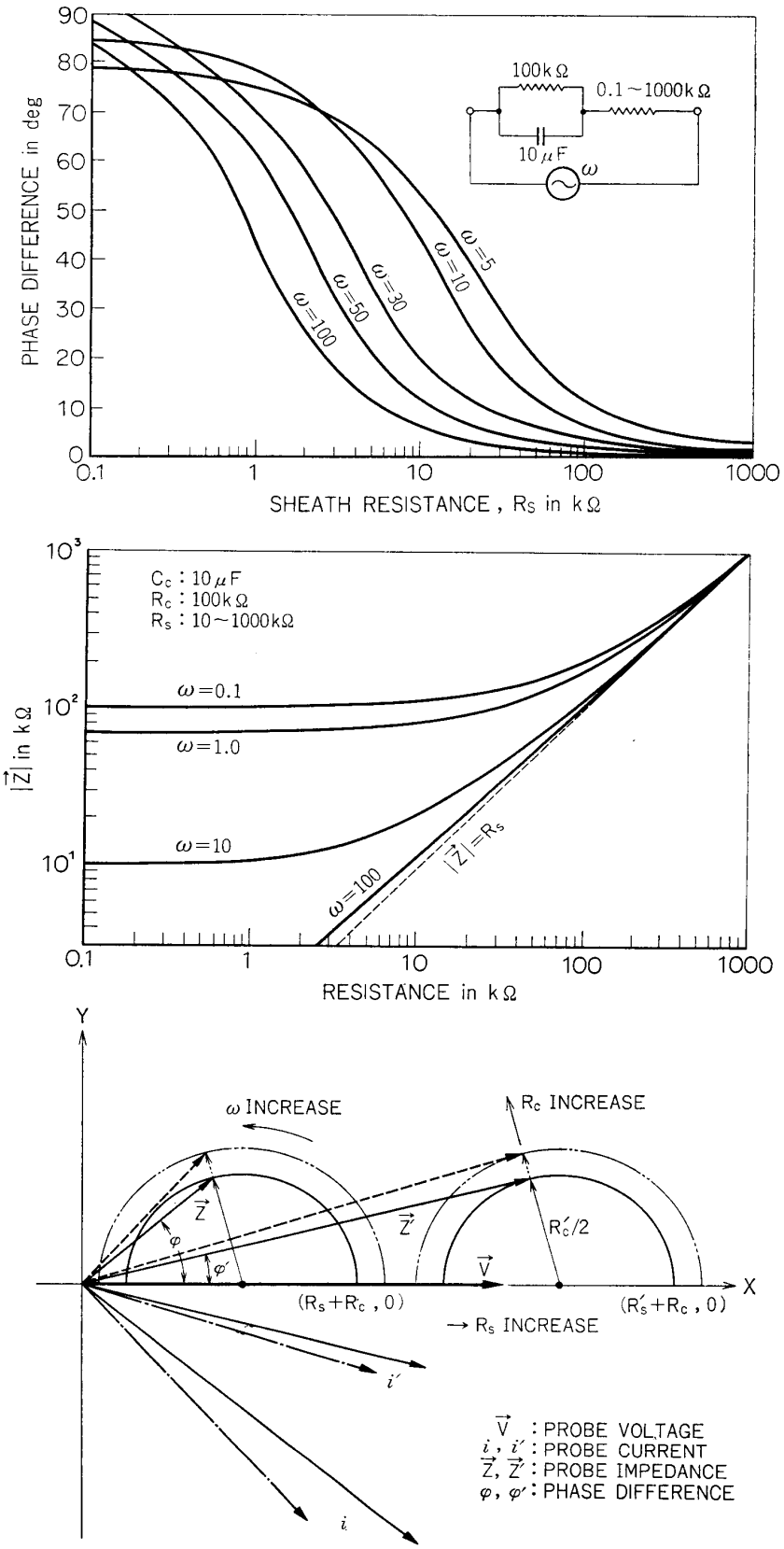

FIG. 19. Phase difference (a) and impedance (b) of the equivalent circuit corresponding to the density dependence and vector locus (c) obtained by combining phase difference and absolute value of impedance. Here R_p is assumed 0.

$$Y=\frac{\omega C_c R_c^2}{1+\omega^2 C_c^2 R_c^2} \quad \text{(Imaginary part)} \tag{17}$$

By eliminating ω from the above two equations, we can finally get the following equation relating X and Y.

$$\left(X-R_s-R_p-\frac{R_c}{2}\right)^2+Y^2=\left(\frac{R_c}{2}\right)^2 \tag{18}$$

The above equation is shown in Fig. 19c, where the phase difference is expressed as the angle between the X axis and the vector impedance $\vec{Z}$ and the above-mentioned absolute value $|\vec{Z}|$ corresponds to the length of the vector impedance $\vec{Z}$. At a glance, one can see two special features mentioned previously, (1) the electron density dependence and (2) the frequency dependence. That is, when R_s is large compared with R_c, $\vec{Z}$ is almost defined by R_s and the phase difference becomes quite small. As the increase of ω, $\vec{Z}$ gradually reduces toward R_s starting from $R_p+R_s+R_c$, while the phase difference gradually increases, takes the maximum value and finally goes to zero.

3. Experimental results (Verification of the theory)

In the present section, are shown the various experimental results on the contaminated probe in order to show the validity of the model described above.

3.1 Experimental set up

The experimental results described in the chapter are mainly obtained by the use of space simulation chamber of the Institute of Space and Aeronautical Science,

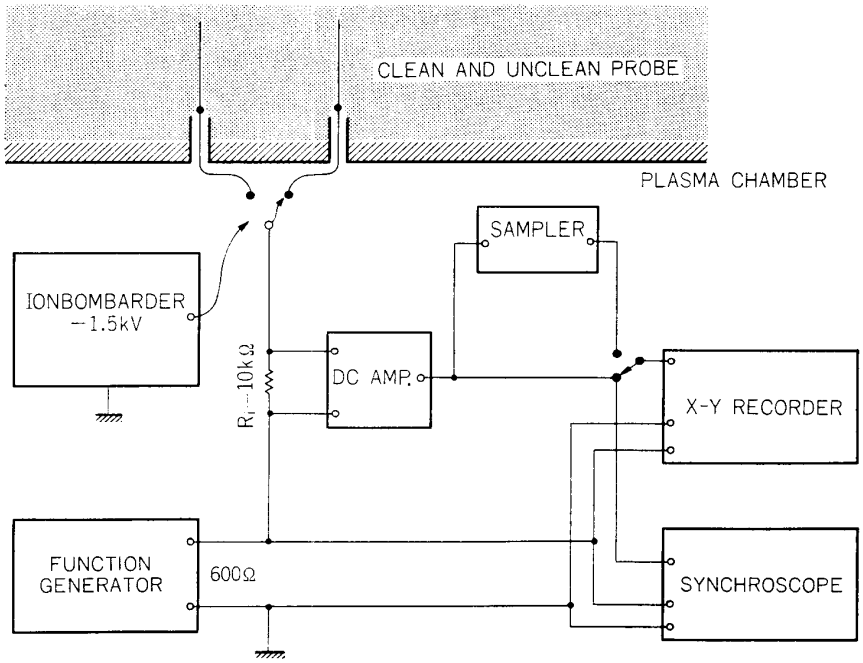

FIG. 20. Experimental set up for a study of a contaminated electrode.

University of Tokyo, whose diameter and length are 2 m and 3 m, respectively. Usually the chamber is evacuated below 2×10^{-7} Torr and Ar gas is filled into the chamber up to about 10^{-4} Torr. Plasmas are produced by the plasma sources of the back diffusion type at both ends of the chamber and are diffused into the measuring space in the chamber. The electron temperature and the density of the produced plasma are in the range from several hundreds degrees to several thousands degrees and 10^{3}–10^{6} el/cc, respectively. The stainless steel cylinder probe (3 mm $\phi\times$20 cmL) is set apart from the ion beam, which is very often produced by the above described plasma sources. To the stainless steel cylinder probe is applied a triangular voltage by means of a function generator through a resistance R_i with the sweep rate of 0.01–50 Hz. The probe current is detected, amplified and recorded by a X-Y recorder or a synchroscope. Sometimes when the response of the X-Y recorder is not enough, "Sampling Recorder" which records quick changes of a curve is used for the study of a frequency dependence of the hysteresis curve.

3.2 Frequency and density dependences

It has already been shown in the theory that the contaminated Langmuir probe gives a hysteresis curve depending on the frequency of the sweep voltage. As the frequency of the sweep voltage increases beyond a point determined by the sheath resistance, the hysteresis decreases and finally vanishes. This process is clearly shown in Fig. 21, which is taken from the experimental circuit described above. In the vanishing part of the hysteresis in higher frequency, it is considered that the probe curve may give a correct Langmuir curve as the theory predicts. The above consideration is quite important in a space plasma observation, which will be discussed later in detail. The simulation is given by the use of simulation circuit of plasma composed of resistance and capacitance. If we take $R_c=100\,\mathrm{K}\Omega$, $C_c=10\,\mu F$, $R_s=\mathrm{diode}+300\,\mathrm{K}\Omega$ and apply the triangular sweep voltage to the circuit, we can get photographs illustrated in Fig. 22, which are quite similar to the results of the real plasma experiments shown in Fig. 21. In order to study the behaviour of the hysteresis more quantitatively, we take the difference of the floating potentials (the potential where ion and electron currents are equal) which are obtained by increasing and decreasing of bias, as a measure of the degree of the hysteresis. The increase of the difference of two floating potentials is considered to represent the increase of the hysteresis. Fig. 23 gives the frequency dependence of the hysteresis curve by means of the difference of floating potentials with a parameter of the electron density. It is clearly shown that the difference in floating potentials decreases with the increase of the frequency of applied voltage. The figure shows at the same time that the increase of the electron density causes the increase of the difference of the floating potentials, that is, the density dependence of the hysteresis curve. The second prediction which is derived from the theory is also thus verified.

3.3 Langmuir curve obtained with the rapid sweep voltage

In the section 3.2, we could find no difference between the curves of decreasing and increasing biases in the case of fast repetition of the probe bias, that is, it cor-

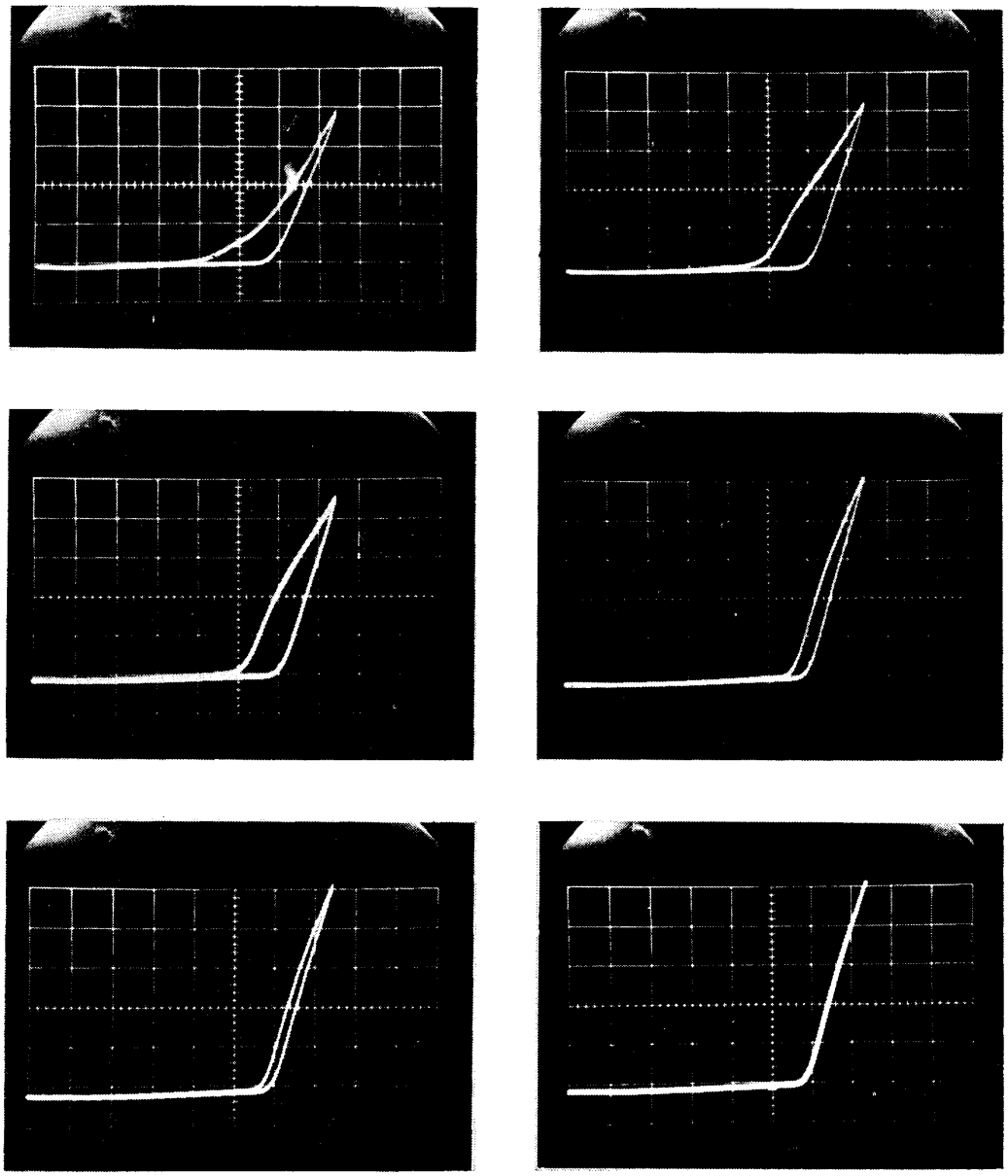

FIG. 21. Frequency dependence of a v-i curve obtained with a contaminated brass cylindrical Langmuir probe, 3 mm$\phi \times$24 mmL. Vertical axis; probe current 4 μA/div. Horizontal axis; probe potential 1.8V/div. Ar gas; 6×10^{-4} Torr. Repetition period; 0.01, 0.05, 0.1, 0.5, 1.0, 5.0 Hz respectively, from upper left to lower right.

responds to the disappearance of the hysteresis. At the stage of the disappearance of the hysteresis, the v-i characteristic curve is considered to give the true electron temperature as is predicted by the equivalent circuit model. Because this fact seems quite important for the space plasma observation, further experiments are carried out. In the space simulation chamber, two kinds of cylinder probe of the same dimension and of the same material are set, one is cleaned by an ion bombardment, the other remains uncleaned which is set apart 10 cm from the former. Two stainless steel cylinder probes give different v-i curves corresponding

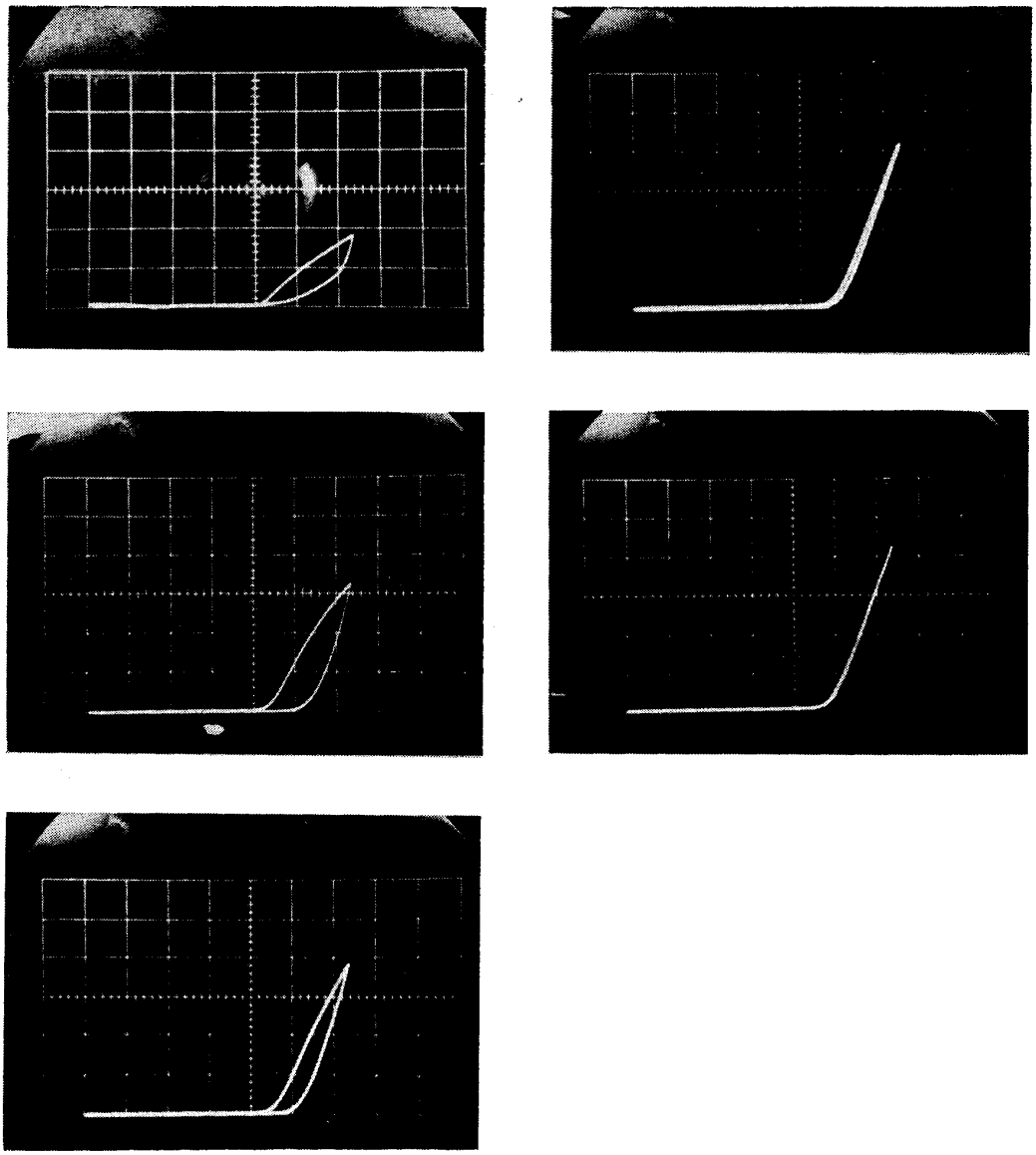

FIG. 22. Frequency dependence by the use of the equivalent circuit shown in Fig. 17. Vertical axis; 1 μA/div, Horizontal axis; 0.4V/div, sweep rate; 0.01, 0.05, 0.1, 0.5, 1 Hz respectively from upper left to lower right.

to the degree of contamination of uncleaned probe as shown in Fig. 24. The contaminated Langmuir probe in a slow sweep of 0.03 Hz gives a seriously distorted Langmuir curve from which we can't evaluate the electron temperature. However, if the probe voltage is quickly swept (10–40 Hz), the hysteresis vanishes even when the probe surface is contaminated. As is illustrated in Fig. 25, it is found that at the time of the vanishment of hysteresis, the semi-logarithmically plotted v-i curve is quite linear and the electron temperature evaluated from the curve is the same as that from the clean probe which is swept with 0.03 Hz.

The behaviour described above is also simulated by the use of the equivalent circuit shown in Fig. 17, where $R_c = 100$ KΩ, $C_c = 1$ μF, R_s = diode and $R_p = 1$ KΩ. In that case, a series connection of diode and 1 KΩ is referred to the clean probe (1), while a circuit including C_c and R_c is analogous to the contaminated probe (2).

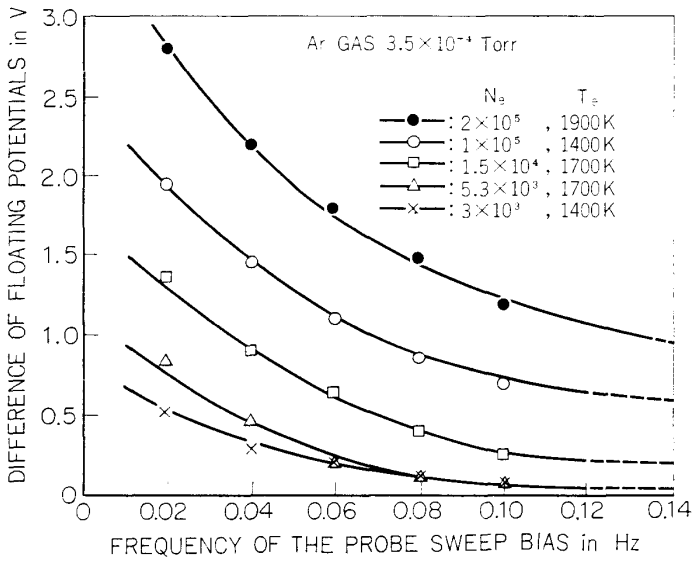

FIG. 23. Density and frequency dependences illustrated by the difference of floating potentials of the v-i curves obtained with a contaminated probe.

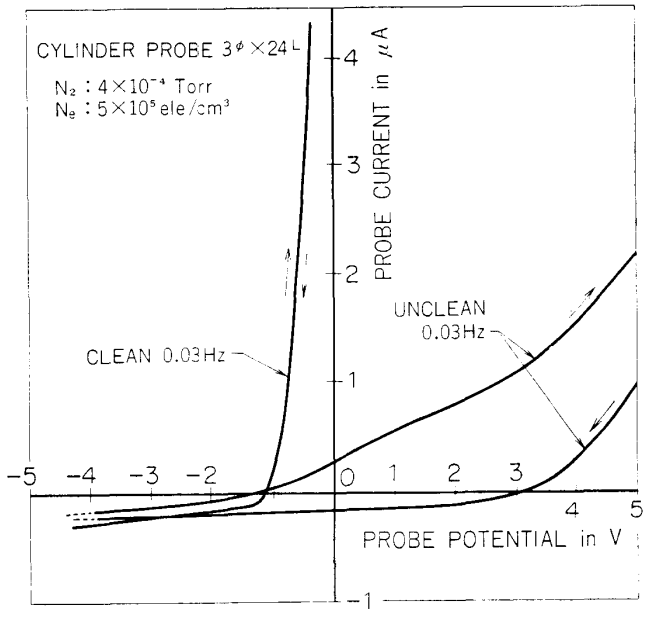

FIG. 24. V-i characteristic curves obtained with contaminated and clean probes.

The results are illustrated in Fig. 26 (a). The left curve is taken by the connection (1) in very slow sweep potential, the right is by the connection (2) under much higher frequency to avoid the hysteresis effect. We can't find any difference between them except the shift of the curve along the horizontal axis accompanied with the connection (2). It should be noted that when the contaminated probe is swept rapidly the shape of the v-i curve coincides with that from the clean probe, but the voltage where the current begins to increase is different. For a further comparison of the real plasma experiment with the above described equivalent circuit model, Fig. 26 (b) is presented, where the left curve is obtained with the

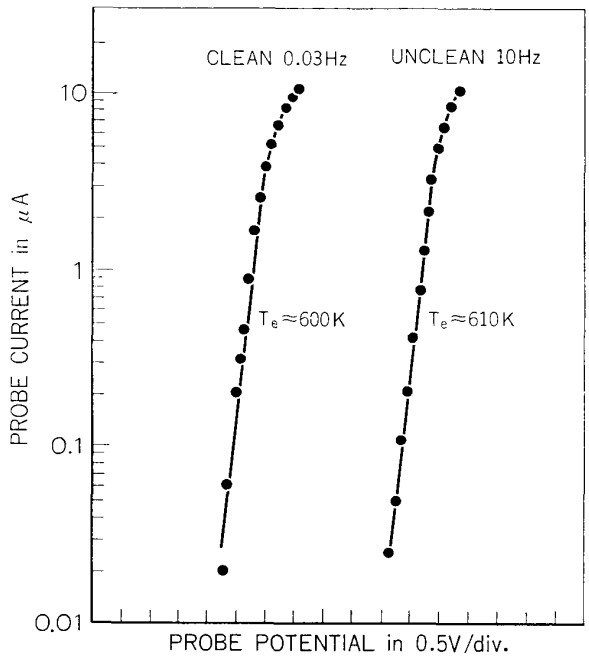

FIG. 25. Electron temperatures evaluated from the contaminated probe and clean probe. The repetition periods of the probe bias are 0.03 Hz and 10 Hz for clean and unclean probes respectively. Coincidence of the electron temperature of the clean probe and that of the contaminated probe is quite good.

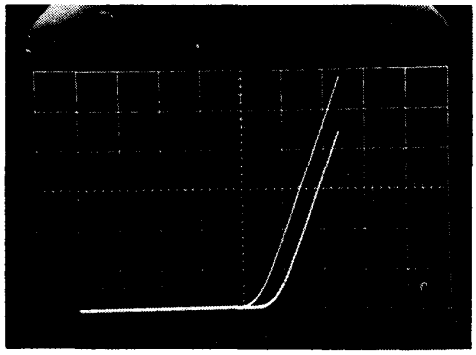

FIG. 26a. Simulation experiments of a quickly-swept bias by the use of equivalent circuit. Right; sweep rate 10 Hz, $Rc = 400\,K\Omega$, $Cc = 1\,\mu F$, Rs=diode (IN34), $Rp = 100\,K\Omega$. Left; sweep rate of 0.1 Hz, Rs=diode (IN34), $Rp = 100\,K\Omega$.

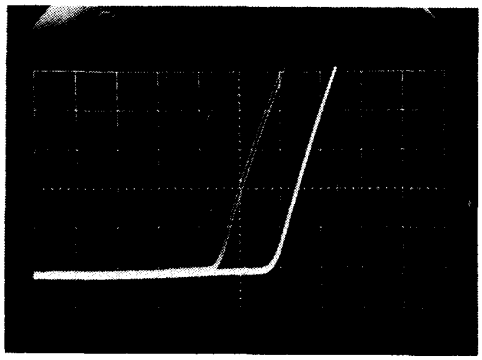

FIG. 26b. Comparison study for a quickly-swept bias.
The probe voltage of a clean probe (left curve) is swept at 0.1 Hz, while that of unclean probe (right curve) has a repetition period of 10 Hz.

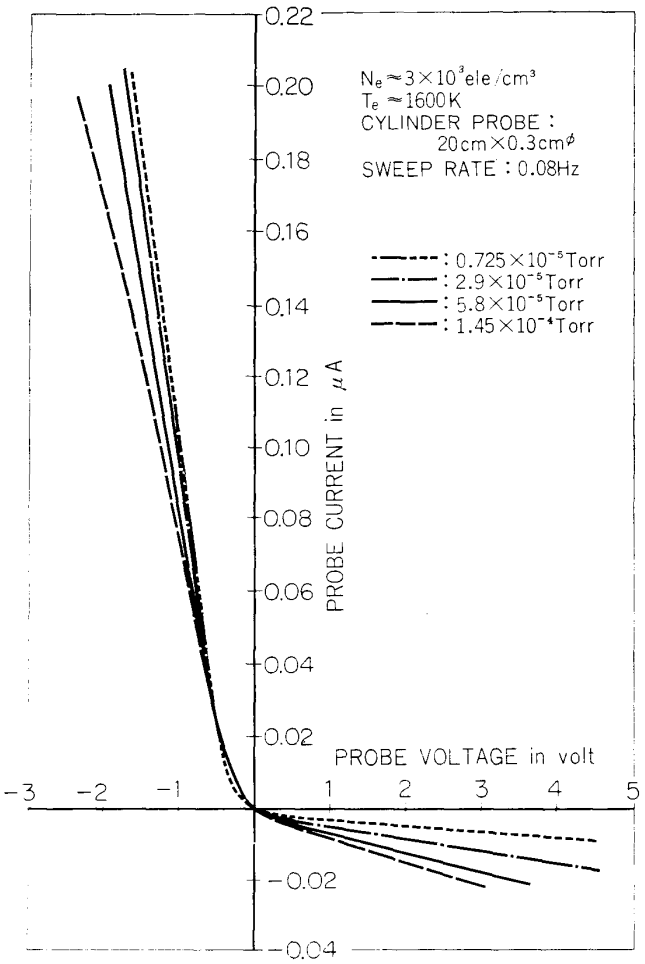

FIG. 27. Apparent enhancement of the ion current in high neutral gas pressure.

use of clean probe which is ion-bombarded and the right curve is obtained with the unclean probe. The sweep rates of the probe voltage are 0.1 Hz for the clean probe and 10 Hz for the unclean probe, respectively. From the results of Figs. 26 (a) and (b), we can conclude that the contamination layer model very well expresses the effect of surface contamination of the actual probe.

As is described above, it is concluded that the high frequency sweep gives nearly the correct temperature. However, strictly speaking, it is found that the slope of the ion saturation current is rather steeper than that of the clean probe. This phenomenon is more enhanced as the increase of the neutral gas pressure as is shown in Fig. 27. Although the ion current enhancement is not completely understood [*57a*, *57b*], it is possible that neutral molecules with metastable state collide to the probe surface and emit the secondary electrons, which consequently increases the apparent ion current. However from the practical point of view, it is found that the apparent enhancement of the ion current scarcely affects the evaluation of electron temperature.

3.4 The effect of contaminated electrode on an electron temperature probe [58]

As in the case of high frequency sweep, the equivalent circuit shows another important and interesting characteristics on the application of small ac signal. As the impedance of contamination layer is reduced for the ac signal, the use of the high frequency can avoid the effect of the contamination capacitance. For example the electron temperature probe of Wrenn et al. may not be influenced by the contamination layer because the high frequency signal is applied at one bias point of exponential region of v-i characteristic curve and electron temperature is calculated from the basic and second harmonic components of probe current. Our electron temperature probe is also classified into the same category which is not influenced by the contamination layer. Besides the advantage that the electron temperature probe uses ac signal which eliminates the contamination effects, the input impedance of electron temperature probe is very high, which will reduce the potential variation of probe surface caused by the flowing cuurrent (see section 4 of chapter 3). The above description concerning the electron temperature probe is easily confirmed by using two cylindrical probes as follows. The two probes are cleaned and uncleaned probes, which give the Langmuir curve as shown in Fig. 28. The Langmuir curve obtained with the ion-bombarded probe has no serious hysteresis and the slopes of the semi-logarithmically plotted Langmuir curve are same for both increasing and decreasing biases, whilst the Langmuir curve from

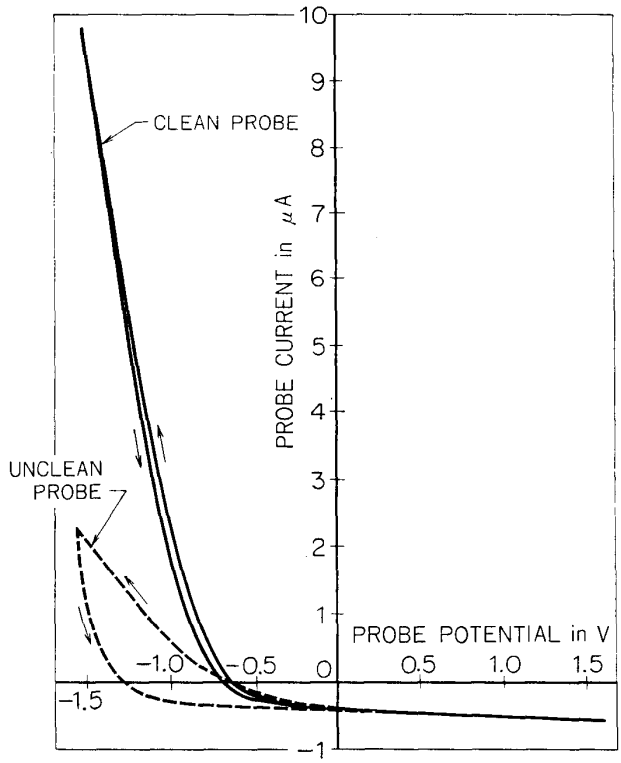

FIG. 28. V-i characteristic curves obtained with contaminated and clean probes for the study of the electron temperature probe. T_e of 950°K is obtained from semilogarithmic plotting of the v-i curve of a clean probe.

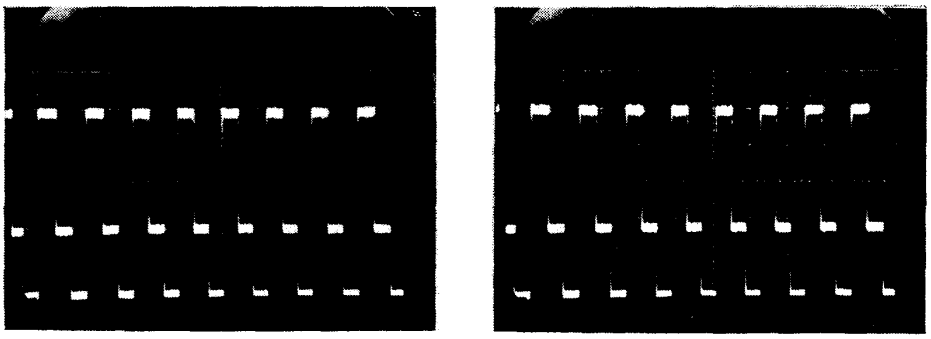

FIG. 29. Output signals obtained from contaminated (left) and clean (right) probes used for electron temperature probe. The evaluated from output signal is 1000°K in both cases, which shows a good agreement with clean dc probe value.

the contaminated probe is quite distorted and has no linear part when it is semi-logarithmically plotted. However if the electronic circuit of the electron temperature probe is connected to the uncleaned probe, the output signal is found to be completely equivalent to that by the clean probe. In Fig. 29 the left output is obtained from the uncleaned probe, whilst right signal is from the cleaned probe. We can find no difference between them and can conclude that even the contaminated probe can give a correct electron temperature when it is used as electron temperature probe. Incidentally the electron temperature obtained with the electron temperature probe with both cleaned and uncleaned electrodes is 950°K, whilst the clean probe gives 1000°K when it is used as a usual dc Langmuir probe.

4. CLEANING OF THE PROBE

In order to get a reliable information with the Langmuir probe, it is strongly required to keep the probe surface as clean as possible. The word "clean" is very ambiguous because molecules of the ambient gas more or less adsorb to the metal surface. The word "to clean the probe" used here is to keep the probe "clean" to the extent that the electron tmperature evaluation becomes reliably available with vanishing hysteresis. A chemical cleaning by the use of Aceton, Alcohol and so on is not effective at all [59]. Long time baking of the probe during the evacuation of the plasma vessel is an effective procedure. One of other cleaning methods is to apply negative or positive voltage to a probe, that is, ion- or electron-bombardment. This section mainly describes the latter method because the first one will be described in detail in chapter III for the discussion of an ionospheric plasma probe.

4.1 Contamination substances

When a probe is biased to a highly negative voltage, ions of the ambient plasma are accelerated into the sheath and impact to the probe. Molecules or atoms adsorbing to the probe surface will gain enough energy from the accelerated ions to depart from the probe surface, consequently the probe surface is cleaned. The

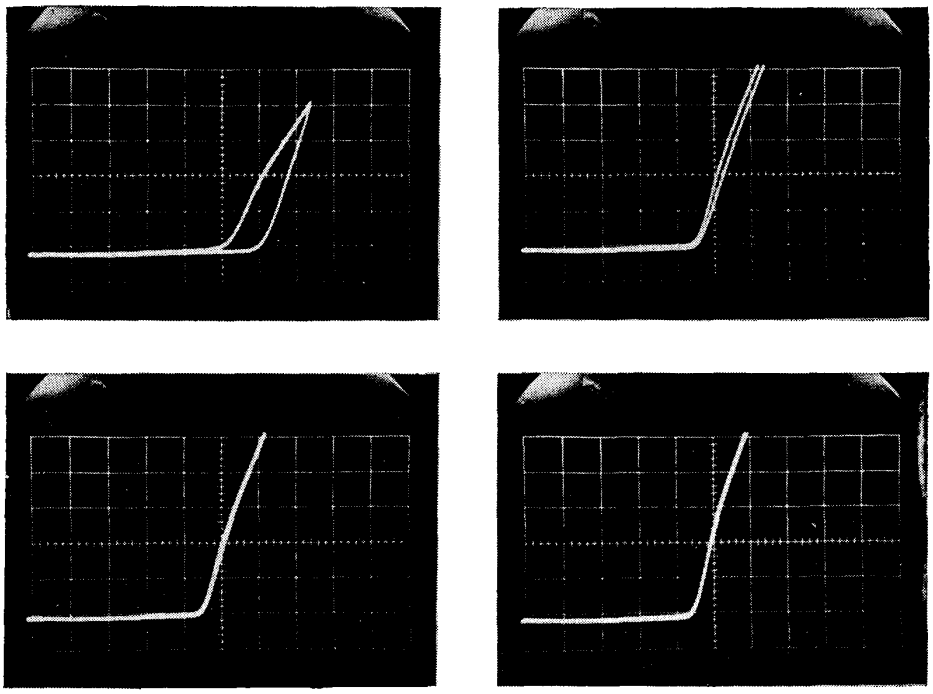

FIG. 30. Variation of the Langmuir curves due to the ion-bombardment of a brass cylinder probe. Bombardment durations are 0 minutes, 3 minutes, 10 minutes and 25 minutes respectively from upper left to lower right.

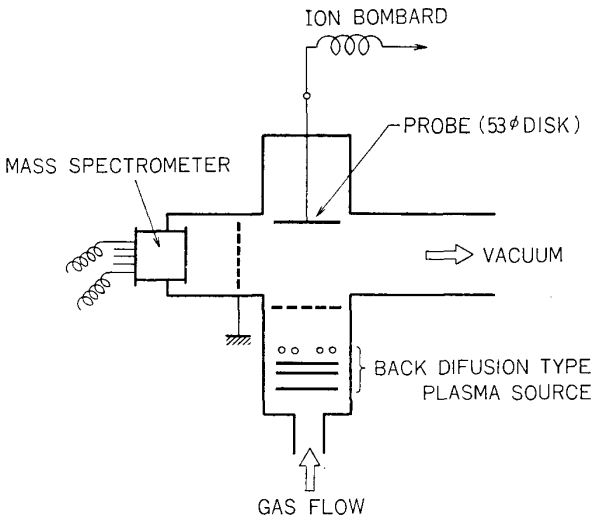

FIG. 31. Configuration for mass analysis of the residual gas in a plasma vessel.

probe surface will be kept more clean if the duration of the bombardment is longer. Fig. 30 shows the cleaning process of the probe surface by the ion-bombardment. As the duration of the ion bombardment becomes longer, the difference between the curves from increasing and decreasing biases decreases and the maximum current at the same probe potential becomes larger. It is also noted that the curve shifts to the left as the increase of ion bombardment duration. This is because that voltage drop induced through the contamination layer by charging capacitance

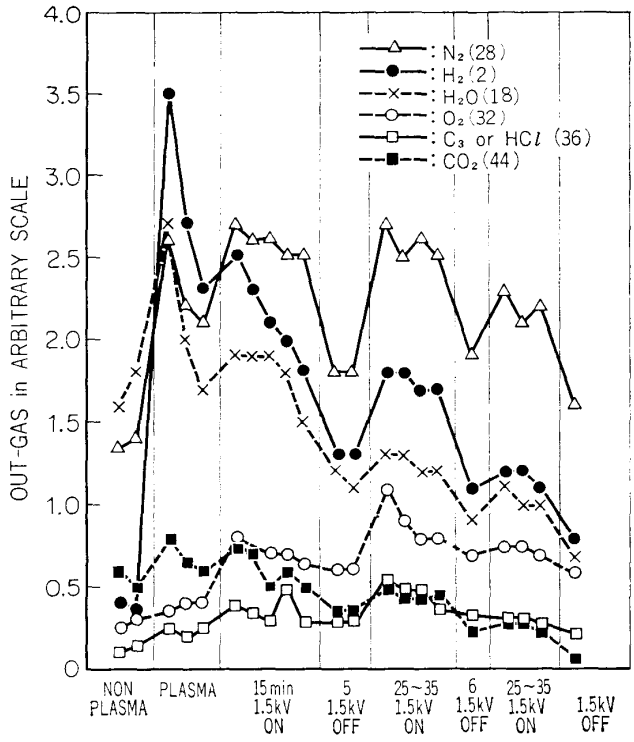

FIG. 32. Contamination substances detected by massspectrometer.

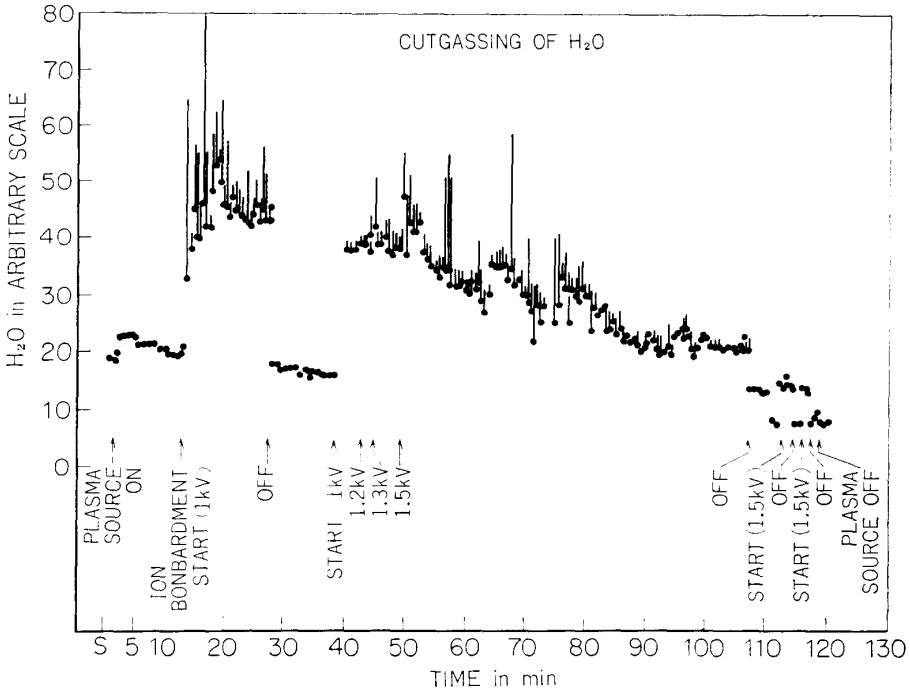

FIG. 33. Behavior of a water vapour from the probe surface during outgassing.

gradually decreases as the capacitance of the insulation layer gradually decreases by the ion-bombardment.

It is also instructive to know what contaminators cover the probe surface and

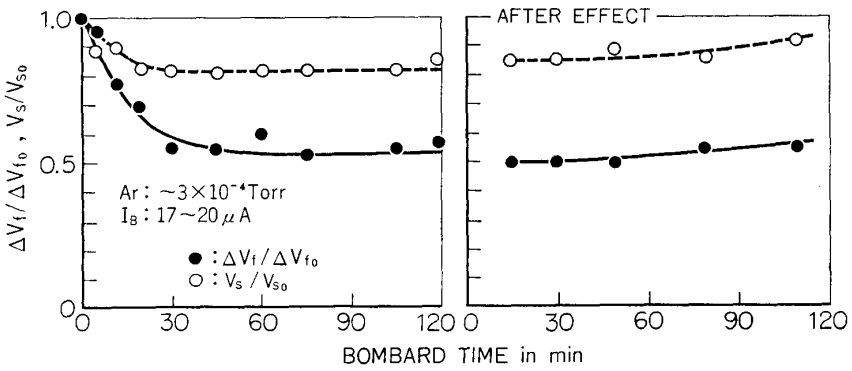

FIG. 34. Recovery of a clean probe to the contaminated probe after ion-bombardment (Dote [60]).

induce the large capacitance described above. In order to detect the contaminators the mass analysis of the outgas during the bombardment is carried out in the configuration of Fig. 31. Massanalyzer continuously detects the residual gases while the probe is ion-bombarded with 1.5 kV negative voltage. Various gases, such as H_2O, N_2, O_2, HCL, and CO_2 are detected as shown in Fig. 32. Among the contaminators detected, H_2O seems the most effective impurity because the contaminator is assumed to have a large capacitance of large dielectric constant, considering that Langmuir curve obtained with the contaminated probe is quite distorted and has different paths according to the direction of the bias sweep. Other traces such as C_3, HCL, and CO_2 are assumed to be derivatives of the diffusion pump oil. Then we fix the analyzer's range on mass-number 18 (H_2O) and watch the behaviour of the water during the experiments.

When the ion bombardment is on, the amount of H_2O gas suddenly increases and at the moment when the ion bombardment is off, it decreases rapidly as shown in Fig. 33. Finally after about 2 hours, a detected amount of H_2O is almost not observable.

4.2 *Recovery of the clean probe to the contaminated probe* [60]

Photograph mentioned in Fig. 31 qualitatively shows that the probe surface is cleaned by the ion-bombardment. However very often, after the cleaning, the cleaned Langmuir probe is found to return to the original state, to the uncleaned probe. Therefore it is quite interesting and instructive to know how long the surface is kept clean after the bombardment. Fig. 34 shows one of the results obtained by Dote. As the bombardment starts, normalized floating potential difference gradually decreases, which means "hysteresis becomes smaller" and when the bombardment finishes, the floating potential difference slowly begins turning to the original point almost within 120 minutes. In the figure, floating potential difference V_f is normalized by the original floating potential V_{fo} before the ion-bombardment. The figure also shows that the space potential in the contaminated condition of the probe is observed higher than the true value. It is noted that the recovery time to the original point is not short, namely not within a minute or

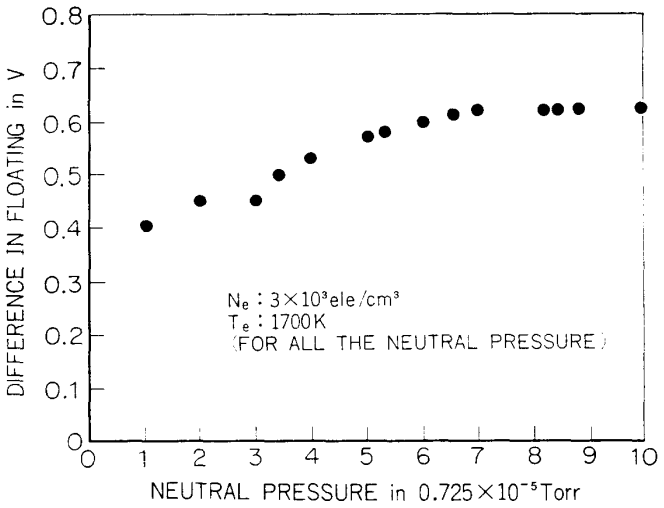

FIG. 35. Neutral gas density dependence of the hysteresis curve. Hysteresis becomes higher as the increase of the neutral pressure.

so. This slow recovery time is also found in an atmosphere of 760 Torr; when after the satisfactorily cleaned probe is exposured in the atmosphere of 760 Torr for 10–20 minutes it is dipped into the plasma in the evacuated chamber, it will not show so serious hysteresis phenomenon. The above results give a quite useful information for an application of a glass sealed Langmuir probe, because even if the glass which seals a probe is broken by the shock of rocket launching, the probe surface will not be seriously contaminated in the atmosphere during a short time such as the rocket flight duration.

4.3 Neutral density dependence of the hysteresis curve

The contamination layer model is explicitly independent of the effects of the ambient neutral particles upon the probe curve. Nevertheless, in the commercially available gas which is used for a plasma production, we can find the effect of the neutral gas pressure upon the v-i characteristic curve; the decrease of the neutral pressure gives a decrease of the hysteresis as is shown in Fig. 35. In the figure the pressure of Ar gas inside the chamber is changed from 1×10^{-5} to 1×10^{-4} Torr. Over all pressure range the electron density of the ambient plasma is kept almost constant in order to avoid the confusion from the electron density dependence. The amount of the hysteresis is measured as the difference in floating potentials of the Langmuir curves which are selectively obtained by changing the direction of the bias sweep.

The above phenomenon which is not predicted by the contamination layer model may be due to the impurity gases such as H_2O included in commercially available Ar gas as a minor constituent (the purity of the gas used is 99.99%). An impurity gas which may exist in proportion to the main neutral gas density is adsorbed to the probe surface and forms an insulation layer. The thickness of an insulation layer may be proportional to the impurity gas included. Consequently the increase of neutral gas density will increase the hysteresis.

5. Contaminated elelctrodes of a retarding potential trap analyzer [61]

It is easily considered from the Langmuir probe experiments that electrodes of a retarding potential trap are also contaminated and may give erroneous results. The present section is devoted to the discussion of the contamination effects upon

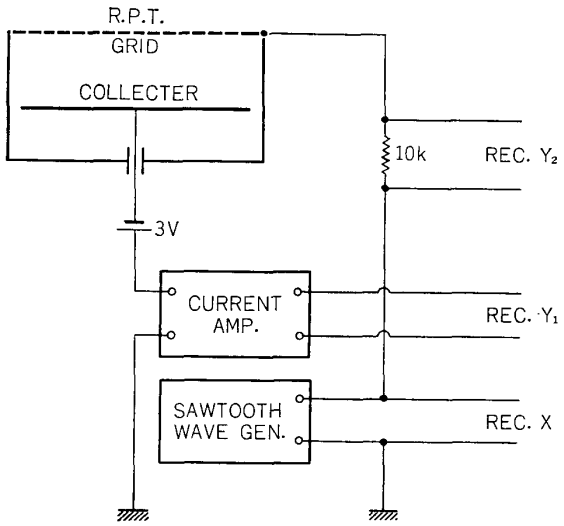

Fig. 36. Configuration for a retarding potential trap experiment. In this experiment, two-electrodes analyzer is used.

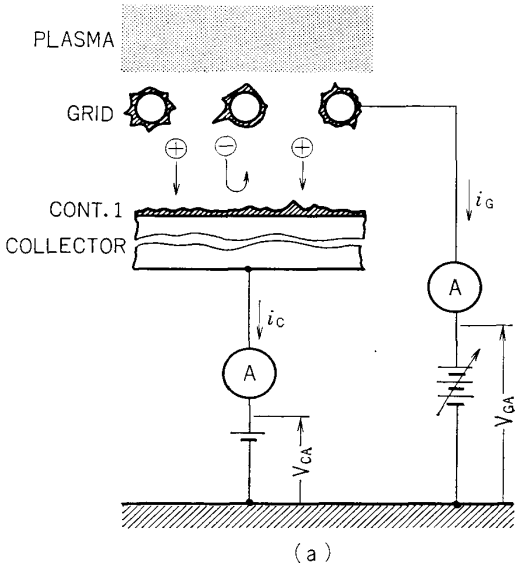

(a)

Fig. 37a. Situation of the contaminated electrodes in R.P.T.

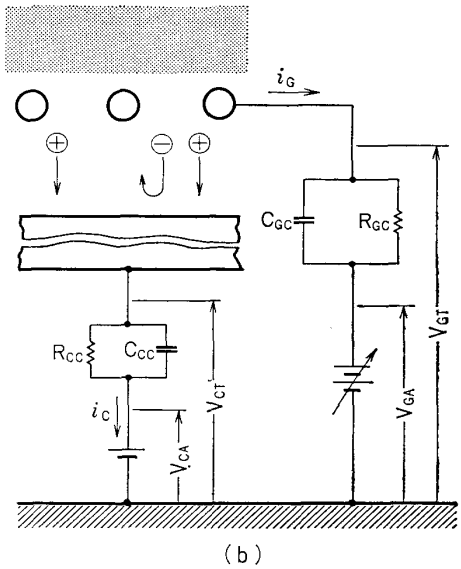

(b)

Fig. 37b. Contamination layer of the electrode is expressed as the parallel combination of resistor R_c and capacitor C_c. V_{CT} and V_{GT} are the voltages of contaminated electrode surfaces. V_{CA} and V_{GA} are actually-applied voltages from out side.

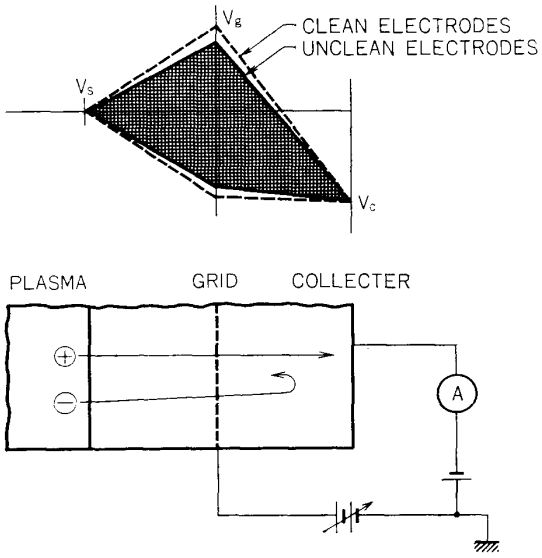

FIG. 38. Potential distribution of the R.P.T. analyzer with clean and unclean electrodes (hatched part).

the two-electrodes analyzer measurement. The use of the two-electrodes analyzer is sufficient for our essential discussion and the discussion will not lose the generality by using such simple analyzer. In such analyzers swept voltage is generally applied to the grid and the collector potential is negatively fixed for the ion collection. V-i characteristic curves obtained from the first grid potential versus the grid current and from the collector current versus the grid potential give electron and ion temperatures in the configuration of Fig. 36. In analogy to the Langmuir probe, the electrodes of the analyzer are seriously contaminated if they are not baked in vacuum. Contamination layer of the electrodes is found to have a large capacitance and resistance. Therefore the measurement system including contaminated electrodes is quite schematically expressed by the equivalent circuit as is shown in Fig. 37. Although the circuit is superficially complicated, the most essential part is the capacitance and resistance due to the contamination layers. The model predicts the followings, the same as in the case of Langmuir probe.

In the low frequency range of the sweep of voltage, where the capacitance effect is negligible, the voltage applied to the electrode is divided by the contamination and sheath resistances. Therefore the voltage applied to the grid is much more influenced by the contamination resistance than that applied to the collector, because the resistance determined by grid current and voltage is much lower than that determined from collector current and grid voltage due to the small ion current.

Especially, the contamination of the grid is much serious because grid potential has direct relation with the evaluation of electron and ion temperatures. Consequently the decrease of the grid voltage caused by the voltage-dividing effect of the contamination layer leads to the overestimation of the ion and electron temperatures. The potential distribution discussed above is illustrated in Fig. 38.

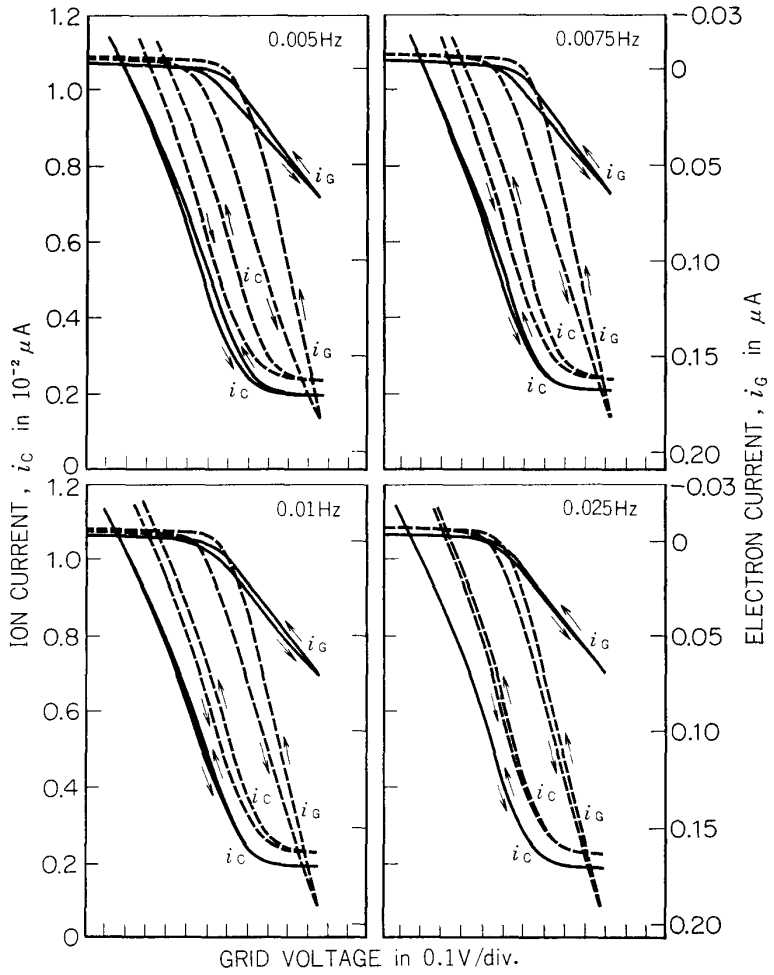

FIG. 39. Effect of the contamination layers of the electrodes on the v-i characteristic curves obtained with two electrodes analyzer.

As the frequency of the voltage sweep becomes higher, the contamination resistance parallel to the capacitor is shortened by the low impedance due to the contamination capacitance. In the similar way of discussion for Langmuir probe, the high sweep rate of the grid bias gives the same v-i characteristic curve as is given by a clean electrode. The above idea is easily confirmed by the simple retarding potential trap experiment. As is clearly shown in Fig. 39, Langmuir curve obtained from the relation of first grid voltage and grid current has a serious hysteresis like the ion current characteristic curve obtained from the relation of grid voltage and collector current. The degree of the hysteresis gradually decreases as the sweep rate of bias, which is applied to the grid, decreases. The experiment carried out in the plasma density of 1×10^3 el/cc and of 2.5×10^3 el/cc shows that the hysteresis is smaller in lower plasma density.

The above two characteristics accompanied with contaminated electrodes may be called "Frequency dependence" and "Density dependence" by analogy with the Langmuir probe.

6. Discussion

We discussed about the effect of contamination layer of a Langmuir probe and retarding potential trap on the evaluation of electron and ion temperatures. The contamination layer was systematically studied by a use of equivalent circuit which was newly proposed in the present paper. The distortion obtained by a contaminated Langmuir probe is now attributed to the effect of capacitance and resistance of insulation layer not to the work function variation of the probe surface which has long been considered. Here we will briefly touch the unvalidity of the work function model by considering some experimental evidences.

It has long been said that the v-i curve must be taken in a short time interval during which the work function does not change. This fact does not conflict our conclusion that the sweep frequency of probe voltage must be high enough to diminish the capacitance effect. The pulse technique used by Waymouth [*62*] is therefore considered as the visualization of the above idea. The work function model loses its validity in explaining the density dependence of the hysteresis curve. It seems reasonable that the work function will not be changed by the electron density of the ambient plasma, though Wehner et al. [*55*] thought that the work function will be lower at smaller collected electron currents. Therefore we can conclude that the contamination layer model is basically correct and can explain the effects of a contaminated probe, though in detail we must have some points to be refined in the future.

The presented model shown in Fig. 17 is based on the assumption that all the probe surface is covered with the contamination. In fact, taking some Langmuir probe results which have been reported by many authors (chapter V) into consideration, we can conclude that the probe surface is almost covered with the contamination layer. However we might have another situation, that is, the probe surface is partly contaminated and partly clean, which is schematically illustrated in Fig. 40a. Similarly to the previous model, we can briefly study the behavior of the partly contaminated probe by using the equivalent circuit which is shown in Fig. 40b. In the figure C_{ci} and R_{ci} are capacitance and resistance of the contamination and R_{ssi}, resistance of sheath contacting to its contamination layer and R_{spi}, resistance of sheath contacting to the clean probe surface. In this case, response of the hysteresis curve to the electron density of ambient plasma is slightly modified; the phase difference between the current and the voltage applied to the probe gradually increases, takes the maximum value and decreases as the density of the ambient plasma decreases. One of the evaluation of the above behavior is shown in Fig. 41 with quite a simple calculation. In that figure $\Sigma R_{ssi}=\Sigma R_{spi}$ is assumed for a simple calculation which means the contaminated surface area to be approximately equal to a clean surface area. In the model shown in Fig. 40 if $R_{spi}=0$, the circuit reasonably approaches to the model which was shown in Fig. 17.

As described in the first part of this section, these patchy structures of the contamination layer don't appear so often. Patchy structure will be formed when the surface of contaminated probe is partly ion-bombarded, or when the cylindrical

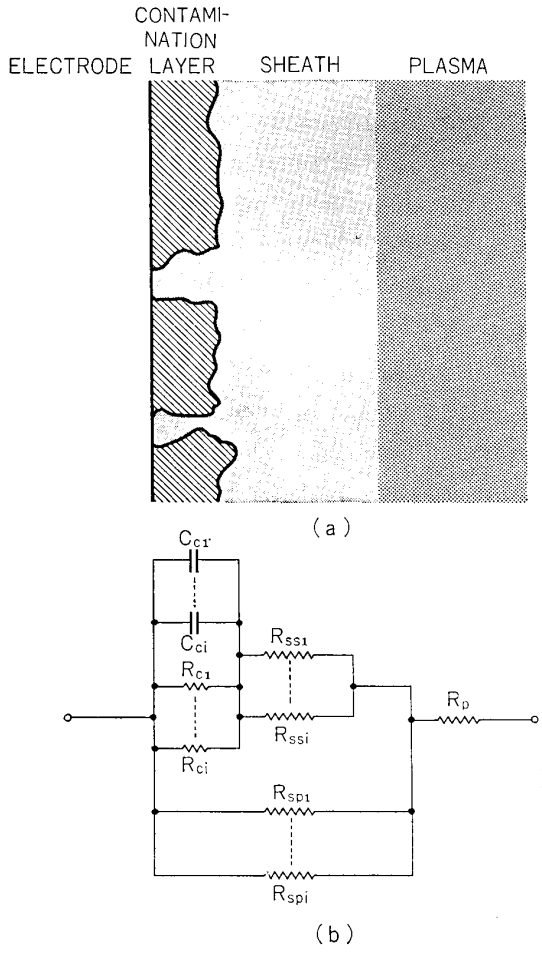

FIG. 40a. Situation of a partially contaminated probe.

FIG. 40b. Equivalent circuit corresponding to the above.

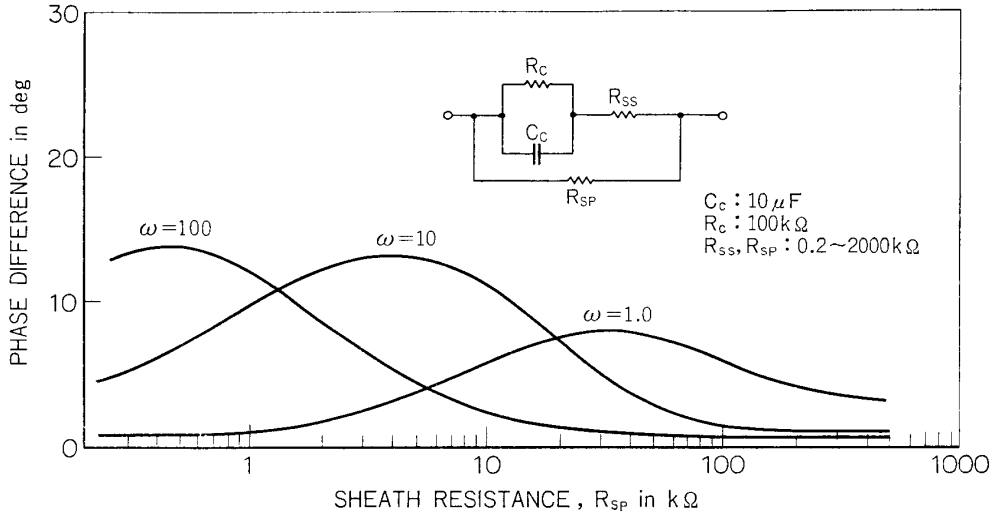

FIG. 41. Density dependence of partially contaminated probe.

or spherical probe is exposured in the circumstances where E.U.V. radiation and anisotropic energetic particle flux are extremely strong. Therefore in the 5th chapter we will proceed our discussion under the assumption that probe surface

is completely covered with contaminators, though the thickness of the insulation layer may not be uniform on the whole probe surface.

7. Concluding remarks

Langmuir probe gives an erroneous effect on the evaluation of charged particle temperature when it is used without cleaning. Generally speaking, the temperature is estimated higher than the true value with such contaminated probe.

In laboratory plasmas, contamination substances can be easily removed away by the ion bombardment or baking in the vacuum. Whilst, situation becomes much serious in space plasma especially in rocket experiments which have insufficiently short duration for baking or ion bombardment of a probe.

In order to get reliable electron temperature by using a contaminated probe, two solutions may be considered.

Firstly we can get almost reliable electron temperature by means of a rapid sweep Langmuir probe. However this method is applicable only when a telemeter channel has a frequency response high enough to follow the rapid change of the v-i curve obtained.

Secondly, a satisfactory information can be obtained by applying the resonance probe theory to the ionospheric plasma. The contamination effect upon the electron temperature evaluation can be conclusively vanished by applying small ac signal to the probe at one bias point of the exponential region of Langmuir curve and detecting the DC voltage variation of the probe. In space plasmas we strongly recommend the second method because it has not strict limitation of the telemeter response as experienced by the rapid sweep Langmuir probe. The results obtained by the second method will be given in the next chapter.

Chapter III. Langmuir Probe in Ionosphere Plasma

1. Introduction

In chapter II, we showed that the contamination effect is quite serious in the diagnostics of a laboratory plasma. In fact, some papers include implicitly the contamination effects in their Langmuir probe measurements. Nevertheless, few one has paid attention to this problem in the space plasma measurement. Recently, Carlson and Sayers [*63*] (1970) insisted that discrepancy of the charged particle temperature should be studied from an aspect of the probe surface. Furthermore, D. Smith [*64*] has just concluded from his afterglow plasma studies that Langmuir probe gave quite erroneous results, especially for the measurement of a low electron temperature ranging from several hundreds degrees to several thousands degrees and that accurate measurements of a low temperature were obtained only after cleaning of the probe and the reference electrode. He suggested also that the laboratory results are such as to place considerable doubt on the accuracy of ionospheric in-situ

measurements of electron temperature, particularly low electron temperatures occuring in the lower ionosphere. We have the same opinion as him and presented some serious problems in the previous chapter which were found in the laboratory plasma. In this chapter are given some evidences that the contamination effect of Langmuir probe is one of the main causes of the erroneous evaluation of electron temperature in the ionospheric plasma.

2. Langmuir probe measurement in space plasma

The electron temperature measurement in the space plasma has a serious problem especially in the ionospheric E region. Although many temperature profiles have been reported up to now, there are many debatable points. For example, Smith's [*65*] data give different electron temperature profiles in both upleg and downleg. The electron temperature profile obtained by Brace et al. [*66*] shows unexpectedly high value around 150 km, which suggests a non-equilibrium situation of the electrons. If this is true, we must consider another kind of heat sources for the electron heating except the solar E.U.V. Therefore, first of all, the subject of the measurement reliability is the most essential problem to supply the reliable data on the discussion of energetics of the ionosphere. Considering that such high temperature does not actually exist but will be observed by the use of the contaminated Langmuir probe, we have continued the study of probe reliability using several sounding rockets. One of such studies [*67*] is to see the effect of the contaminated probe upon the evaluation of electron temperature by comparing the values obtained from the different methods. Electron temperature observed with the contaminated probe and that with the electron temperature probe will give some useful clues for the discrepancy in the results of in-situ measurement in the ionosphere. From the standpoint described above, experiments were carried out with two rockets, K-9M-28 and -29 with almost the same instrumentation. The block diagram and the photograph of the instrument are shown in Figs. 42 and 43. One of the electron temperature profiles was evaluated from the v-i characteristic curves obtained with a disk planar probe of 100 mm diameter. The probe voltage was changed from -3V to $+3$V with the sweep rate of 3 Hz for K-9M-28 and 5 Hz for K-9M-29. If the difference exists between v-i curves obtained from increasing and decreasing biases, we can conclude that the same phenomenon which is found in laboratory plasma also occurs in the ionospheric plasma. The other value of the electron temperature was derived from the electron temperature probe which determined the ratio of two successive floating potential deviations caused by the application of the two levels of high frequency signals. As was described in the previous chapter, the electron temperature probe which uses high frequency signals can give correct electron temperature even if the probe surface is contaminated. Electron temperatures thus obtained from the two instruments are shown in Figs. 44 and 45.

The electron temperature obtained with the electron temperature probe shows 1550°K with a standard deviation of 70°K at around 300 Km (K-9M-28) and is

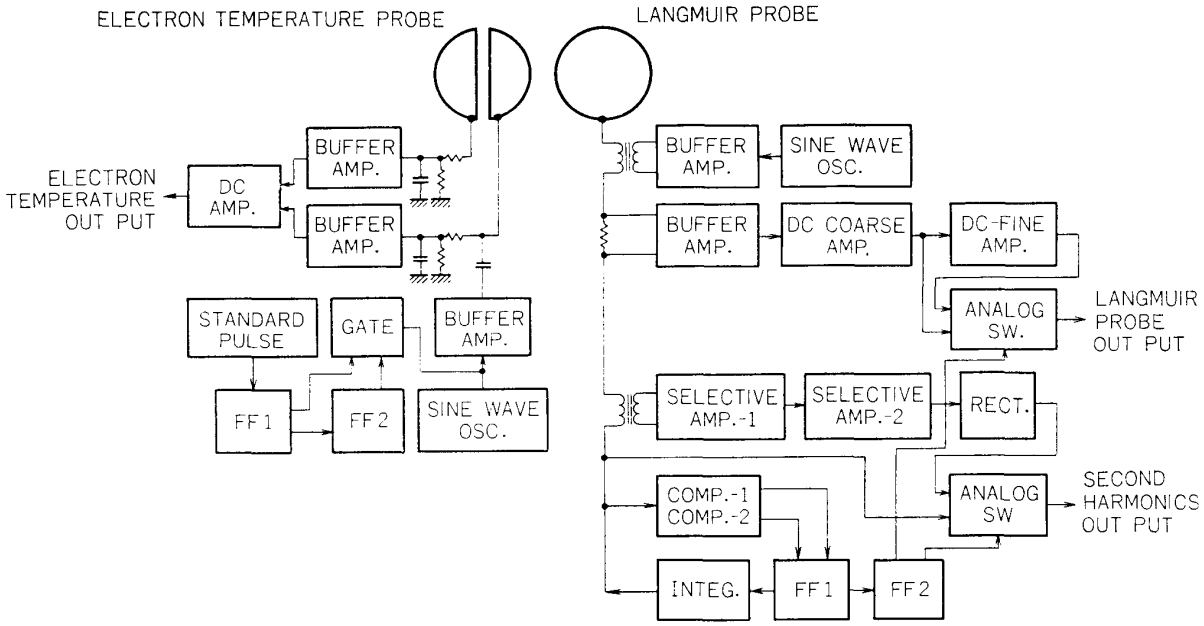

FIG. 42. Block diagram of an electron temperature probe and of a Langmuir probe instrument carried on K-9M-28 and -29.

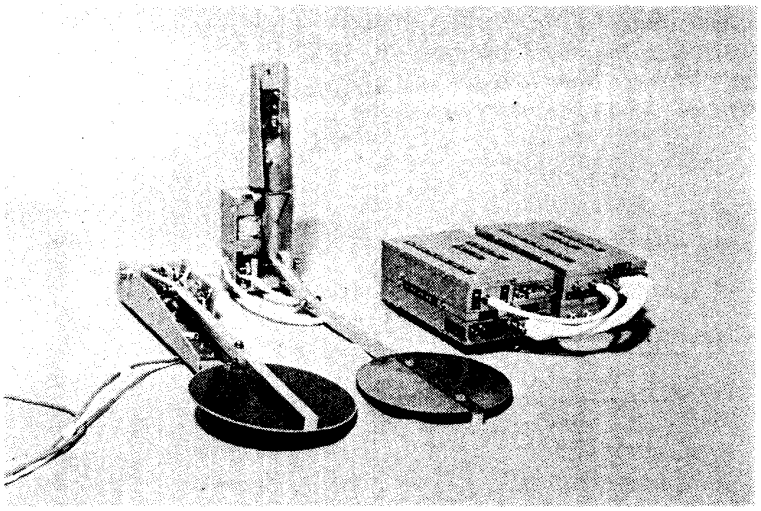

FIG. 43. Photograph of the Langmuir probe instrument carried on K-9M-29.

quite reasonable considering the neutral temperature evaluated from Jacchia 1971 model. [68] Whilst the electron temperature obtained from the semi-logarithmically plotted Langmuir curves is fairly higher with large uncertainty than the value by the electron temperature probe. Such large uncertainty of the electron temperature comes from the uncertainty of the linear-fitting of the semi-logarithmically plotted Langmuir curve. Although the non-linearity of the v-i curve may be attributed to the non-maxwellian energy distribution of electrons, the fact that two probe curves of both increasing and decreasing biases are different states that the non-linearity is caused by the contaminated Langmuir probe.

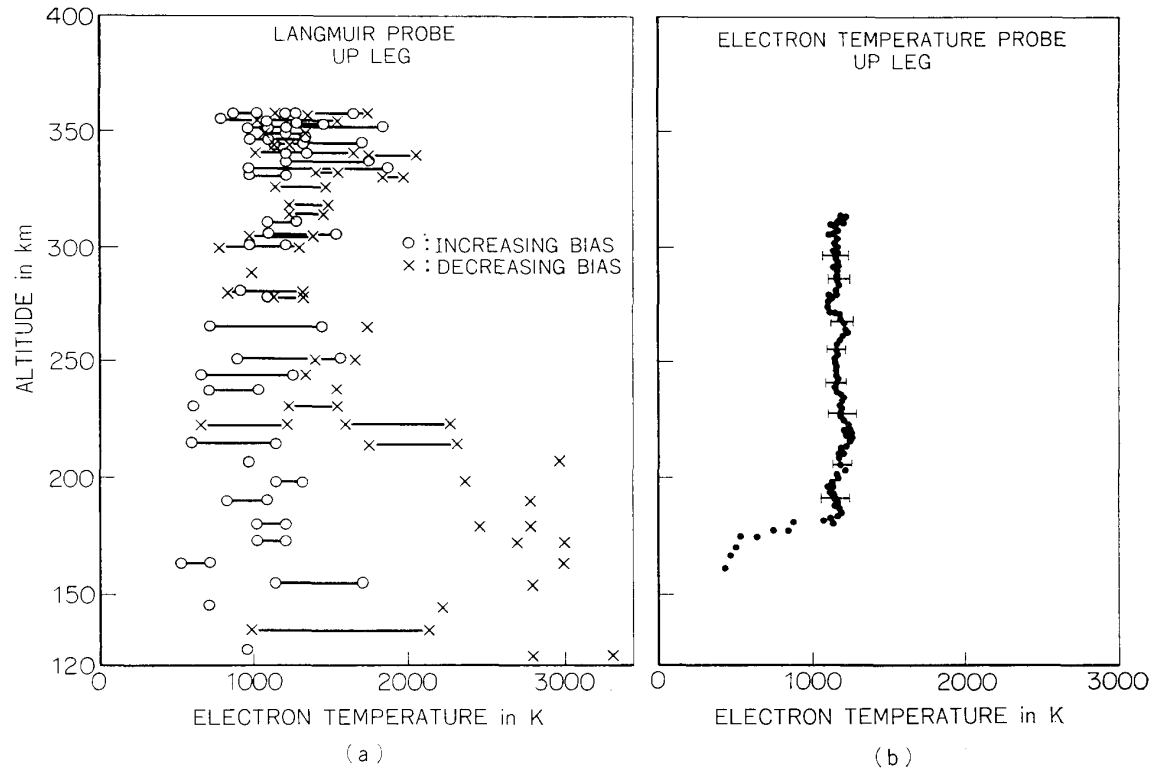

FIG. 44. Electron temperature profiles obtained with E.T. probe and Langmuir probe on K-9M-28 launched on Jan. 25, 1970.

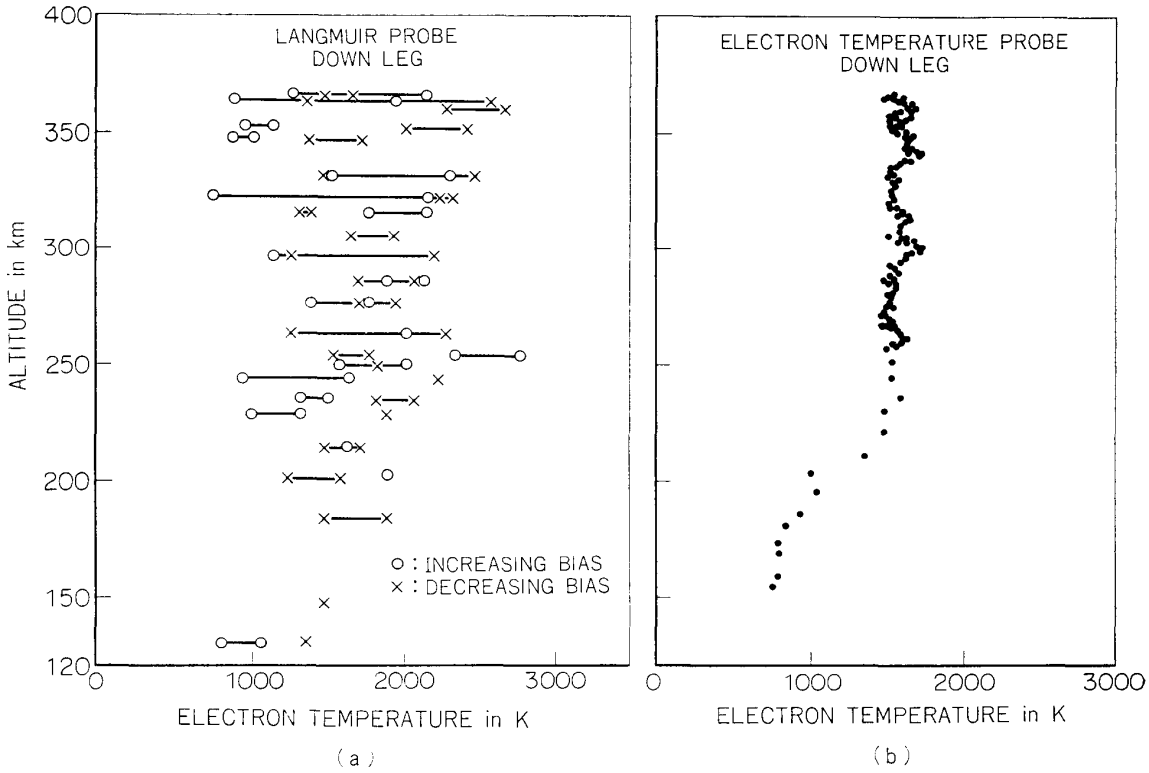

FIG. 45. Electron temperature profiles obtained with E.T. probe and Langmuir probe on K-9M-29 launched on Jan. 27, 1970.

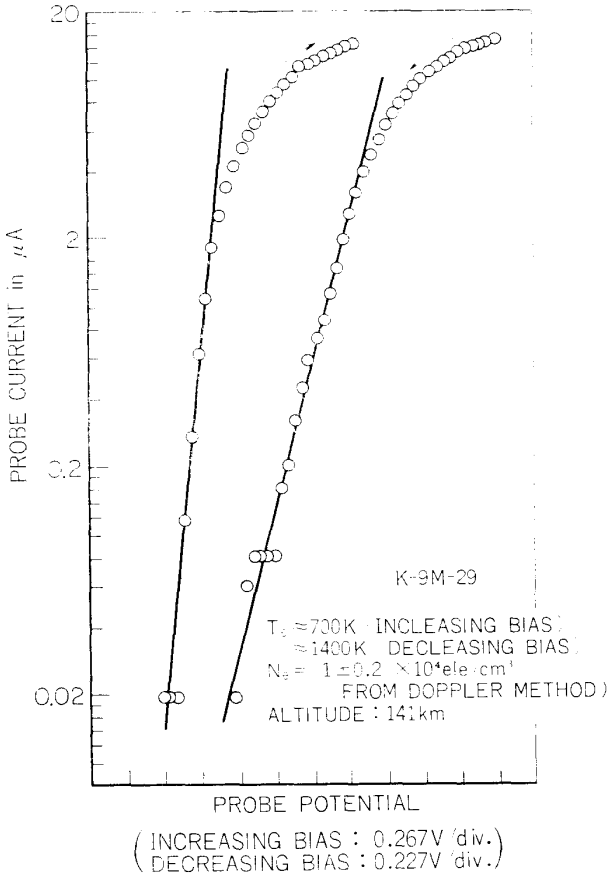

FIG. 46. Semi-logarithmically plotted Langmuir curve obtained at the height of 141 Km by K-9M-29. Note that the semi-logarithmically plotted Langmuir curves obtained with contaminated probe are still linear.

Below the height of 250 Km, the electron temperature by Langmuir probe shows much higher values and sometimes it reaches up to 3000°K degrees, which is not observed in the electron temperature probe data. Although it seems quite bold to attribute the large difference of the electron temperatures obtained from the two probes only to the resultant of the use of contaminated Langmuir probe, this fact seems to be an useful clue to solve the discrepancy of the electron temperature in the E-region which has long been discussed. For the energy distribution of electrons mentioned above, one more interesting and quite suggestive fact is recognized from the following results of experiments. In the evaluation of "electron temperature", it is necessary condition that the semi-logarithmically plotted v-i curve must be linear. By this time we have considered that the linearity of the semi-logarithmically plotted v-i curve appears only when the energy distribution of electrons is maxwellian. However it is found that even when the probe surface is covered with contamination substances, the probe will give a good linearity for the semi-logarithmically plotted curve, although the slopes of the semi-logarithmically plotted curves are different for both increasing and decreasing biases as is shown in

Fig. 46. These curves are the example which were obtained semi-logarithmically from the Langmuir probe characteristic at the height of 141 Km with K-9M-29. The electron temperatures obtained from the increasing and decreasing biases are 700°K and 1400°K respectively, whilst the value obtained with electron temperature probe shows 400°K at the height of 160 Km. Though the electron temperature probe could not be used below this altitude, lower value is reasonably expected, say 350°K or so, at the height of 141 Km, where the above Langmuir curves were obtained. Therefore it is quite evident that Langmuir probe values are about 300°K higher than the E. T. probe value, which is considered correct because the electron temperature probe is not influenced by the contamination of probe surface. Therefore in order to get a reliable electron temperature, it is necessary to assure the coincidence of the slopes of the semi-logarithmically plotted Langmuir curve deduced from both increasing and decreasing biases.

3. Cleaning of a probe in space [69]

3.1 Glass sealed Langmuir probe

As was described in chapter II on laboratory experiments and also mentioned here for ionospheric plasma, cleaning of a probe surface is considered to be essential problem to get reliable results from Langmuir probe experiment. In laboratory plasmas we can clean the probe surface by means of the ion bombardment in the plasma or baking of the probe in a good vacuum. However in space experiment, one can not accept the above procedures because the flight duration of a sounding rocket is not enough for bombardment or baking. Therefore, the probe is baked in the high vacuum like 10^{-8} Torr during 10–20 hours in high temperature of 500–600°K and sealed in a glass tube before the payload integration. When the probe comes into the ionospheric plasma, the glass tube is destroyed

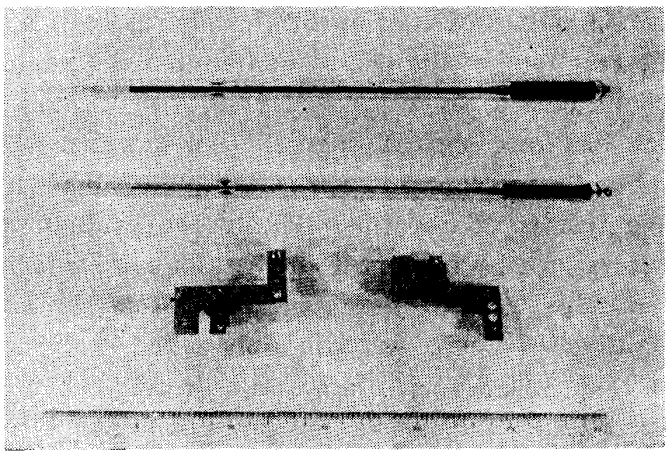

Fig. 47. Glass sealed Langmuir probes and cutters for the destruction of the glass tube.

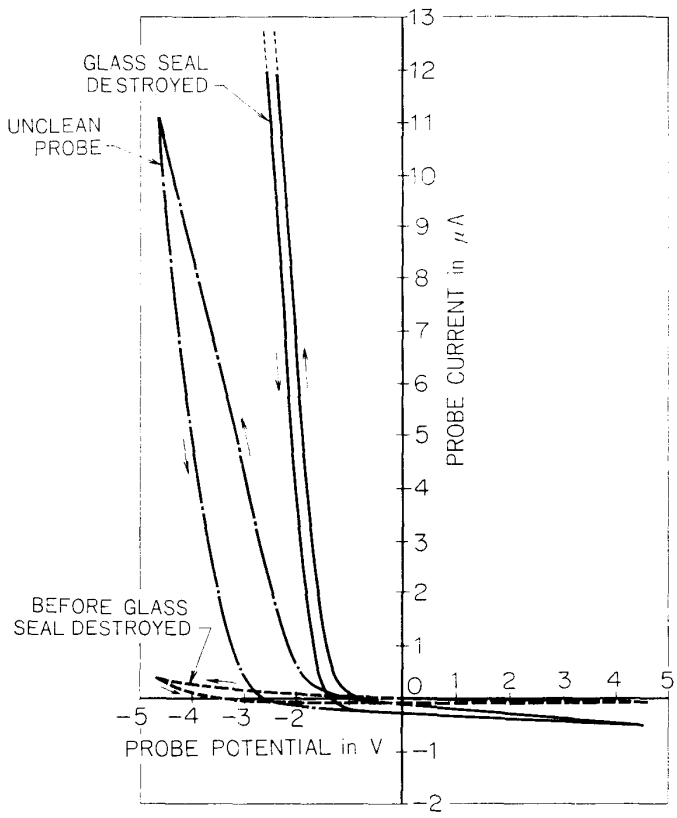

FIG. 48. Langmuir curves obtained with unclean and glass sealed Langmuir probes.

and the probe is exposured into plasma. Fig. 47 shows a glass sealed Langmuir probe which is developed from the above ideas. The glass tube which seals cylindrical Langmuir probe of which diameter and length are 3 mm and 200 mm, respectively, is destroyed by hitting the root of the supporting rod with spling-actuated edge which is also shown in Fig. 47. The glass sealed Langmuir probe was first tested in the space simulation chamber of our institute. The same instrumentation described in 3.1 of the 2nd chapter is used for the testing. The pressure inside the simulation chamber is first evacuated down to 1×10^{-7} Torr. After Ar gas is introduced into the chamber up to 1×10^{-4} Torr, plasmas are produced by back diffusion type plasma sources. Langmuir probe sealed into a glass tube with cutter and the naked probe are set 10 cm apart from each other inside the chamber. The behaviour of the two probes are studied by taking the v-i characteristic curves alternately and comparing them after sealing glass is removed by the strong shock given by the metal hammer. The result is illustrated in Fig. 48. Langmuir curve obtained from the unclean probe has much bigger hysteresis than that from the clean probe. Although the v-i characteristic curve obtained with the clean probe is recognized to include a slight hysteresis, serious effect is not found in the evaluation of electron temperature. This experiment shows that the glass sealed Langmuir probe is useful for the measurement of electron temperature

if the probe is sufficiently baked and cleaned in vacuum before the launching.

3.2 *Application of a glass sealed Langmuir probe* [70]

As we described in the previous sections, Langmuir probe in the space plasma is found to have a difficulty in the reliable observation of electron temperature because of the contamination effect of the probe surface. As we mentioned in chapter II, rapid sweep Langmuir probe is evidently one of the solutions to get a reliable electron temperature. However this method has some difficulties when we apply it to the observation of lower ionosphere where the electron temperature is 300–600°K. In order to get a reliable electron temperature from a rapid sweep Langmuir probe by the use of contaminated electrode, a sweep rate of the probe bias must be at least 10 Hz (period; 0.1 sec) or more for the voltage sweep of from 0 to 2 V. Whilst for the evaluation of electron temperature of 300°K from Langmuir probe method, the voltage resolution of at least 0.03 V is required. In order to get such voltage resolution for the voltage sweep of 0–2 V/0.1 sec., the time resolution of 0.0015 sec is needed. This value corresponds to a frequency response of 600 Hz, which needs so high response for the telemetry channel.

Taking the above fact into consideration, we hope that the glass sealed clean Langmuir probe can be used instead of the rapid sweep Langmuir probe method. In order to test the performance of this glass sealed probe, an experiment was carried out with the rocket S-210-7. The rocket S-210-7 carried the electron temperature probe, the glass sealed Langmuir probe and the non-cleaned Langmuir probe of the same dimensions as glass sealed Langmuir probe whose diameter and length were 3 mm and 200 mm, respectively. The probe voltage was applied to both two probes from −3 V to +3 V and from +3 V to −3 V within one second. The current flowing through the probes were picked up as a voltage drop through 10 KΩ resister and amplified by the three amplifiers with different gain. The payload which included these instruments is shown in Fig. 49. The glass sealed Langmuir probe began operating after the rocket went into ionospheric plasma. At the same time the contaminated Langmuir probe also gave a v-i characteristic curve. Fig. 50 shows a set of v-i curves obtained during increasing and decreasing biases. In the clean probe, the same slopes, that is, the same electron temperatures were obtained, whilst the slopes of the semi-logarithmically plotted curves from the contaminated probe were different between increasing and decreasing biases. The different slope of the Langmuir curve means that the contaminated Langmuir probe gave the hysteresis.

Although the rocket S-210-7 behaved quite so abnormally in its attitude that we were impossible to get the data over all the altitude range, the results obtained at around apogee are summarized in Fig. 51. The figure shows that the electron temperature obtained with the glass sealed Langmuir probe agrees with the neutral temperature from Jacchia's static model, whilst the contaminated Langmuir probe presents the scattered electron temperatures depending on the direction of the probe voltage sweep. In the figure the value from the electron temperature probe is also plotted to compare with Langmuir probe data. The value coincides with the clean

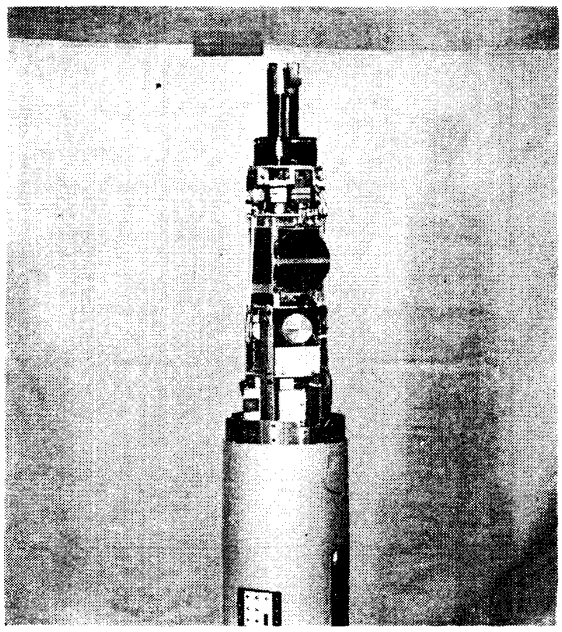

FIG. 49. Payload of S-210-7 rocket for comparison study of unclean and glass sealed Langmuir probes.

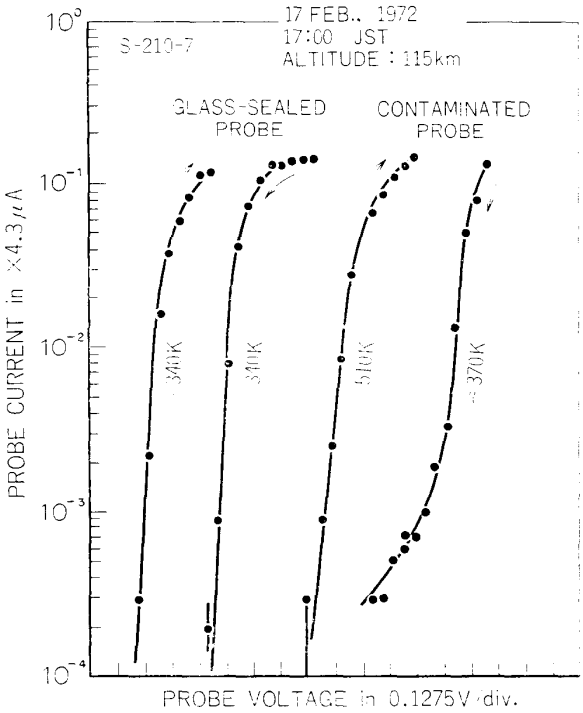

FIG. 50. An example of the Langmuir curves obtained with contaminated and clean probes on S-210-7.

Langmuir probe data. From the above fact, the glass sealed Langmuir probe is considered to be fully available to the ionospheric plasma with good accuracy.

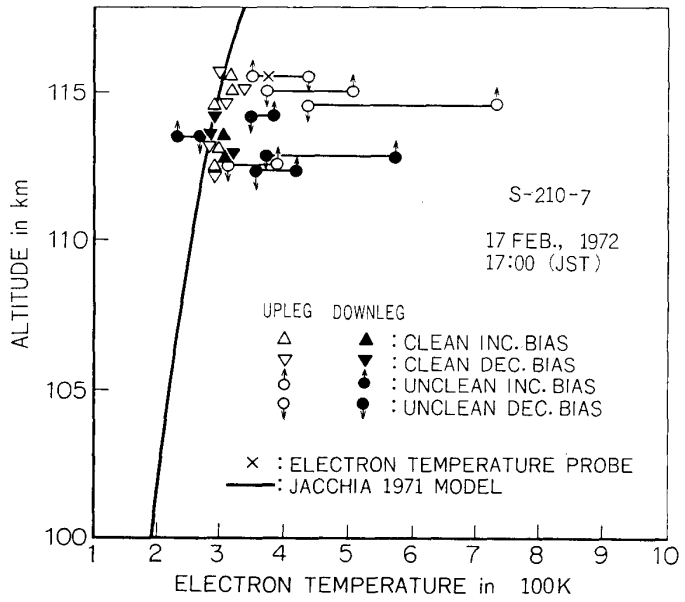

FIG. 51. Electron temperature profile obtained with contaminated and glass sealed Langmuir probes.

4. EFFECT OF A ROCKET BODY (contaminated counter electrode)

In the previous section we showed that the glass sealed Langmuir probe and sometimes the rapid sweep Langmuir probe are quite useful for laboratory and space plasmas. However we did not mention the contamination effect of the counter electrode which is necessary for the validity of a single Langmuir probe theory (including the retarding potential trap). Langmuir probe theory requires a counter electrode which should be much larger than the probe surface area. Consequently, we come to a question "Does the contamination layer of a counter electrode influence the evaluation of electron and ion temperatures?" The result obtained with the rocket S-210-7 appears to show that no consideration is necessary for this problem. However it is quite worthwhile to check the problem for the future application of the glass sealed and the rapid sweep Langmuir probes.

In laboratory experiments, counter electrode of Langmuir probe is very often a cathode of plasma source which is directly or indirectly heated. Contamination substances will move away from the heated cathode and heated cathode will not have large capacitance. Therefore, no consideration seems to be needed for the contamination of the counter electrode. For the glass sealed Langmuir probe, the sweep rate of the probe voltage can be very low and the sweep rate for the contaminated probe must be high enough to diminish only the capacitance effect of the probe surface. While, Langmuir probe and the multi-electrodes probe in the space plasma use a rocket or a satellite body as their counter electrodes. The surface area of the body is always covered with the contamination layer formed by the adsorption of the various substances. The situation is illustrated in Fig. 52. Therefore the contamination layer of the rocket body is considered to have a capac-

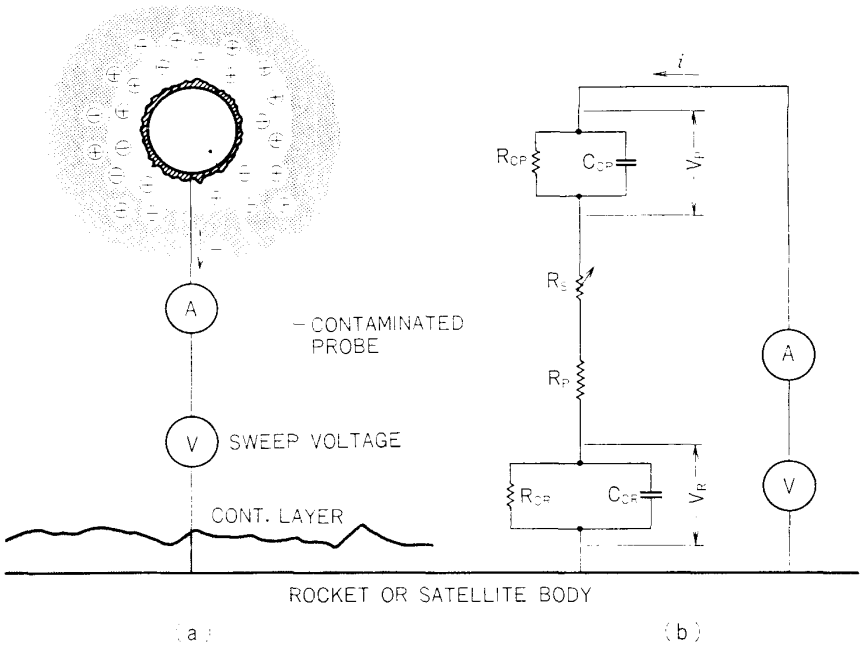

FIG. 52. Situation of a contaminated rocket body.

itance and resistance similarly to the probe surface, which may influence the probe measurements. However if the effect of contamination layer of the counter electrode is removed by a rapid sweep of the probe voltage we can expect the correct temperature. Therefore the subject of our discussion exists in that in what frequency of voltage sweep, the effect of rocket contamination can be eliminated. In order to get a general understanding, we pick up a contaminated Langmuir probe.

The capacitance of the insulation layer will become larger according to the larger surface area of the counter electrode. In most cases, the surface area of the counter electrode is much larger than the surface area of a probe, which means that the capacitance of the rocket body (C_R) is larger than that of the probe (C_p), namely $C_R \gg C_p$.

As the probe current flowing through a circuit will raise the potentials of the rocket body and of the probe, we can write the potential variations of the probe surface and of the rocket body in the followings,

$$\text{for rocket potential} \quad V_R = \frac{1}{C_R}\int i dt \quad \text{or} \quad \frac{dV_R}{dt} = \frac{i}{C_R} \tag{19}$$

$$\text{for probe potential} \quad V_p = \frac{1}{C_p}\int i dt \quad \text{or} \quad \frac{dV_p}{dt} = \frac{i}{C_p} \tag{20}$$

Therefore by taking the above description $C_R \gg C_p$ into consideration, we can get $dV_R/dt \ll dV_p/dt$, which means that the potential variation of contaminated rocket body is much smaller than that of probe. Generally speaking, it can be said that the potential of a rocket body does not change by the application of probe voltage.

The experiment with S-210-7 rocket seems to support the above consideration.

Therefore we can conclude that the contamination effect of a rocket or satellite body will not influence on Langmuir probe experiments as long as the surface area of a counter electrode is sufficiently large.

5. Electron temperature obtained with electron temperature probe

It was shown in chapter II that the electron temperature probe, a sort of ac mode probes, is not influenced by the contamination layer of a probe and gives a correct electron temperature. This section presents electron temperature profiles obtained with the electron temperature probe with a brief geophysical discussion. Profiles observed by the foreign authors from the point of probe reliability will be discussed in the 5th chapter.

5.1 Geophysical condition for the obtained data [27]

Sounding rockets were launched from the Kagoshima Space Center, its location being shown in Fig. 53. Geomagnetic location of the K.S.C. is 20°0 N and 198°4 E and dip angle is about 40°. One important feature of the location of the K.S.C. is that the center of geomagnetic dynamo current passes frequently over there wandering to north or south. Therefore, data obtained at the geophysically par-

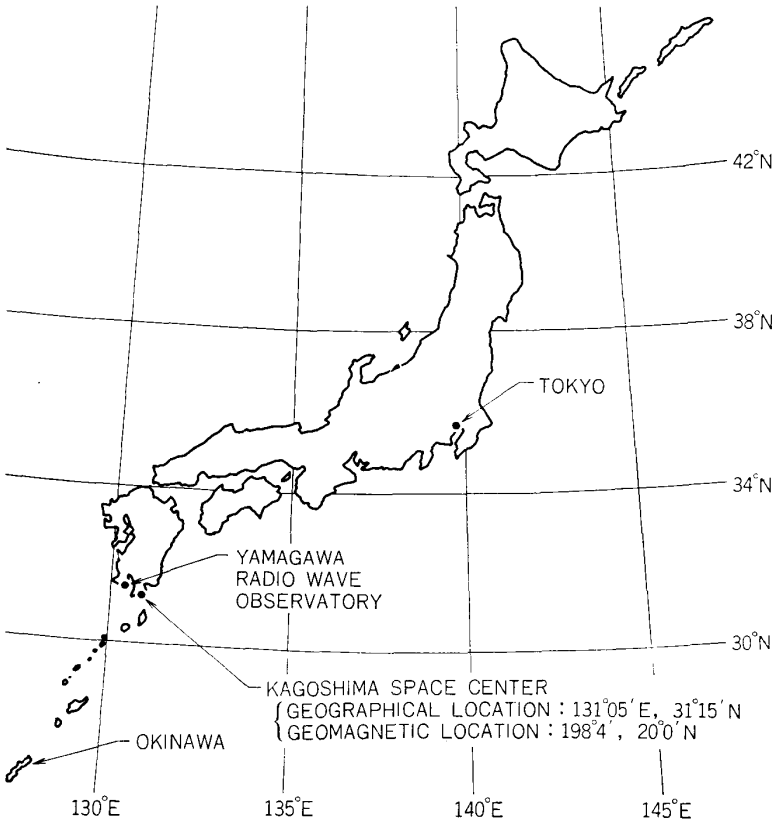

Fig. 53. Geophysical location of K.S.C.

TABLE 3. List of sounding rockets and geophysical conditions.

Rocket	Data	Time	Zurich	$F_{10.7}$	K_p	Remarks
K-9M- 9	1965 3/27	14 : 01	1	72.1	1	
K-10S- 6	1965 8/28	11 : 02	18	73.2	2	Q
L-3H- 6	1970 1/21	11 : 00	120	177	0	
K-9M-28	1970 1/25	14 : 00	99	149.5	1	Q
K-9M-29	1970 1/27	19 : 20	132	163.0	1	
K-9M-32	1970 9/27	15 : 42	87	145	3	D
S-210- 4	1971 1/16	11 : 00	65	136.4	3	
K-9M-30	1971 1/16	16 : 15	65	156.4	3	
K-9M-34	1971 1/24	11 : 00	99	177	2	
K-9M-33	1971 8/26	19 : 35	82	138.8	3	
K-9M-38	1972 2/22	15 : 00	167	180.4	0	
K-9M-40	1972 9/20	14 : 00	44	149.5	1⁻	QQ
L-3H- 7	1971 9/ 3	21 : 00	24	92.5	1	
S-210- 6	1972 1/21	11 : 24	78	127.9	2⁻	
S-210- 8	1973 1/16	8 : 40	11	93.8	3	
K-9M-39	1972 2/18	18 : 28	146	184.4	1	
K-9M-42	1973 2/23	18 : 38	33	91.4	5	D

ticular point is expected to give unique results. Electron temperature profiles obtained with sounding rockets are summarized in Table 3, including date, time, sunspot number Rz, solar flux $F_{10.7}$ and *Kp* index. It is noted that data were obtained in relatively high solar activity condition.

5.2 Daily variation of the electron temperature profile

Although we don't have enough data to discuss in detail, electron temperatures at Uchinoura can be basically grouped into three categories depending on the time, those are, around 10–12 hours, 14–16 hours and evening time, as were already shown in Figs. 8 a, b and c. In the figure, dotted and dashed curves are the electron temperature profiles obtained by individual rockets, while full curves are their mean values. In the Fig. 8 b, mean value is taken by avoiding the K-9M-30 result, because the profile obtained with K-9M-30 is considered to be quite special one as will be discussed in more detail.

5.3 Solar flux dependence of the electron temperature in isotherm region

The electron temperature in an isotherm region is found to have a solar flux dependence. When we evaluate the electron temperature deviation from the neutral temperature deduced from CIRA [*71*] and Jacchia 71 model around at the height of 300 Km, we can find two interesting features. One of them is that the temperature difference decreases with the increase of solar flux intensity, which is shown in Fig. 54.

In the Fig. 54, T_{n65} and T_{n71} are the neutral temperatures deduced from CIRA 65 and Jacchia 71 static model respectively, by taking into account the solar flux

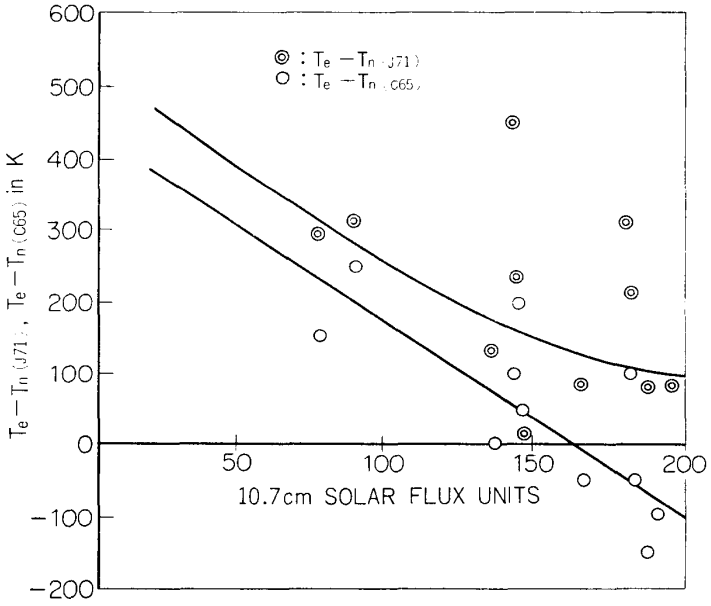

FIG. 54. Solar flux dependence of the electron temperature from neutral temperature in isotherm region.

intensity and K_p index. The figure shows that the electron temperature is lower than the CIRA 65 model neutral temperature in the higher intensity of solar flux. From an energetics point of view, it is difficult to consider that the electron temperature is lower than the neutral one. Therefore, we may be able to conclude that CIRA model overestimated the neutral temperature in the higher intensity region of the solar flux. In contrast to CIRA 65 model, Jacchia 71 model seems to be reasonably improved if we look it from the electron-neutral temperature relation.

The decrease of $T_e - T_n$ with the increase of solar flux intensity may be explained by the increase of electron cooling, because the increase of electron density is accompanied with the increasing loss rate by Coulomb encounters with ions expressed as $L_{ei} \approx 4.82 \times 10^{-7} N_e^2 (T_e - T_n) T_e^{-3/2} eV/\text{cm}^3/\text{sec}$.

The second feature is that electrons are never in thermal equilibrium with neutral particles in the lower solar activity if the Jacchia 71 model is assumed correct. The tendency is as much enhanced as in the much lower solar activity. If the Jacchia model 71 does not express the behaviour of the actual neutral temperature, the above description is invalid. However, when the solar flux dependence of $T_e - T_n$ described above is reasonable, the non-equilibrium with electrons and neutral particles seems quite sure. In order to confirm this fact, simultaneous observations of T_e and T_n are necessary.

5.4 *Electron density dependence of the temperature profile*

Among the electron temperature profiles obtained during afternoon, profiles obtained with K-9M-30 are particularly different from those of others. The electron temperature increases almost monotonously as the height increases. Whilst other data which are considered quite typical in the afternoon, have maximum

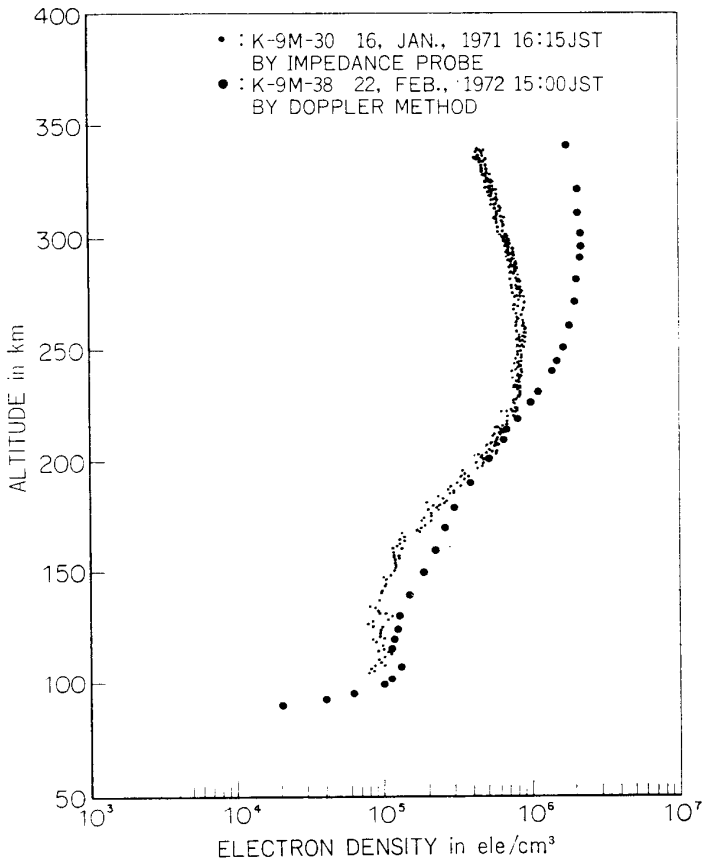

FIG. 55. Electron density profiles for K-9M-30, 38.

values around 220 Km and gradually decrease.

In this section we discuss the special feature of the profiles of K-9M-30 by considering the electron density profile obtained simultaneously with the same rocket. Electron density and temperature profiles are shown in Figs. 55 and 56 which show that the electron density for K-9M-30 is 3 times lower than that of K-9M-38 around 300 Km. In order to check whether an incoming energy flux exists or not, the heat production rate (loss rate) is calculated by assuming the neutral temperature, the density and the composition of Jacchia 1971 model. The evaluation shows that no difference between them exists, which means that no heat flux from the protonosphere can be considered. This fact says that the electron temperature seems to be influenced mainly by the electron density. The relation N_e versus T_e–T_{n71} is shown in Fig. 57 for K-9M-30 and -38 together with the results obtained with the incoherent backscatter technique at Jicamarca. The result also shows that the electron temperature is nearly influenced by the electron density. As a next step of this study, it would be interesting to know what mechanism attribute to the decrease of electron density. From the data of magnetogram and ionogram shown in Fig. 58, we can investigate the ionospheric condition when the observation was carried out.

In normal case (K-9M-38), the deviation of the horizontal intensity from an average value of the geomagnetically quiet days was quite small. In contrast to

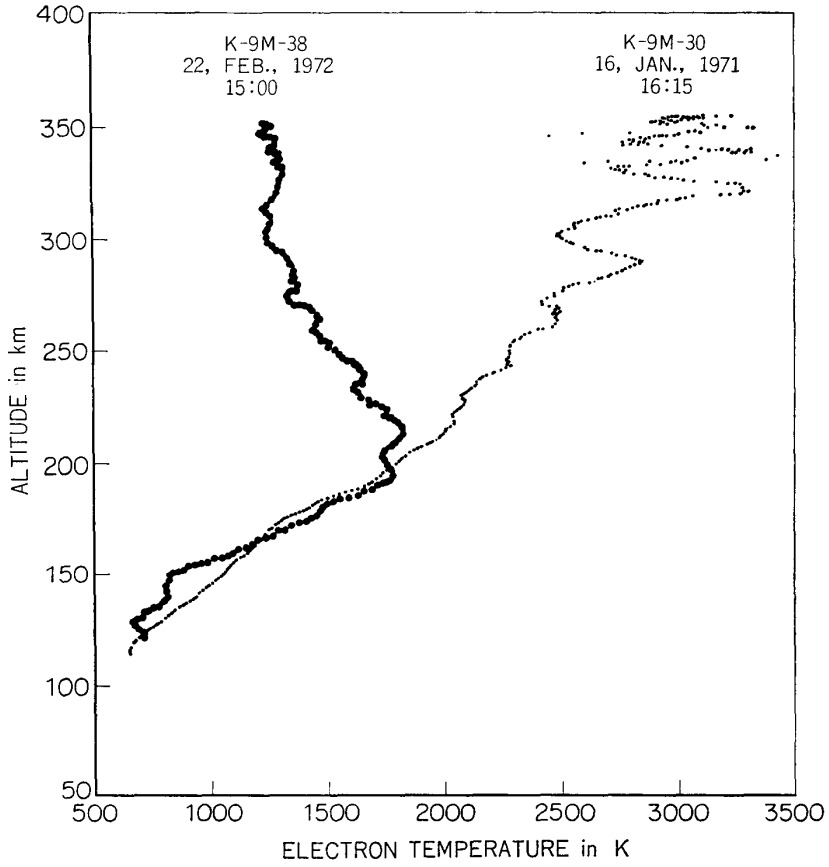

FIG. 56. Electron temperature profiles for K-9M-30, 38.

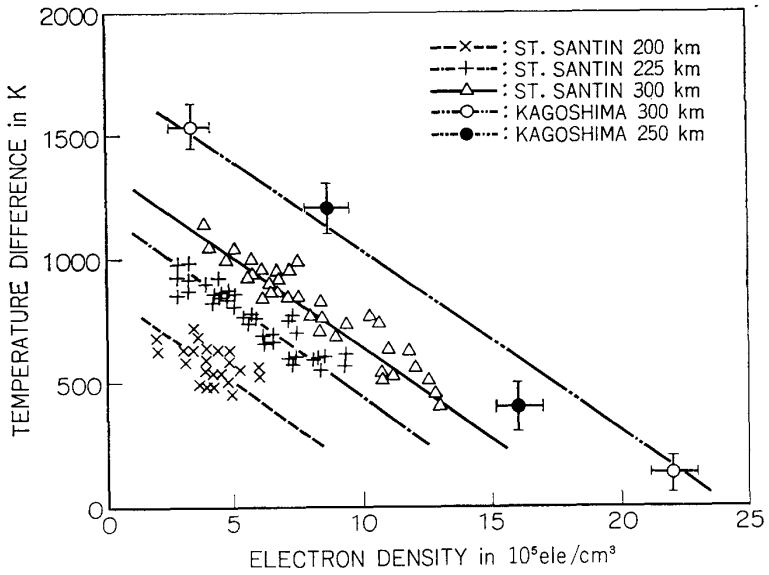

FIG. 57. Relation between electron density and electron temperature (for reference, St. Santin's result is also shown).

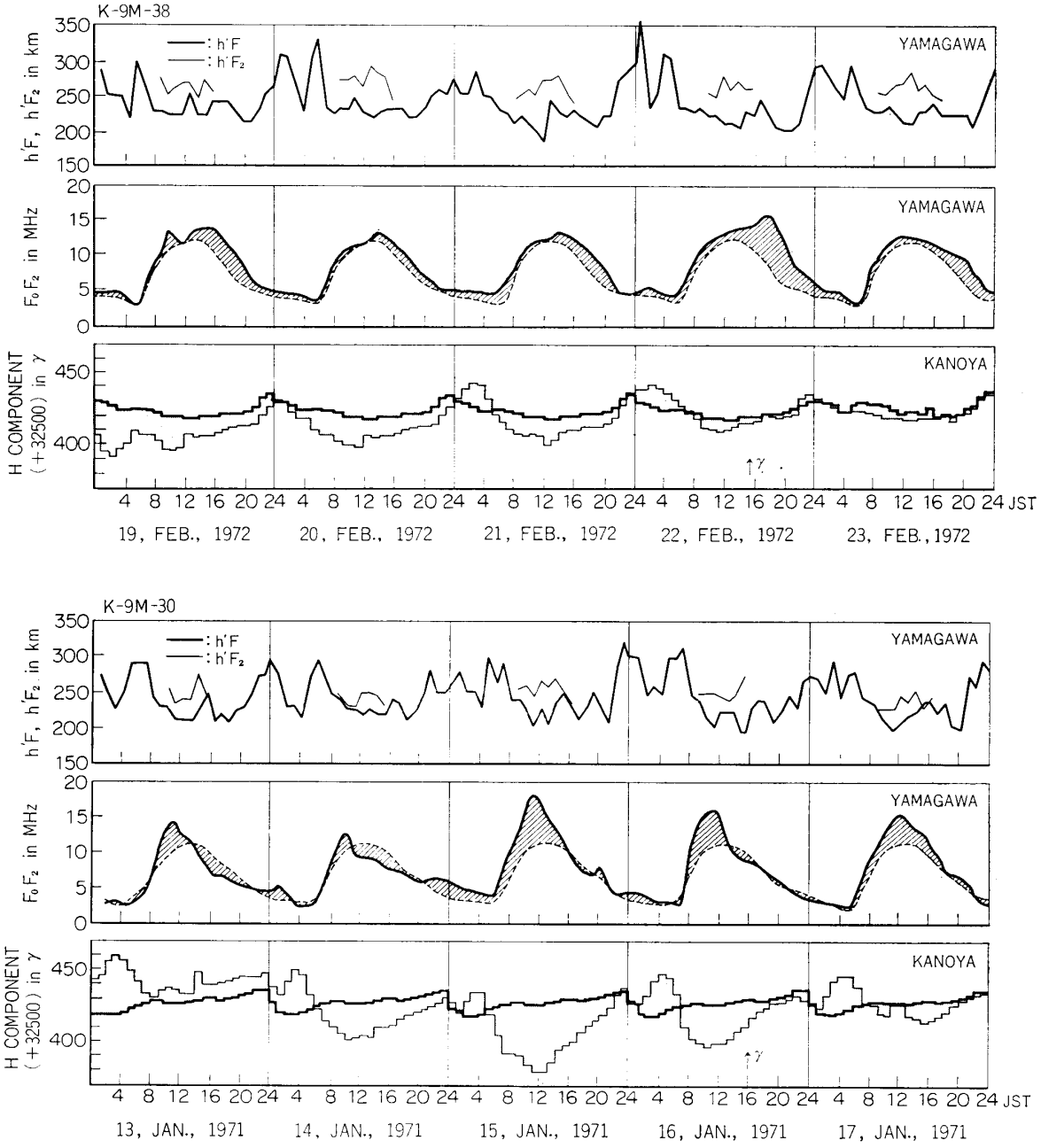

FIG. 58. Geophysical condition for K-9M-30, 38. Upper; *h'F*, middle; critical frequency for *F*. Dotted lines are monthly mean values. lower; horizontal intensity of the geomagnetic field. Full lines are mean values of the 5 quiet days.

that, the case for K-9M-30 experienced a quite large deviation from the mean value of foF_2 and the average value of horizontal intensity of the geomagnetic field. Virtual height of F layer, h'F, also showed a clear change. When the rocket observation was started, h'F suddenly increased. At the same time foF_2, which had been higher than the mean value before the rocket launching, decreased below the mean value. The time of observation corresponded to the very transient time of the ionospheric condition.

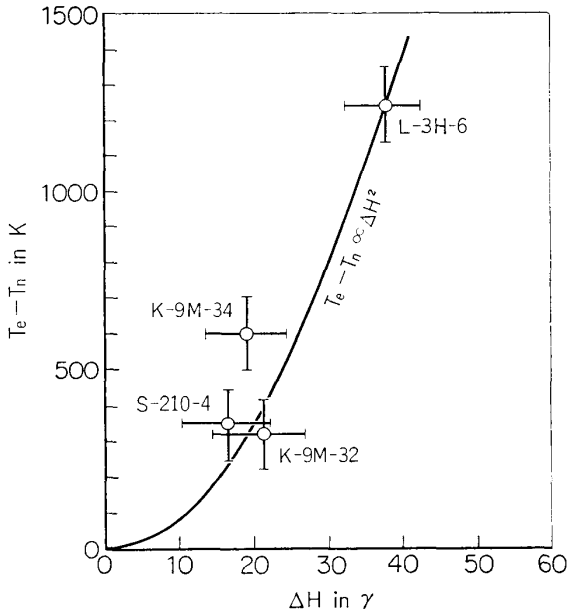

FIG. 59. Relation of electron temperature increase in temperature maximum and diurnal variation of the horizontal intensity of geomagnetic field observed on the ground.

As described above, the high electron temperature observed by K-9M-30 is considered to be a result of the electron density decrease accompanid with an ionospheric disturbance. However the cause of the decrease of electron density in the disturbed condition is not yet clear in spite of immense efforts of many scientists. Therefore when the mechanism of ionospheric storm concerning the electron density becomes clear, the behavior of electron temperature profile such as experienced by K-9M-30 may be also resolved.

5.5 High temperature layer around 100 Km

As was mentioned in Fig. 15 in chapter I, thin layer which has the higher temperature than surroundings was found to appear around 11 hours in local time. The electron temperature begins increasing from 100 Km, reaches the maximum value at about 105 Km, takes the minimum value at around 110 Km and then again increases gradually. The height of the maximum temperature is slightly different for each rocket; 112 Km, 110 Km, and 106 Km for S-210-4, L-3H-6, and K-9M-34 rockets respectively. The value of the maximum electron temperature seems to be dependent of the diurnal variation of the horizontal intensity of geomagnetic field as shown in Fig. 59. Such increase of electron temperature can not be explained by the Joule dissipation so far as we take the neutral temperature from Jacchia 71 model into account. Even if the real neutral temperature is higher than a model temperature as was reported by Blamont [*72*] or Wand [*73*], the Joule dissipation can not still explain such phenomenon.

We are afraid that the electron temperature probe can't give a correct electron temperature when the electrons are not in maxwellian. When electrons deviate from the Maxwell energy distribution and have much higher energy especially in an

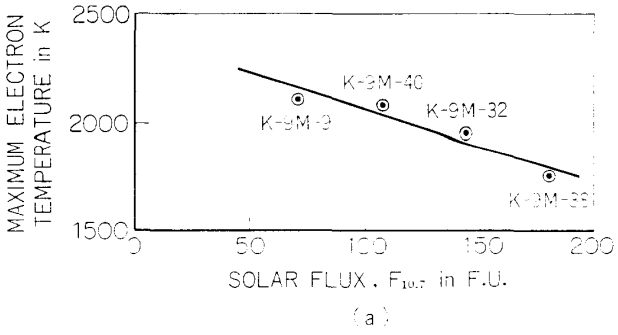

FIG. 60a. Solar flux dependence of temperature in the maximum temperature region.

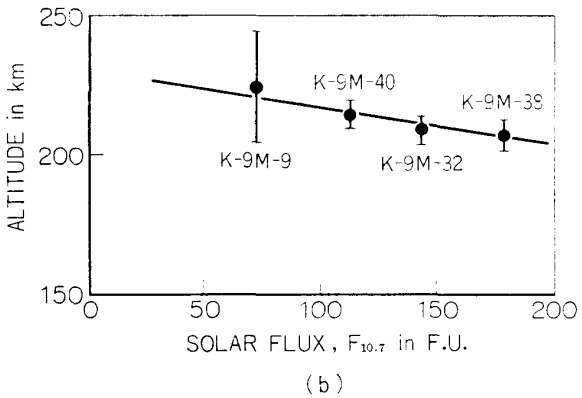

FIG. 60b. Solar flux dependence of height of the temperature maximum (numbers correspond to the rockets K-9M-9, 32, 38 and 40 respectively).

energy range corresponding to the floating potential, the electron temperature probe will present a different value which is higher than the true value. Therefore our observation suggests that (1) the high electron temperature layer really exists, or (2) electrons are not in a maxwellian energy distribution. If the energy distribution of electrons is not maxwellian, high energy tail must exist. In order to identify the above two candidates we are planning to measure the electron energy distribution around at the height of 100 Km by the use of a glass sealed Langmuir probe in 1974. Whether the result supports (1) or (2) will present quite interesting problem.

5.6 *Solar flux dependence of electron temperature and height at temperature maximum*

As shown in Fig. 8 b, the electron temperature first gradually increases up to around 250 Km and begins to decrease toward 300 Km in the afternoon. It is found that the electron temperature at maximum level depends on the intensity of solar flux, the maximum temperature decreasing with the increase of solar flux (Fig. 60 a). The height of the maximum temperature also shows the solar flux dependence; the increase of solar flux intensity causes the decrease of the height of electron temperature maximum (Fig. 60 b). These interesting features contradict with the theory developed by J.R. Herman and S. Chandra [20] who solved the electron continuity and the heat conduction equations simultaneously.

Chapter IV Some Other Factors Which Cause Unreliable Evaluation of Charged Particle Temperatures

1. Introduction

In the previous chapter, it was shown that the contamination of Langmuir probe and the retarding potential trap is one of the most serious reasons to cause errone-

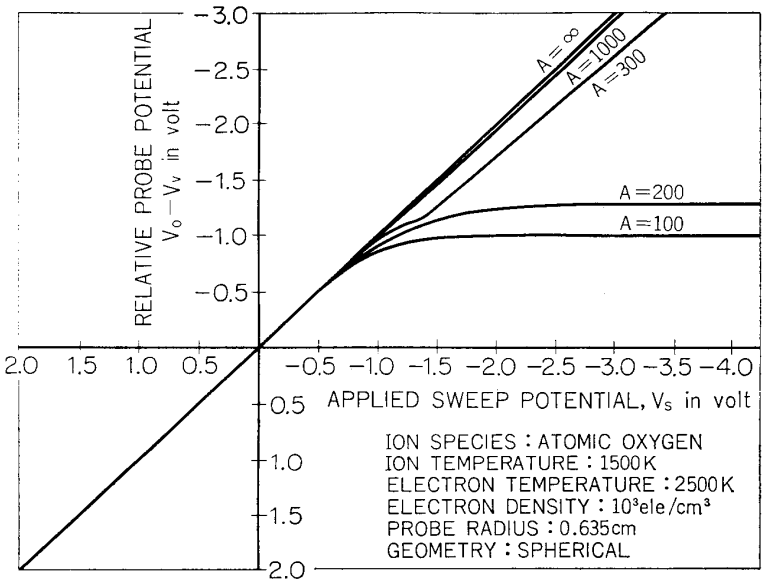

FIG. 61. The applied voltage versus probe (to plasma) voltage characteristic of bipolar Langmuir probes of various area ratios and ambient conditions.

ous results. Because of the insulation layer formed on the probe surface, the electron temperature is estimated higher than that of the true value. On the other hand, we can list up some other possible reasons to cause erroneous results besides the contmination layer. Then we will be able to find any reasons to cause the discrepancy in the space plasma measurement which was briefly reported in the previous chapter. Therefore, this chapter presents and discusses some other possibilities which are considered to cause erroneous results on those probes. The discussion made in this chapter will be used again in the next chapter to find out the possible reason.

2. POSSIBLE CAUSES OF ERROR

2.1 Area of a counter electrode

A rapid time variation of the vehicle potential has been almost ignored by many investigators but this may lead to a significant error. For instance, Fig. 61 shows characteristics of the applied voltage versus the probe voltage characteristic of double probes of various area ratios under many conditions [*74*]. It is evident that for an area ratio of 300, for instance, an appreciable portion of the applied sweep voltage appears as a "vehicle potential bounce" and that the proble potential is appreciably less than that actually applied one. If we plot the current against the applied voltage semi-logarithmically, the resultant slope may be interpreted in terms of the electron temperature. The distortion in the sweep curve will lead to the overestimation of the temperature in a similar way discussed in the contamination effect. In this paragraph we discuss this problem in more detail referring to Dote's [*75*] work.

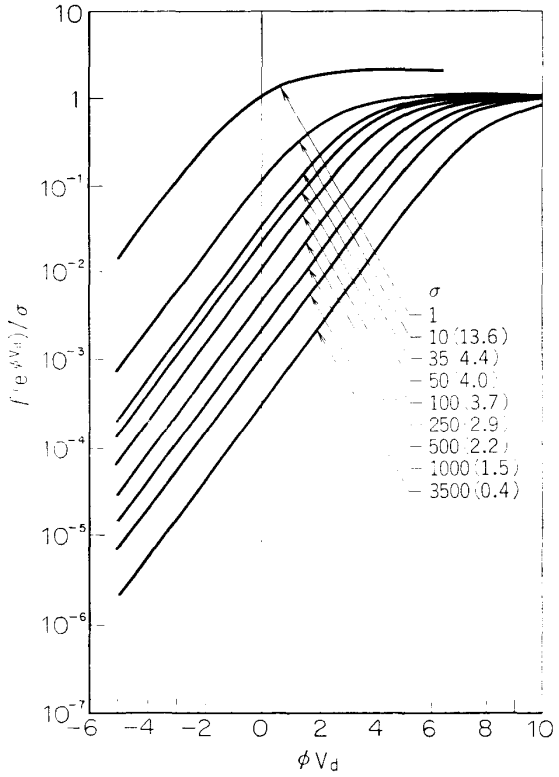

FIG. 62. Semi-log. plotted Langmuir curves for the various counter electrode surface (Dote et al. [75]).

According to the double probe theory as described by Johnson et al., the electron current J_e, flowing into the probe will be expressed as follows,

$$J_e = J_{o+} A_1 (1+\sigma)/(1+\sigma\, e^{-\phi V_d}) \tag{21}$$

where J_{o+} is the random ion current, A_1 and A_2 are the surface areas of the probe and the rocket, respectively. V_d is the probe potential referring to rocket body, $\phi = e/kT_e$, $\sigma = A_2/A_1$, e is electronic charge, and V_s is the potential of the body when the rocket and the probe is in the same potential.
When $V_d = 0$, equation (21) gives the following equation

$$J_e = J_{o+} A_1 = J_{oe}\, e^{-\phi V_s} \tag{22}$$

Therefore Eq. (21) can be rewritten

$$J_e = J_{oe}\, e^{-\phi V_s}(1+\sigma)/(1+\sigma\, e^{-\phi V_d}) \tag{23}$$

If $\sigma \gg 1$ and $e^{-\phi V_d} \gg 1$ in this equation,

$$J_e = J_{oe} A_1\, e^{-\phi(V_s - V_d)} \tag{24}$$

This means that if the probe area is enough small compared with the area of counter electrode, the probe characteristic is equivalent to the general Langmuir probe.

If the conditions $\sigma \gg 1$ and $e^{-\phi V_d} \gg 1$ are not valid, Equation (21) can be rewritten again

$$J_e = J_{eo} A_1 \, e^{-\phi(V_s - V_d)} \cdot f(\phi V_d, \sigma)$$

$$f(\phi V_d, \sigma) \equiv (\sigma + 1)/(\sigma + e^{\phi V_d}) \tag{25}$$

If Fig. 62 the semi-logarithmically plotted Langmuir curve is illustrated which shows that the electron temperature evaluated from the slope will not have so serious errors even if the ratio σ is small, for example $\sigma \equiv 10$. In Fig. 62 evaluated errors in the electron temperature are also shown in parenthesis, where the electron temperature is evaluated in the region of $\phi V_d > 0$.

In order to check the significance of the counter electrode, we consider a S-210-type sounding rocket, which is the smallest sounding rocket in Japan (whose outer diameter; 210 mm). Supposing that the length of rocket body as the counter electrode is 10 cm (surface area ≈ 610 cm^2) and the cylindrical probe of 20 cm in length and 3 mm in diameter which is in general use (surface area 20 cm^2), the surface area ratio will be 30. In reference to Fig. 62 we can see that the evaluated error is only about 4.4% in the above described case. Therefore we can conclude that the surface area ratio will be rather satisfactory as long as the electron temperature measurement onboard a rocket is concerned.

2.2 *Effect of a geomagnetic field* [76]

The effect of geomagnetic field is a factor which can not be ignored according to the dimension of the probe and the intensity of the magnetic field. The problem of the influence of a magnetic field on the probe will be divided into two parts; one is the influence upon the electron temperature and the other is that upon the electron density. This paragraph discusses only the effect of the geomagnetic field upon the evaluation of electron temperature according to Dote's [75] paper. The effect of the geomagnetic field is discussed from the point whether the Larmor radius is larger than the sheath radius or not. When the surface of the planar probe and the axis of cylindrical probe are parallel to the magnetic field, the electron current flowing into the the probe is expressed as follows.

For the planar probe;

$$J_e = J_o/2[1 - erf((d/a)(1 - y/y_0)) + \exp(y)(1 - erf((d/a)(1 + y/4y_0)))]$$

$$a = 2/\omega_{ce} \cdot \sqrt{kT_e/m_e}, \quad y_o = d^2/a^2, \quad \omega_{ce} = eB/m_e C, \quad J_o = N_e e \sqrt{kT_e/2\pi m_e}, \quad y = \frac{eV_p}{kT_e} \tag{26}$$

In the region $y \ll -y_o$, $J_e \approx J_o \exp(-y)$, that is, in the negative potential region far from space potential, the v-i characteristic curve will not be affected by the magnetic field.

For the cylindrical probe:

$$J_e = 2\pi \cdot r_p \cdot L \cdot e \cdot J_o \cdot \Psi \tag{27}$$

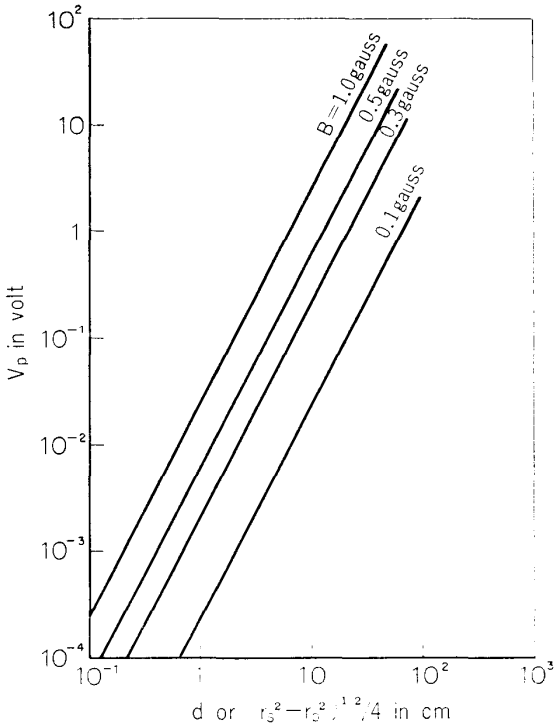

FIG. 63. The retarded probe potential above which the effect of the magnetic field can be neglected for electron temperature measurements as a function of d or $(r_s^2-r_p^2)/4$ with the magnetic field as a parameter (Dote [76]).

$$\Psi=\exp(y)-1/2[\exp(y)\cdot\{erf(r_p/a(\sqrt{q+1}+1))+erf(r_p/a(q\sqrt{1+\alpha}-1))\}$$
$$-q\{erf(r_p/a(\sqrt{1+\alpha}+q))+erf(r_p/a(\sqrt{1+\alpha}-q))\}] \tag{28}$$
$$d=y/y_o', \quad y_o'=r_p^2/a^2(q^2-1), \quad q=r_s/r_p$$

In the region $y<y_o'$, the above equation will be written as follows,

$$J_e=2\pi\cdot r_p\cdot L\cdot J_o\cdot e\cdot\exp(y), \tag{29}$$

where e the electron charge, m_e the electron mass, V_p the retarded potential difference between the probe and the plasma, B the geomagnetic field, C the light velocity, d the sheath thickness, r_p the probe radius, r_s the sheath radius, and L the probe length. The conditions of $y\ll -y_o$ for planar probe and of $y<y_o'$ for the cylindrical probe give the situation in which the semi-logarithmically plotted Langmuir curve of the electron current against the probe potential is a straight line. The following critical values of V_p are shown in Fig. 63 as a function of d or $(r_s^2-r_p^2)/4$ for several values of B.

$$\text{Planar probe; } V_p\gg eB^2d^2/2C^2m_e=8.8\times10^{-2}B^2d^2 \tag{30}$$
$$\text{Cylindrical probes; } V_p\gg eB^2(r_s^2-r_p^2)/8C^2m_e=2.2\times10^{-2}B^2(r_s^2-r_p^2) \tag{31}$$

Since B is about 0.3 gauss and the sheath thickness is considered to be of the

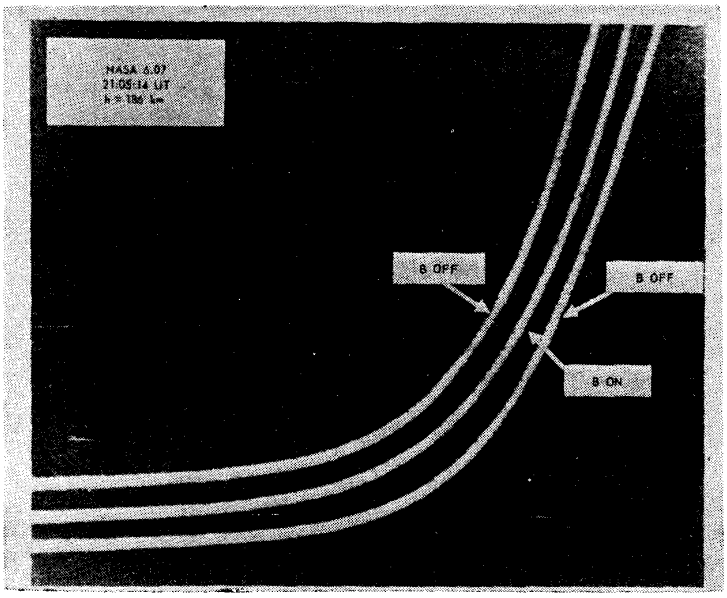

FIG. 64. Photograph of a sequence of retarding regions with a 4 gauss field applied (B on) and removed (B off). (Brace [*109*]). Note that no change appeared in two curves.

order of 1 cm in the ionosphere, the critical value of V_p deduced from this figure is about 1 mV.

Recently Sanmartin [*77*] performed an asymptotic analysis for a spherical probe in a magnetic field. His theory also seems to show that the effect of the geomagnetic field is negligible in the evaluation of the electron temperature, although he considers the geomagnetic field as one of the possible reasons of the discrepancy of electron temperatures between from Langmuir probe and the backscatter technique. From a view point of the experiment Brace et al. [*79*] checked the effect of the geomagnetic field upon the probe characteristic curve on board the rocket. They compared Langmuir curves under the existences of the magnetic field of 4 gauss and of only geomagnetic field. The results are shown in Fig. 64 which shows no difference between two curves.

2.3 Errors accompanied with retarding potential trap

2.3.1 Errors caused by non-uniformity of the grid potential [*80*]

Most planar retarding potential analyzers use a transparent grid for the retarding element in order to evade some electronic difficulties that arise from sweeping the potential of the current collector. The temperature and the composition of ions are then derived by assuming that only ions with the energy greater than the applied grid potential can reach the collector. The hazards of this assumption have long been recognized (Hanson and Mckibbin [*81*], 1961, Knudsen [*83*], 1966).

Potential depressions occur between the grid wires because adjacent elements (e.g., other grids) are usually held at a lower potential and the actual voltage

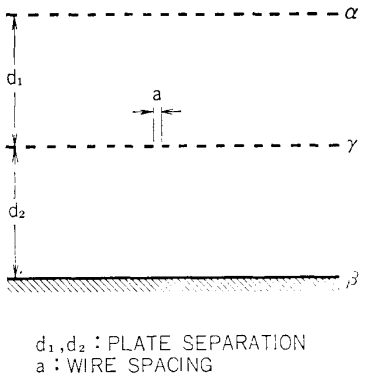

FIG. 65. Configuration for R.P.T. for the study of non-uniformity effect; d_1, d_2 the plate separation, a the wire spacing.

sweep is somewhat smaller than that directly applied to the grid. As a result, ions with energy less than the applied retarding potential sometimes do penetrate the grid openings and the derived ion temperature is too high. W. B. Hanson et al. estimated the effective potential V_e when V_r is applied to the grid r as shown in Fig. 65.

$$V_e = V_r\{1-(\delta+r/\pi)/(d+\delta)(1+2r/a)\} \tag{32}$$
$$d = d_1 d_2/\{d_1+d_2-(d_1V_\beta+d_2V_\alpha)/V_r\}$$

where d_1 and d_2 are the plate separations, r the wire radius, a the wire spacing, δ a characteristic length of the shielding effectiveness of the grid, essentially independent of d_1 and d_2 and of the form $\delta = a \cdot f(r/a)$

The function f is different for each type of geometry (e.g., linear, square mesh, stocking mesh), but depends only on the ratio of wire size to a characteristic mesh length for a given geometry. According to the equation (32), Hanson et al. estimated the error for R.P.T. which was used in Ogo. 4 and Ogo. 6.

TABLE 4. Evaluated error of ion temperature observed on Ogo. 4 and Ogo. 6.

Exp.	d_1, mils	d_2, mils	δ, mils	$1-V_e/V_r$	T_i correction
Ogo 4	157	157	5.7	0.0736	−15 %
Ogo 6	100	235	0.67	0.0145	− 2.9%

The evaluation is described in Table 4. Comparisons of the ion temperature observed on Ogo. 4 with that by the Jicamarca radar, which will be mentioned in the next chapter, indicate that the correction of −15% shown in Table 4 have the correct sign, but are too small if the radar values of T_i are correct. In addition to the above-described effect of a decreasing of the effective retarding potential, the potential non-uniformities have the further effect of perturbing ion trajectories. When the potential of a grid is retarding, the perturbation of the trajectory is such that the particle tends to pass the grid through the point where the potential is

minimum (i.e., less retarding). Both of these trajectory perturbations made the apparent temperature of the ions (as inferred from the ideal grid analysis)) higher than the real temperature. According to Goldan et al. [*82*], the temperature obtained with the retarding potential trap of Ogo. 4 must be lower at least 32%.

2.3.2 Curved sheath effect [*83*]

A curvature of the sheath boundary causes two effects; first, the area of ion collection becomes larger than a plane sheath, and second, ions collected through the opening have a deviation of angles of attack from normal to the opening

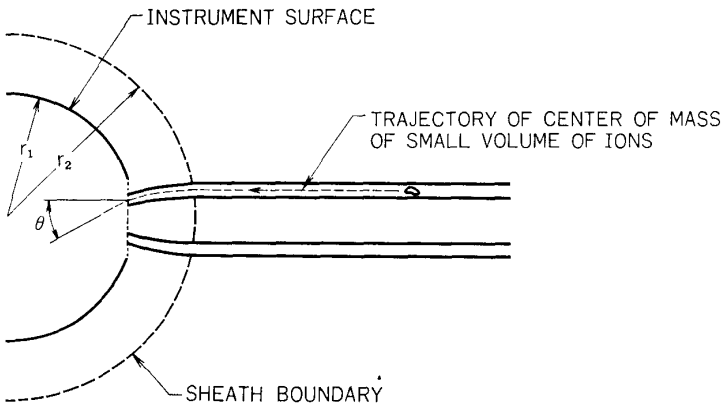

FIG. 66. Evaluation of the effect of sheath curvature on derived ionospheric quantities (Knudsen [*83*]).

TABLE 5. Effect of sheath curvature on derived quantities.

Trap Opening radius cm	r_1 cm	r_2-r_1 cm	a	Ψ_o volts	n_1/n^-	n_2/n^-	T^+/T_o^+	$\Psi-\Psi_o$ volts
1.0	7.0	5.7	7.8	−15	1.38	$<5\times10^{-5}$	0.995	0.03
1.0	3.5	5.7	7.8	−15	1.60	$<2\times10^{-4}$	0.985	0.1
1.0	3.5	2.5	7.8	− 5	1.17	$<3\times10^{-5}$	0.997	0.00
1.0	3.5	0.8	7.8	− 1	1.02	$<2\times10^{-6}$	1.000	0.00
1.0	7.0	1.2	2.0	− 2	1.15	$<2\times10^{-2}$	0.967	0.01
1.0	7.0	0.5	2.0	− 0.5	1.02	$<2\times10^{-3}$	0.996	0.00
1.0	7.0	1.2	0.7	− 2	1.53	0.0*	0.915	0.02
1.0	7.0	0.5	0.7	− 0.5	1.09	0.0*	0.983	0.00

a: Speed of satellite in units of the most probable ion thermal speed
T_o^+: Ion temperature assumed in deriving theoretical characteristic curve (=1000°K)
n^-: Total ion concentration assumed in deriving theoretical characteristic curve. Only O^+ was assumed to exist
n_1: Concentration of O^+ derived from the least-squares fit
n_2: Concentration of $(NO^+ + O_2^+)$ derived from the least-squares fit
T^+: Temperatures of ions derived by least-squares fit
Ψ: Vehicle potential derived by least-squares flt
*: n_2 set equal to zero and other quantities recomputed if initial least-squares fit gave a negative value for n_2.

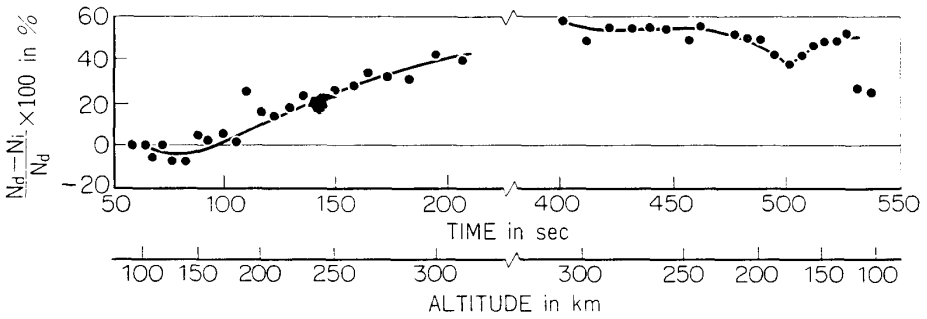

FIG. 67. Electron density measurements observed by Doppler method (N_d) and impedance probe (N_i) carried on rocket K-9M-38. Deviation is caused by the decrease of electron density around rocket (Kimura [85]).

surface. The first effect produces an error in the calculated concentration, and the second may cause errors in the derived ion temperature, vehicle potential, and ion composition. Although the error in the ion temperature caused by the curved sheath can't be investigated rigorously now, Kundsen evaluated the problem as following. To simplify the computation of particle trajectory, the opening of the R.P.T. is assummed to be located in the hemisphere of radius r_1 and the edge of the sheath is assumed located at a distance r_2. It is further assumed that the potential varies as $1/r$ between r_1 and r_2. This last assumption is far from the reality but permits the assessment of the effect of particle trajectory on the derived quantities. The potential at r_1 is assumed less than at r_2. His evaluation is summarized in Table 5.

From the calculation, he concludes that the error in ion temperature introduced by the curved sheath around an instrument carried abroad a satellite is seen to be less than 2% for the most severe case, namely a small instrument and large vehicle potential (−15 volts) and also concludes that the largest temperature error, 9%, occurs when the trap is moving with a velocity less than the thermal ion velocity and the vehicle potential is relatively large. The concentration is 1.6 times larger than the assumed concentration in one of the cases examined.

2.4 Disturbance due to the spacecraft charging

The rocket and satellite have a certain equilibrium potential with an ambient plasma to make the total current to a body equal to zero [*84*]. Generally the equilibrium potential ranges several minus volts referring to the space potential in case of K-9M-type rocket. Sometimes the equilibrium potential is found to reach the extremely negative value, generating the thick disturbed region around the vehicle.

If the equilibrium potential becomes large, the sheath thickness around the rocket or satellite becomes large and almost all of the thermal electron can not reach the probe. Therefore electron density will be inevitably evaluated lower than the ambient plasma density, if the measurement is carried out in this disturbed region. The good example is shown in Fig. 67. The electron density observed with the impedance probe is lower than that from Doppler method [*85*]. The discrepancy becomes larger as the time after launch lasts. This must be due to

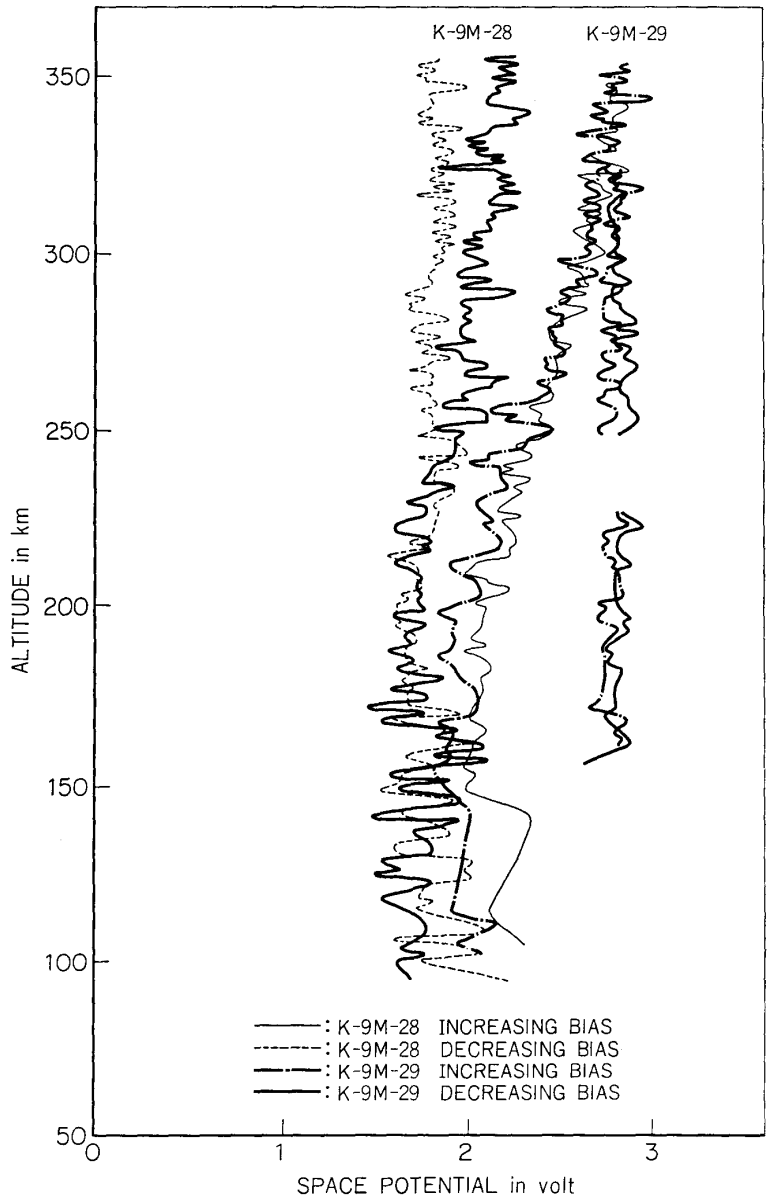

FIG. 68. Floating potential variation of the rocket experienced on K-9M-29 (Same situation was experienced on K-9M-38 rocket).

the gradual decrease of electron density in the disturbed region which is caused by the gradual increase of the equilibrium potential. Such kind of the potential increase is caused by the rectification effect of a large high frequency signal applied to the probe whose surface area can not be neglected compared to the conducting surface area of the spacecraft. The similar variation of rocket body potential was observed in K-9M-29 on which an impedance probe instrument also was installed. It is also reported that if the satellite goes further, energetic particles play a serious role. The ATS 5 satellite [*86*] in geosynchronous orbit was charged up to 4200 V, which is considered to be due to the bombardment with the energetic particles.

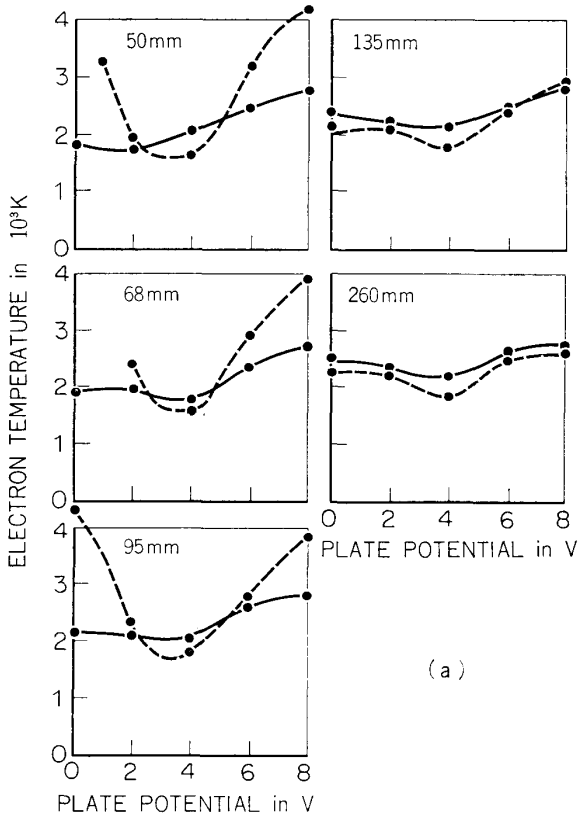

FIG. 69a. Electron temperature observed in the disturbed plasma. Abscissas; voltage applied to the disturbing plate. Ordinates; electron temperature obtained from front (dashed lines) and back (full lines) probes. Space potential of the ambient plasma is 4 volts. Distance of the two probes from a disturbing plate is taken as a parameter.

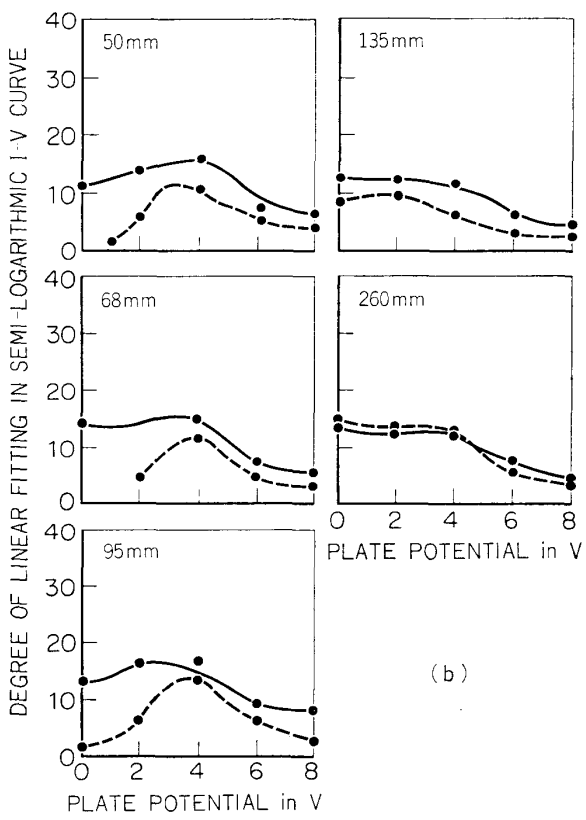

FIG. 69b. Degree of Maxwell distribution of electrons in the disturbed region. Note that "electron temperature" is apparently increased as the linearity of the semi-logarithmically plotted curve becomes worse.

The electron temperature measurement in the disturbed region which is produced by the potential sink of spacecraft as described above becomes quite serious because a large part of the thermal (low energy) electron can not jump over the potential barrier established around the rocket or satellite body and either can not reach the probe or trap in the disturbed region.

In order to understand these situations, simulation experiments are carried out in the space chamber [*87*]. On the disturbing plate acting as the satellite or rocket body is applied a dc potential to get a disturbed region around it. In front of the disturbing plate two retarding potential traps are set, one is faced to the disturbing plate (front probe), the other is anti-faced to the disturbing plate (back probe.) The front probe is supposed to collect the electrons reflected from the disturbing plate, while the back probe to collect the incident electrons from the plasma region. The disturbing region was changed by changing the dc voltage applied to the plate.

One can see from the figure that if the voltage of the disturbing plate departs from the space potential, the "electron temperature" derived from the front probe is elevated. However it is strongly noted that the increase of the electron temperature is merely apparent. That is, as shown in Fig. 69b, the range of the linear part of the semilogarithmically plotted curve decreases as the potential of the disturbing plate departs from the space potential. The above fact presents an important conclusion that we are apt to everestimate the electron temperature because of the short range of the linearity of the semi-logarithmically plotted Langmuir curves as will be mentioned in 2.2 of chapter V. Therefore sensor electrode for the electron temperature measurement should be deployed into the undisturbed plasma. When the vehicle circumstance is widely disturbed, disturbed plasma region can be reduced by controlling the vehicle potential. The vehicle potential control will be easily done by emitting electron or ion beam from the vehicle.

2.5 *Deviation from the Maxwell energy distribution* [88]

The temperature of charged particles has a definite meaning when their energy distribution is maxwellian. We have a question, what happens if particles are not in the Maxwell distribution. Hoegy evaluated the above case and applied his conclusion to explain the discrepancy between the probe and the back scatter data. He assumed the isotropic electron distribution function $f(v)$, (*a*) as a sum of two Maxwell distributions at temperatures T_1 and T_2 with populations 1-p and p, respectively

$$f(v)=(1-p)\cdot\left(\frac{m}{2kT_1}\right)^{3/2}\exp\left(-mv^2/kT_1\right)+p\left(\frac{m}{2kT_2}\right)^{3/2}\exp\left(-mv^2/kT_2\right) \tag{33}$$

and (b) as a Laguerre polynomial expansion

$$f(v)=\left(\frac{m}{2\pi kT}\right)^{3/2}\exp\left(-mv^2/2kT\right)\cdot\sum_{l=0}^{\infty}A_l L_l^{(1/2)}\left(\frac{mv^2}{2kT}\right)\qquad A_0=1,\ A_1=0 \tag{34}$$

The thermodynamic electron temperature T_{th} is determined from the average energy of the entire electron population

$$3/2kT_{th}=\int dv\tfrac{1}{2}mv^2 f(v) \tag{35}$$

The radar backscatter electron temperature T_b [89] is defined as follows.

$$m/kT_b=\int dv(1/v^2)f(v) \tag{36}$$

and the probe temperature T_{plate} corresponds to the temperature measured by the ac mode Langmuir plate (Wrenn, 1969) [90]. This device measures the ratio of

the first to the second derivative of the electron current versus probe potential by operating in the ac mode.
Thus T_{plate} is defined by

$$T_{\text{plate}}=\frac{m}{k}\int_{(2eV/m)^{1/2}}^{\infty} vdvf/f(v)\left(\frac{2eV}{m}\right)^{1/2} \tag{37}$$

The temperature T_{cyl} corresponding to the temperature measured by the cylindrical electrostatic probe, which is determined from the best fit to the net current by a computer

$$i_{\text{net}}=C_1 \exp\left(-eV/kT_{cyl}\right)+C_2+C_3V \tag{38}$$

Shkarofsky [*91*] discussed the computer reduction problem described above in more detail. He evaluated cylindrical probes which are placed parallel (probe 1) and normal (probe 2) to satellite velocity vector. The ion current to probe 1 is always smaller in magnitude but exhibits a greater variation with applied voltage than in probe. 2. As the computer reduction using Eq. (38) assumes that the ion current can be accurately represented by a linear function of the probe voltage, the larger variation in probe 1 magnifies the non-linear variation of the ion current. This causes a higher temperature in general. Consequently perpendicular position was recommended.

The temperature T_{trap} corresponds to the temperature measured by the planar electron trap (Donley [*92*], 1969). This device measured the retarded electron current over a wide voltage range and thereby enables it to detect both the thermal and the energetic electrons
We define T_{trap} from the slope of *In i* versus V.

$$T_{\text{trap}}=\frac{m}{2k}\int_{(2eV/m)^{1/2}}^{\infty} vdv\left(v^2-\frac{2eV}{m}\right)f(v)\Big/\int_{(2eV/m)^{1/2}}^{\infty} vdvf(v) \tag{39}$$

In the figures, he included an evaluation of the degree of departure parameter L (Lunc [*93*]) in order to connect that distribution function with the degree of departure of the ionospheric electrons from the equilibrium.

The parameter L is defined by

$$L^2+1=\int dvf^2/f_{eq} \tag{40}$$

where f_{eq} is the equilibrium-distribution function. The state of the electron is considered far from the equilibrium when L is much greater than 1, close to equilibrium when L is much less than 1 and in a transition regime when L is close to 1.

2.6 Effect of a probe surface material

The Langmuir probe theory shows that the electron temperature and the density can be derived from the v-i characteristic curve, independently of the probe surface

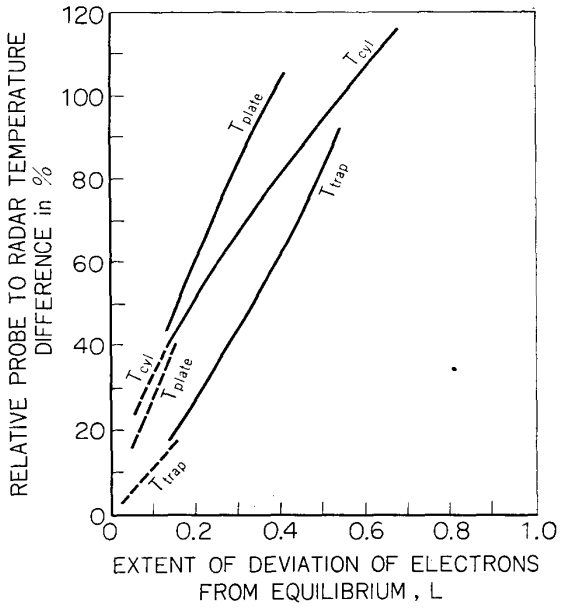

FIG. 70. Relative temperature difference between probe and radar (Hoegy [*88*]) correlated with the extent of deviation of electrons from equilibrium. Solid curves computed with polynomial expanded distribution; dashed curves computed with two temperature distribution.

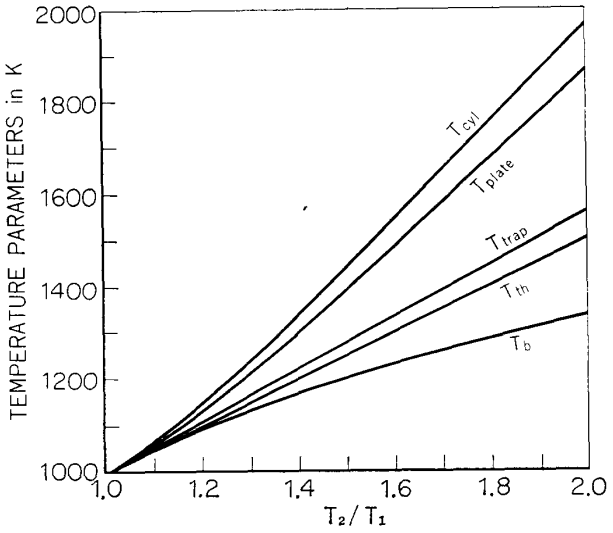

FIG. 71. Variation of the five temperature parameter with temperature ratio T_2/T_1.

material used. However it is not unworthy to check the effect of the probe surface material. According to the experiment made by L. H. Brace et al., they could not find any difference between electron temperatures obtained with various probes made of rhodium, stainless steel and platinum probe, concluding that surface material has little influence on the value of T_e derived. One of their conclusions is

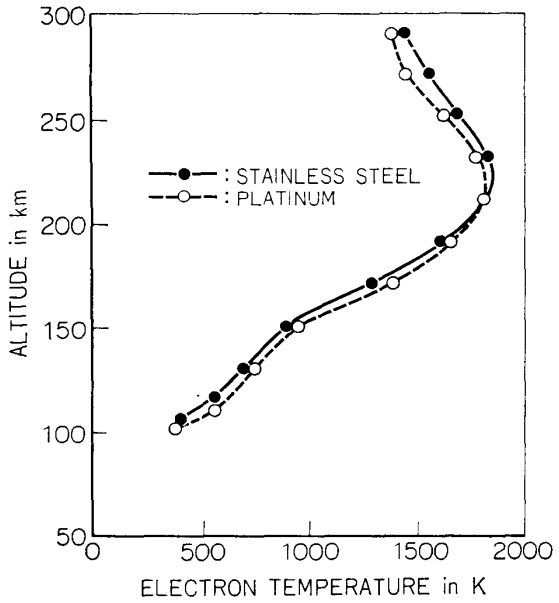

FIG. 72. Comparison of the electron temperatures obtained with stainless and platinum Langmuir probes (Brace et al. [109]).

illustrated in Fig. 72. We also made a simple comparison experiment with cylindrical probes made of copper, brass, stainless steel, aluminum and tungsten. The electron temperature evaluated from these probes agreed within a error of reduction.

2.7 Aerodynamical effects

Aerodynamic effect will become important only in the D-region where the mean free path becomes smaller than some typical rocket dimensions and a shock wave and its associated heating effects will appear. Smith [*65*] et al. noted a tendency in their nosetip probe experiments that the higher electron temperature is obtained in the ascent than in the descent of the rocket trajectory even in the E region, as due to aerodynamic effect. However we consider that it is rather explained by the cleaning effect of the contamination of a probe surface.

3. SOME OTHER SOURCES FOR THE ERRONEOUS EVALUATION

L. H. Brace et al. carried out systematic experiments for a probe reliability in the evaluation of electron temperature by the use of cylindrical Langmuir probe. In atempting to uncover and evaluate the sources of experimental error the following effects have been examined.

(1) the consistency of the volt-ampere curve with retarding potential theory
(2) the effect of collector geometry, by comparing data from different type of probes on the same satellite
(3) the effect of translational velocity, by comparing data from identical probes on rockets and satellite passing in close proximity

(4) the function of the guard electrode, by changing its potential from that of the collector during rocket flights
(5) the influence of photoemission from the spacecraft, by examining data obtained during the satellite traverses of earth's shadow under the conditions of very low electron concentration.

These investigations have failed to identify any of these factors as sources of error in the measurement of electron temperature. Those suggested, however, that in the E region altitude, the probe surface condition may influence the accuracy of the measurement. Although those could not confirm any of the above effect as a most serious cause, the probe surface contamination appears to be the most reasonable for the sources of experimental error and this is the objective of the present thesis.

Chapter V Present Problems and Their Solutions

1. Introduction

Since the frontier work of Reifman and Dow, the electron temperature has long been measured in the space plasma. However even now there exist confusions in the electron temperature measurement as described previously in preface. From 1959 to 1967 (Bogges, Brace and Spencer, 1959 [*5*]; Spencer, Brace and Carigman, 1962 [*94*]; Brace, Spencer and Carignan, 1963 [*95*]; Smith, Weeks and Mckinnon, 1968 [*65*]; Spencer, Brace, Carignan, Taeuch and Nieman, 1965 [*96*]), the electron temperature observed with Langmuir probe was 2 or 3 times higher than the neutral gas temperature in the ionospheric E region. However, backscatter data did not give such high electron temperature there (Carru, Petit and Waldteufel, 1967 [*97*]). In addition to this fact, a readily identifiable heat source for electrons could not be throught of. Therefore, some scientists doubted the reliability of the Langmuir probe. However, in the E region, the electron collision frequency evaluated from the radio wave absorption is higher than that from scattering cross sectional data and that from model atmosphere (Schlapp, 1959 [*98*]). As the electron collision frequency is nearly proportional to the electron temperature, observed collision frequency could be explained with the high electron temperature observed with Langmuir probe. This idea was also presented by Beynon and Owen Jones [*99*], Thrane and Piggot [*100*] (1966). Moreover, J.C.G. Walker tried to explain the high electron temperature in the E region as due to the vibration temperature of the nitrogen molecule (Walker, 1968 [*101*]). In spite of the efforts of many scientists the electron temperature in the E region still remains in question. The satellite observation also has the same type of problem since Hanson et al. reported the difference of electron temperature between radar and probe techniques.

In 1970, Carlson and Sayers [*63*] summarized many probe data. They surveyed the papers concerning the electron temperature measurement and suggested that the high electron temperature may be explained with the surface problem of a probe.

D. Smith [*64*] has expressed the similar opinion as above, which we mentioned in chapter III. Gradually the essential point of the problems seems to be forcussed. Their general and certain conclusion drawn from various past experiments is that an ac mode Langmuir probe [*102*] such as ion probe on the Explore 31 or the electron temperature probe on ESRO-1A and Ariel 1 satellites gives a good coincidence with the incoherent backscatter value. The coincidence of the temperatures obtained from ac mode probe and that from another technique, such as a radar technique seems to support the theory that the confusion which has been discussed for a long time is caused by uses of a contaminated Langmuir probe and retarding potential trap. In this chapter problems accompanied with the measurement of charged particle temperature are discussed mainly from the point of probe surface contamination, standing on the opinion that various discrepancies reported by many scientists have been caused by the contaminated Langmuir probe. The chapter first summarizes the discrepancies caused by a dc mode Langmuir probe and then discuss the ac mode Langmuir probe which appears to give a correct temperature.

2. Informations from dc Langmuir probe

2.1 Electron temperature in the lower ionosphere

The electron temperature in the lower ionosphere has been measured almost mainly by the use of dc and ac mode Langmuir probes. The dc mode Langmuir probe is the probe from whose v-i characteristic curve plasma parameters such as the electron density and temperature can be evaluated. The dumbel probe [*5*], the nose tip probe [*65*], the thermospheric probe [*94*] and the retarding potential trap may be grouped in this classification. While the principle of the ac mode probe is that the electron temperature or density is obtained by detecting the distorted probe signal caused by the non-linearity of a sheath. The remarkable point of the ac mode Langmuir probe is free from the contamination effect of a probe surface. The rapid sweeping DC Langmuir probe will be situated in an intermediate place between dc mode and ac mode probes. In Fig. 73, the electron temperature profiles which have been observed with the probes described above are summarized for the midlatitude ionospheric observation.

In an equatorial region or a low latitude region, electron temperature profiles in the lower ionosphere observed by in-situ probe method seems to be quite few so far as we know, though a large number of electron temperature profiles have been obtained by the backscatter technique above 200 km [*26*]. In the neighbourhood of an aurora and in the auroral zone, additional heating processes are likely to modify the lower ionospheric temperature in general. Since large amount of energy are certainly available in the production of aurorae and the associated high latitude current system, some part of these energy is likely to be dissipated as ionospheric heating source. Further, data obtained in this region are quite few. Therefore we will not pick up the above region and we will limit our discussion to

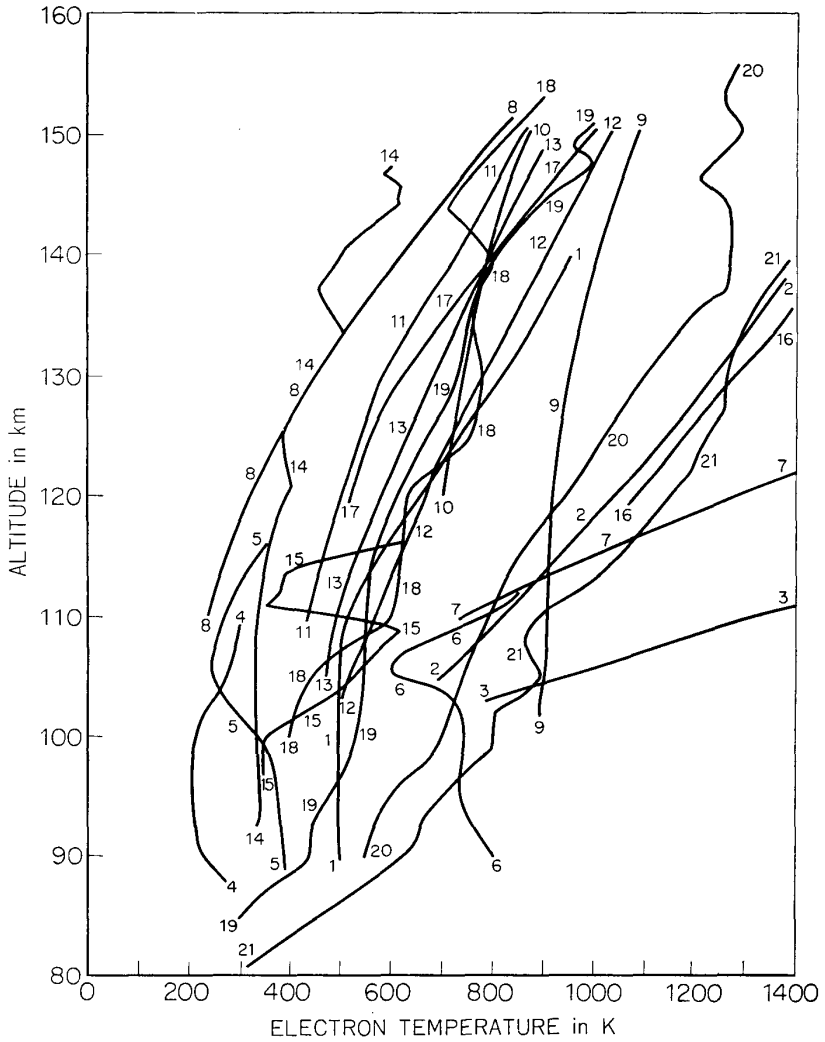

FIG. 73. Electron temperature profiles in the midlatitude ionospheric *E* region observed by means of Langmuir probe.

the electron temperature in middle latitude. The observers and the probes used for the observations are listed in Table 6. In the Fig. 73, one can see the serious scattering of the values. Especially profiles indicated at 2, 3, 6, 7, 9, 16, 20, and 21 show abnormally high temperature. Whilst past neutral temperature experiments [*72*, *73*] show that neutral temperature ranges from about 300°K to 1000°K between 115 km and 150 km. Further, theory shows that electron and neutral particles are in thermal equilibrium under only one heat source of solar E.U.V., because electrons lose most of their energy via elastic and inelastic collisions with neutral particles and consequently have almost the same temperature in the lower ionosphere. Therefore almost all the results shown in Fig. 73 give conclusively too high electron temperature, especially around 100 km. In order to recognize such a high temperature, we must assume extremely high energy source besides the solar E.U.V. heat source. In addition to the above consideration, backscatter data will give useful information for the comparison study. The backscatter

TABLE 6. List of the electron temperature profiles.

Data No.	Date	Time (L.T)	Place	Observer	$F_{10.7}$	*Remarks
1	'66.11.12	13 : 00	Cassino	Smith	128.9	1
2	'67. 1.31	13 : 50	Wallops	Smith	161.9	1
3	'66. 6.14	04 : 18	Wallops	Smith	93.9	1
4	'65.11.10	22 : 10	Eglin	Sagalyn		2
5	'65.11.17	23 : 20	Eglin	Sagalyn		2
6	'65.11.16	12 : 22	Eglin	Sagalyn		2
7	'60. 8. 3	11 : 26	Wallops	Brace	142	3
8	'61. 4.26	11 : 56	Wallops	Brace	121	3
9	'63. 4.18	16 : 04	Wallops	Brace	88	4
10	'63. 7.20	16 : 54	Wallops	Brace	77	4
11	'68. 3.17	15 : 30	Arecibo	Brace	136.6	4
12	'70. 3. 7	13 : 00	Wallops	Brace	171	4
13	'70. 3. 7	13 : 27	Wallops	Brace	171	4
14	'64. 9. 5	16 : 30	Hammaguir	Aubry		5
15	'64. 9. 7	16 : 42	Hummaguir	Aubry		5
16	'66. 3. 2	12 : 59	Wallops	Brace et al.	78	4
17	'69. 4. 3	10 : 35	Woomera	Timothy	189.8	5
18	'68. 3.30	10 : 57	Volgograd	Andreyeva	160	6
19	'69. 1.21	11 : 00	Volgograd	Andreyeva	136.3	6
20	'69. 1.23	14 : 59	Volgograd	Andreyeva	128.8	6
21	'69. 7.10	11 : 04	Volgograd	Andreyeva	159.0	6

* Probes used are (1) nose tip probe, (2) retarding potential trap, (3) Dumbel probe (4) cylinder probe in "thermospheric probe", (5) ac mode Langmuir probe, (6) dc Langmuir probe.

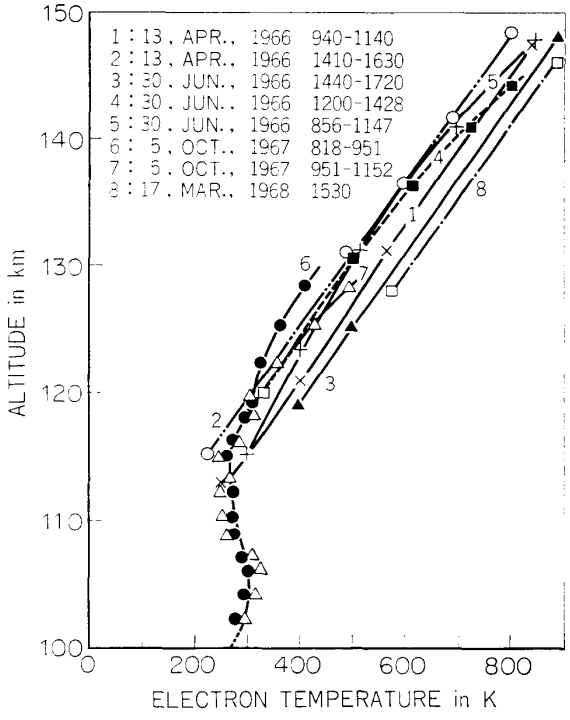

FIG. 74. Electron temperature profiles given by backscatter technique.

technique has some difficulties below 120 km in determining the electron and ion temperatures because of collisional effects. Inevitably quite a small amount of data in these ionospheric region has been reported, which are summarized in Fig. 74. The wavy structure of the curve in the figure observed over Arecibo at around 115 km looks quite meaningful in relation to the high electron temperature reported in the 1st and 3rd chapters, but we don't mention about them here further. General profile obtained with radar technique shows about 300°K around 115 km and gradual increase up to 150 km which is close to the neutral temperature, whilst Langmuir probe shows basically the value ranging from 300°K to 600°K at 115 km and 1000°K at 150 km. Therefore the comparison with Langmuir probe results, though indirect, shows doubtlessly large difference of the electron temperature especially below 120 km.

In chapter III, we showed that Langmuir probe can't give a correct electron temperature at all in usual use. Therefore we may conclude that the discrepancy in ionospheric E region should be first of all attributed to the use of a contaminated Langmuir probe.

2.2 *Simultaneous comparison between the rocket probe and the radar techniques*

Brace [*103*] et al. discussed the discrepancy of the electron temperature by using simultaneous comparison experiments with a rocket and backscatter technique. The results obtained from the comparison studies show a remarkably good agreement in the daytime flight and small disagreement in the night; the electron temperature obtained with the probe technique showing approximately the value interpolated from the radar profiles taken about 25 minutes before and after flights, whilst the night time electron temperature were systematically 10–15% higher than radar results. The altitude range of comparison experiments was 130–290 km in the day and 210–290 km at night. Evans [*104*] also reported the similar results, namely a general coincidence of daytime electron temperatures and small amount of nighttime discrepancy reported by Brace et al. Willmore [*105*] suggested that the discrepancy may be explained by considering the fluctuation of that order in the radar technique.

When we look the above discrepancy from the Langmuir probe measurement, contamination effect of the probe can't explain the discrepancy; contaminated probe gives higher electron temperature in higher density plasma. If the discrepancy is due to the contamination, it must be larger during daytime than at night.

2.3 *Satellite probe and backscatter observation*

The comparison but not simultaneous study made by Evans [*104*] shows that the electron temperature measured by Langmuir probe and the backscatter technique agrees well in daytime, while the average of T_e by the probe is about 20% higher than Millstone radar's monthly average value at night. To our regret the measurement used in the comparison were not simultaneous as described above.

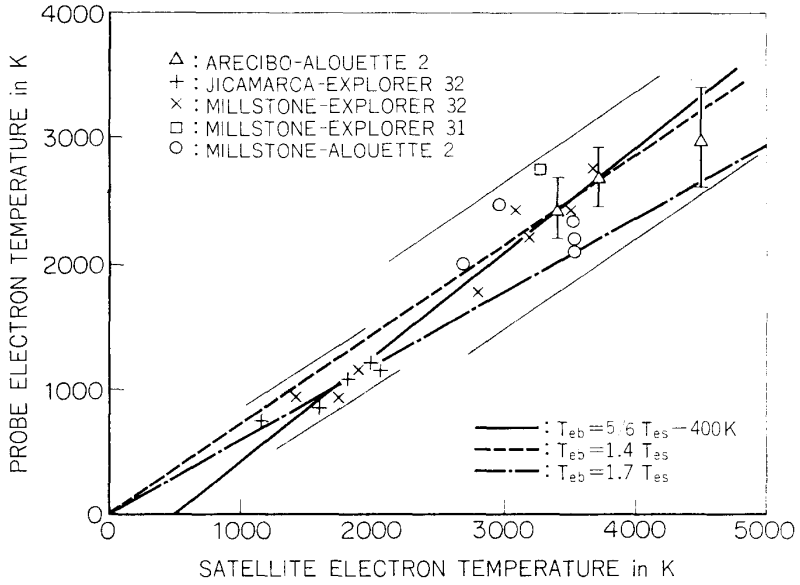

FIG. 75. Comparison of electron temperatures simultaneously measured with satellite probes and backscatter technique.

The first simultaneous attempt to compare probe and incoherent scatter observations was that of Hanson et al. [*106*], using the Explorer 31 passing near the incoherent scatter radar station at Jicamarca. A comparison of the electron temperatures obtained during 5 passes of the satellite distributed in different local time showed the probe results on T_e to be systematically higher by the factor of 1.7 than the backscatter results.

Booker and Smith [*107*] have compared cylindrical probe results (T_{es}) from Explorer 31, 32, and Alouette 2 with incoherent scatter values (T_{eb}) of T_e taken simultaneously at Jicamarca, Arecibo and Millstone Hill and have concluded that the relation between these is $T_{eb}=0.84T_{es}-400$. As for the relation, Carlson and Sayers suggested that the linear relation of T_{eb} and T_{es} may be a useful clue to solve the discrepancy. Furthermore McClure et al. [*108*] reported a similar comparison made by using the retarding potential trap analyzer. The Ogo. 4 and radar T_e measurements conflict by a factor of 1.4 or more in some cases, that is, $T_{es}=1.4_{eb}$. In Figure 75, both relations $T_{es}=1.4T_{eb}$, $T_{es}=1.7T_{eb}$ and $T_{eb}=0.84T_{es}-400°$ are drawn for comparison. It is noted that these equalities will be valid above 1000°K because data were obtained in satellite altitude where charged particle temperatures are more than 1000°K.

2.4 Comparison with rocket and satellite probes

L. H. Brace et al. [*109*] compared the rocket data with satellite one in conjunction with nearby passages of the four satellites. The same type of cylindrical Langmuir probes are carried on both rocket and satellite. The collector of the cylindrical probe is 23 cm long and 0.56 mm in diameter and is usually made of either stainless steel, rhodium, or platinum. A guard electrode of similar length

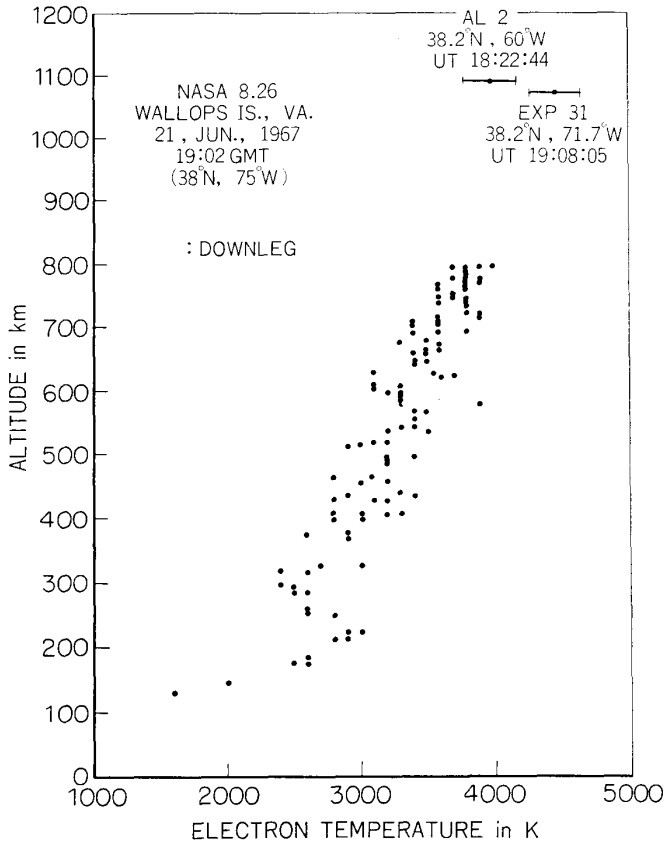

FIG. 76. Comparison of rocket and satellite probe measurements from NASA 8.26 and Explorer 31-Alouette 2. (Brace et al. [*109*]).

covers the collector in the near vicinity of the spacecraft where the plasma properties may be significantly changed from the ambient plasma. The probe is impressed by a sawtooth wave voltage three times per second in rocket. The probe current is recorded by linear detectors having several ranges of current sensitivity. In Fig. 76 are shown the obtained rocket profiles of T_e and the single value of T_e derived from the satellite probe (or probes) described above at closest approach to the rocket path. The agreement between rocket and satellite probes seems to be within an acceptable limit, the differences being 10%. Brace suggested that the comparison tends to show poorer agreement than those made at higher altitude. In addition to the above, the semi-logarithmically plotted Langmuir curve has a very good linear part, which generally means that the electron energy distribution is maxwellian. Therefore they concluded that Langmuir probe is free from faults to cause the discrepancy reported by many authors. Nevertheless, when this value is compared with the incoherent backscatter data, it is found that the electron temperature obtained with Langmuir probe is higher than the incoherent backscatter data. The above fact may be easily understood by considering that even when the probe surface is contaminated, the semi-logarithmically plotted Langmuir curve obtained from it will be linear as will be shown in Fig. 78.

In the experiment they also payed attention to the probe surface study. The satellite had been launched from several weeks to several months earlier, whilst the rocket was in the ionosphere for 5–10 minutes. Because they couldn't find any serious discrepancy between satellite and rocket data, they concluded that the effect of the exposure of the probe and space craft to the space environment seems not to be so large. However we can argue against their opinion by showing that the probe contamination is quite difficult to be taken off from the probe surface even in laboratory experiments. The surface cleaning in the space may be carried out to some extent by the exposure to the E.U.V. but not so effective even for a long time. Therefore the surface condition will not change for a very long time. Brace's result that the electron temperature coincides with each other in probe measurement seems to verify unremovable contamination effect in spite of their conclusion. Further the fact that the comparison at a low altitude tends to show poorer agreement than those at a higher altitude seems to be one of the evidences that the discrepancy is caused by a contaminated Langmuir probe, because the fact itself can be explained as "Density dependence of a hysteresis curve".

2.5 *Intercomparison of the probe data between two satellites* [*110*]

The combined launch of the two spacecrafts, Explorer 31 and Alouette 2 satellites provided an excellent opportunity for the comparison study of plasma parameter measurement. In such a satellite-satellite comparison, Brace and Findlay have reported that an agreement between identical cylindrical probes on Explorer 31 and Alouette 2 was generally better than 10%. The probe bias is swept from −3 V to 10.5 V in every 0.7 sec for Alouette 2 and −1.7 V to 5.1 V in 1.26 sec for Explorer 31. These two satellites were placed in orbit by the same vehicle and separated slowly to carry out combined mission for ionospheric studies. An example of the agreements between two sets of the probe measurement is shown in Fig. 77. The linearity of the semi-logarithmically plotted curve is apparently satisfactory enough to let them consider that the electrons are in good Maxwell distribution. In the region of the probe potential of $7\,kT_e$, the plotted curve is quite linear (Fig. 78). Taking the above fact into consideration, we are tempted to conclude that Langmuir probe has no wrong point. However, when we compare the results obtained by the different methods such as wave phenomenon in Aloutte 2 and the incoherent scatter technique, Langmuir probe is reported to give the higher electron temperature than that of another. Further details will be given in the next section.

2.6 *Intercomparison of the data obtained with different methods on satellite* [*111, 112*]

Explorer 31 was instrumented with many kinds of direct measurement probes which provided measurements of the major ionospheric parameters through different techniques. Probes are of the planar ion trap, the planar electron trap, the planar Langmuir plate, and the spherical ion probe. Among the probes employed,

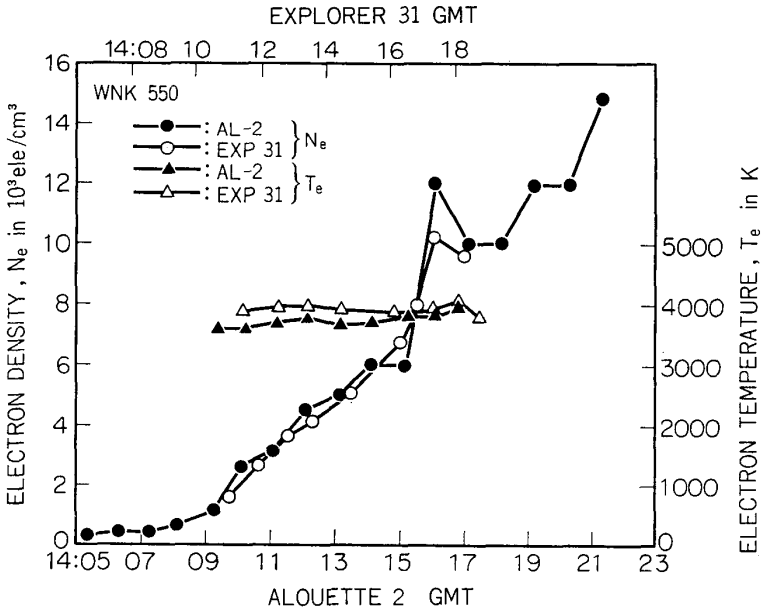

FIG. 77. An example of the agreement between identical probes on Explorer 31 and Alouette 2. (Brace et al. [*109*]) Alternate points from Explorer 31 were obtained with independent but identical cylindrical probes.

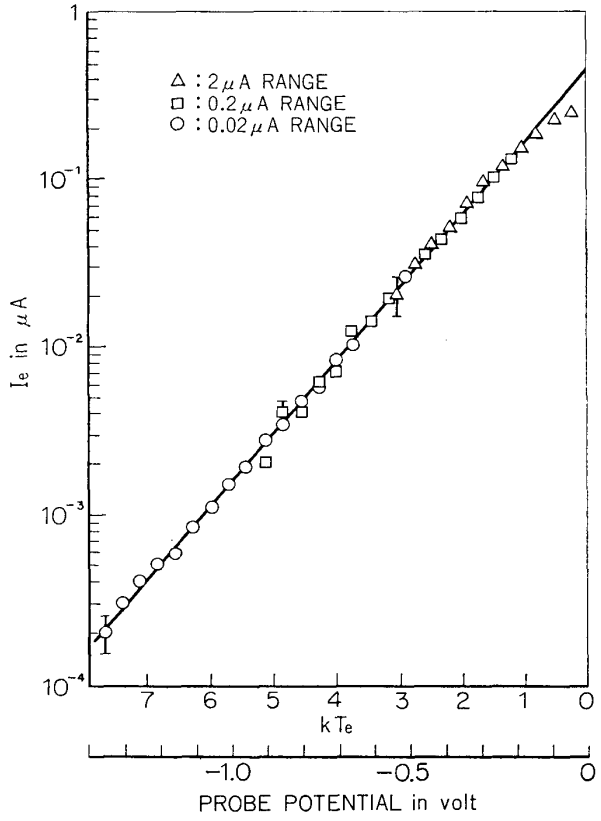

FIG. 78. Evaluation of ionospheric electron temperature measurement by cylindrical electrostatic probe (Brace et al. [*109*]).

FIG. 79. Electron density dependence of the temperature difference (Donley et al. [*110*]).

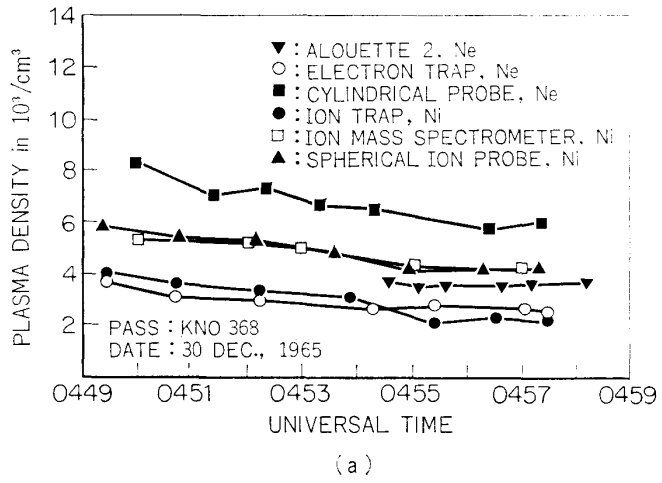

a. Plasma density measurements for the KNO 368 pass on December 30, 1965. Values from the cylindrical probe are up to 60 percent high and values from the ion and electron trap are up to 40 percent low with respect to Aloutte 2 density measurement.

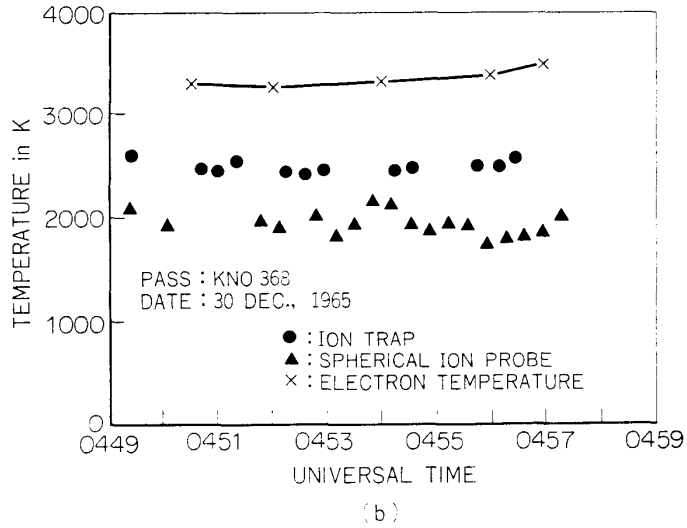

b. Hydrogen ion temperature measurements for KNO 368 pass. Mean electron temperature is also shown.

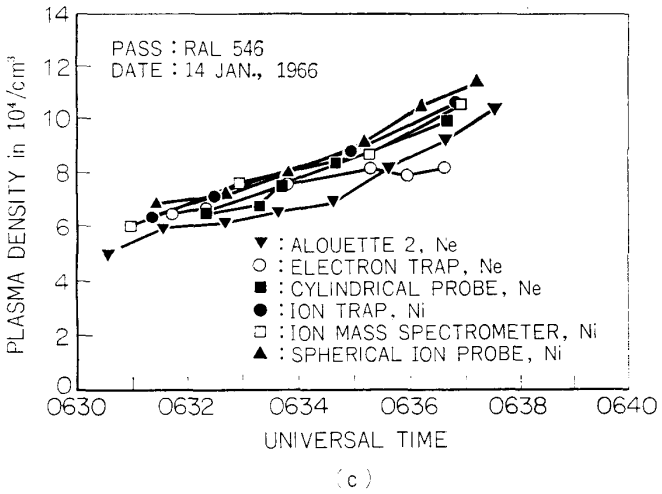

c. Plasma density measurements for the RAL 546 pass on January 14, 1966. Individual data points are connected by straight line.

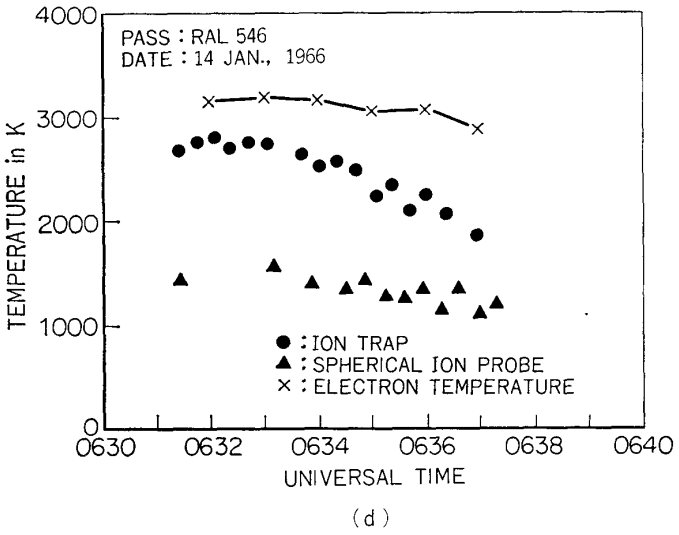

d. Oxygen ion temperature measurements for the RAL 546 pass.

the ion trap, the electron trap, and the Langmuir plate were mounted to the statellite skin. The cylindrical electrostatic probes and the spherical ion probe were mounted on short booms ejected about one foot from the satellite surface. Preliminary results are shown in Figs. 79 a, b, c, and d. In the figures, two observing passes are set in pairs, where the plasma temperature and density are stimultaneously observed. From the figures, one can see a clear difference between three probes in WNK 546 pass and RAL 368 pass. As for the ion temperature, one from the spherical ion probe is lower than that from the ion trap. The difference may be explained by the contamination of the electrode surface, considering that the ion probe operated in the ac mode is not affected by the contamination layer.

In the comparison of Figures 79 b and d, it is generally recognized that the difference of the ion temperatures from two instruments in larger in RAL 546 pass than in KNO 368 pass. In other words, in lower plasma density the ion temperature observed with ion trap approaches to the ion temperature obtained from ion probe. Therefore above two facts seem to show two natures accompanied with contamination effect, frequency and density dependences.

2.7 *Conflict of the data by retarding potential trap* [*113, 114*]

Up to now, the discussion is mainly pointed to the discrepancy which appeared in Langmuir probe measurement. However as we mentioned in section 2.3 of this chapter, measurements with the retarding potential trap (R.P.T.) has a problem similar to Langmuir probe experiments. McClure et al. [*108*] reported from the Ogo. 4 experiments that the ion temperature obtained with R.P.T. is 1.4 times higher than that from the backscatter technique which was simultaneously observed. One of the example of the discrepancies is shown in Fig. 80. They could not find an evidence of a non-maxwellian ion energy distribution in an examination of data. They suggested also the possibility of the geophysical discrepancy but could not find any reason for this. If the conflict is caused by the penetrating electric field of the electrode which has already been discussed by Hanson et al.,

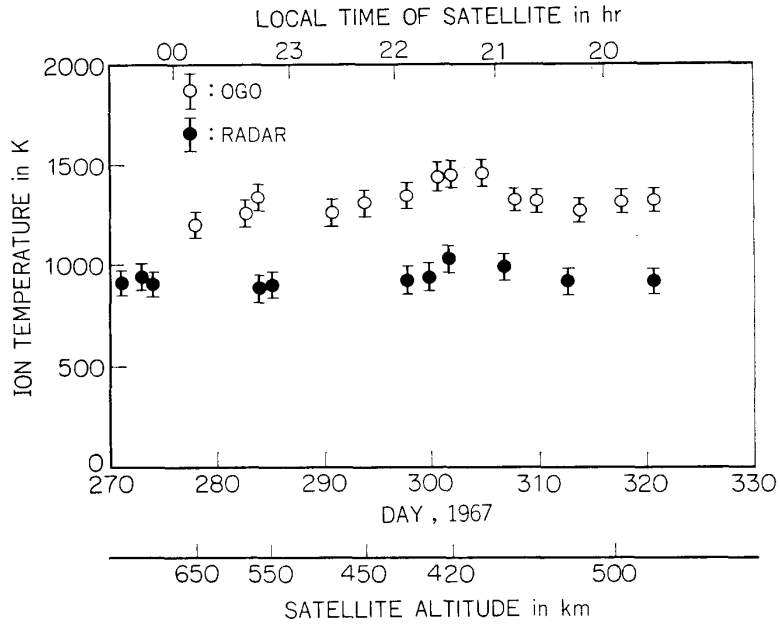

FIG. 80. Conflicting radar and satellite values of T_i. (McClure [*108*])

the ion temperature by retarding potential trap will be 15% less than that observed. By reducing the value in 15%, the corrected R.P.T. value must coincide with the radar value if the backscatter technique is assumed to give a correct value. However observed value is much higher than the theoretical value which is calculated by taking the penetrating electric field into consideration. Therefore the discrepancy can not be explained by the effect of penetrating electric field.

Goldan et al. [*82*] tried to explain the discrepancy reported by McClure et al. in Ogo. 4 to be due to the non-uniformity of the grid plane potential. But we can find a good consistency of the temperature in another observation of Ogo. 4. Fig. 81a shows the ion and electron temperatures obtained on Ogo. 4 and those observed at Jicamarca radar observatory simultaneously on 29 Oct. 1967. The two temperatures measured are 1450°K for the retarding potential trap and 1030°K for the backscatter value in the density of 2×10^6 el/cc and their difference is quite clear as reported by McClure et al. On the other hand in the data obtained by Chandra et al. [*115*] on 18 Sept. 1967 (Fig. 81 b), the ion temperature observed on satellite is 1000°K in the density of 2×10^4 el/cc, whilst the radar value, though not simultaneously obtained, is considered slightly more than 900°K. Consistency of the last two temperatures seems to be pretty good, though a little discrepancy is still found. The above fact shows that the R.P.T. on Ogo. 4 does not always indicate a discrepancy. Although it may be quite reckless to draw a conclusion only from two data, the comparison of two observations shows that the disparity appears in rather high plasma concentration. In the 2nd chapter we mentioned the density dependence of the contamination effect, that is, the contamination effect appears as the increase of plasma density. Therefore the feature of Ogo. 4 measurement appears to show the density dependence of the contamination effect.

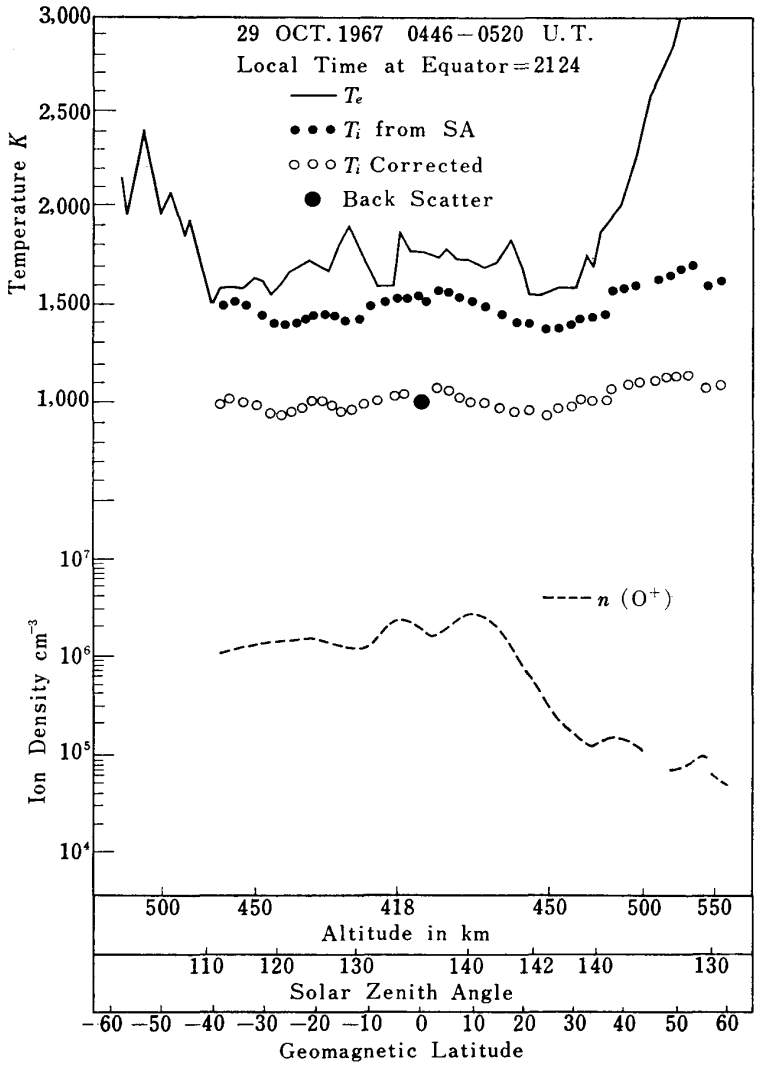

FIG. 81a. Equatorial T_i and N_i values from Ogo. 4 passes on 29 Oct. 1967. The corresponding J.R.O. T_i value is also shown in this figure. Satellite data lowered as 32% of the original value are also indicated.

The surprising coincidence of Ogo. 6 [*116*] (Fig. 82), which is mainly observed in winter night time is also explained in the same way. Although the electron density is not always clear in the paper, the density of winter night time is the lowest among a year. For example in 15 Nov. 1969 when the observation is carried out, the electron density is about 3×15^5 el/cc at 22:00 in the height of 450 Km over Jicamarca. This value is nearly 10 times lower than that of 29 Oct. 1967 when the discrepancy of Ogo. 4 was reported. As almost all the observations were carried out later than 22:00, the plasma density will not have the drastic decrease and keep the same order as described above. Therefore, it is easily considered that the value obtained by the retarding potential trap is close to the correct temperature.

As illustrated in Fig. 81, the ion temperature observed on Ogo. 4 on 29 Oct. 1967 can be fitted to the backscatter value by reducing the original satellite value as 32% according to the evaluation made by Goldan et al. who emphasized the

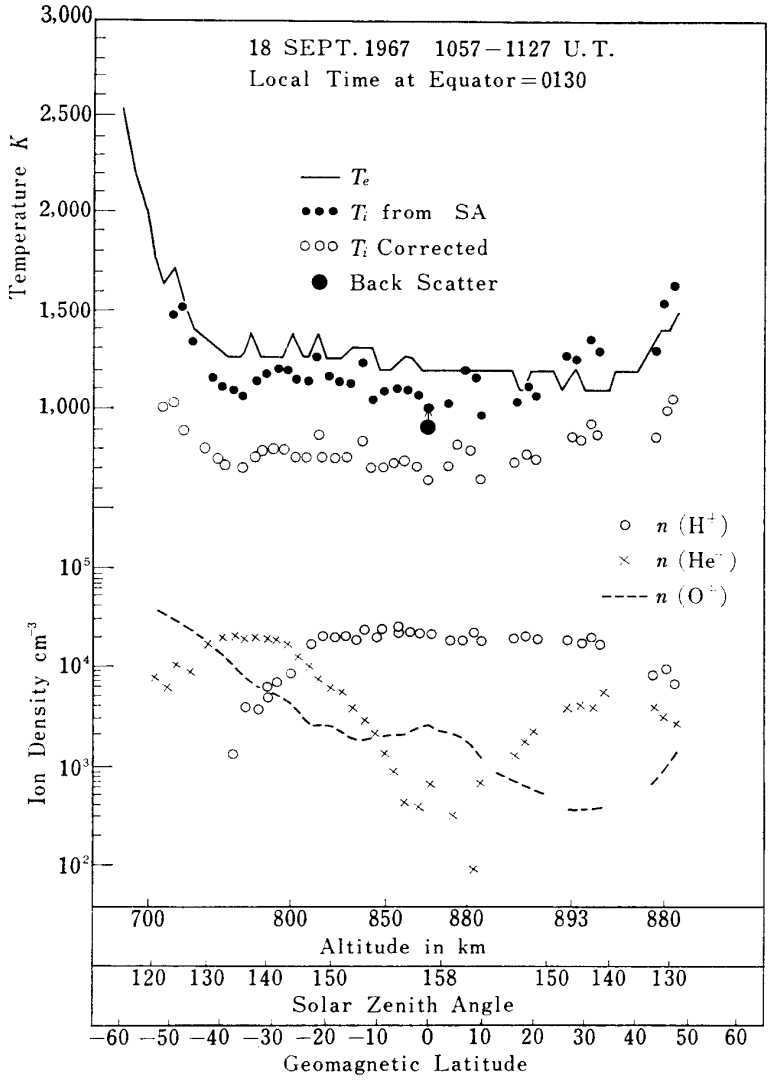

FIG. 81b. Equatorial T_i and N_i value from Ogo. 4 passes on 18 Sep. 1967. The corresponding reasonably assumed T_i value is also shown. Satellite data lowered at 32% of the original value are also indicated.

non-uniformity effect of the grid potential plane. However if the same correction is applied to the 18 Sept. 1967, the R.P.T. data is 200°K lower than the back scatter value, being too low to exist. Therefore the effect by the non-uniformity of the grid potential plane can not explain all the Ogo. 4 data. In summarizing all the above facts, it seems to be quite reasonable that the discrepancy is caused by the contamination of the electrodes.

3. OBSERVATION BY AC MODE LANGMUIR PROBE

In the previous section, we showed mainly the discrepancy between electron temperatures measured with the dc mode Langmuir probe and the incoherent back-scatter technique. Whilst this section summarizes the general agreement between

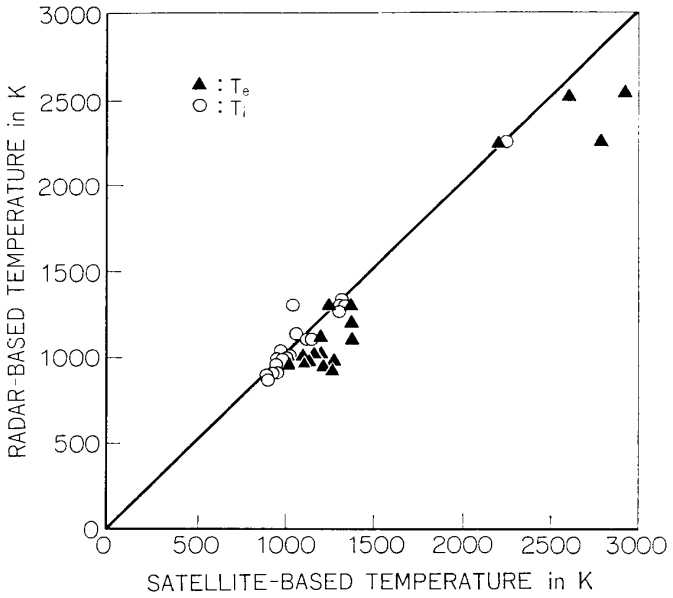

FIG. 82. Good agreement between radar-based and satellite-based T_e (Triangles) and T_i (circles) observed in Ogo. 6. The average satellite to radar temperature ratio $T_{es}/T_{eb}=1.15$ (McClure et al. [*116*]).

the values derived from the ac mode Langmuir probe and the radar technique.

In the rocket experiment, quite few data were given by the ac mode Langmuir probe except ours, as was described in the 3rd chapter. Although we can not precisely identify the validity of these data, the values appear to be quite reasonable looking from the geophysical point of view. The electron temperature which was measured by Aubry et al. by means of the ac mode Langmuir probe is very close to the model neutral temperature around 100 Km. Further, concerning our results obtained at K.S.C. with E.T. probe, the data are quite reasonable as has already been discussed in the 3rd chapter. Therefore we can conclude that the ac mode Langmuir probe in rocket experiments gives reasonable results. Whilst in satellite experiments, we have more data than in rocket experiments. The problem of discrepancy which was first presented by Hanson et al. for satellite dc probes in 1965 [*105*] seemed to get one clue for the solution when Taylor and Wrenn [*112*] reported the agreement of the charged particles temperatures observed with the ac mode probe with those with the backscatter technique. They compared the electron and ion temperatures observed with the ac mode Langmuir probe of Explorer 31 and the incoherent scatter radar at Malvern, England (5.1°N, 2.3°W) during a period of about 2 months in October/December 1968. There was in fact agreeent between the results from two techniques as shown in Fig. 83.

Donley et al. (1969) compared results from all the electron temperature probes on Explorer 31 and concluded from the five passes that the slow sweep cylindrical probe indicated typically higher values and the modulation Langmuir probe gave typically lower values than the mean temperature data of these three probes used.

In 1973 Wrenn et al. reported the coincidence of electron temperatures from Explorer 31 and ESRO-1A modulation probe with the backscatter value. The

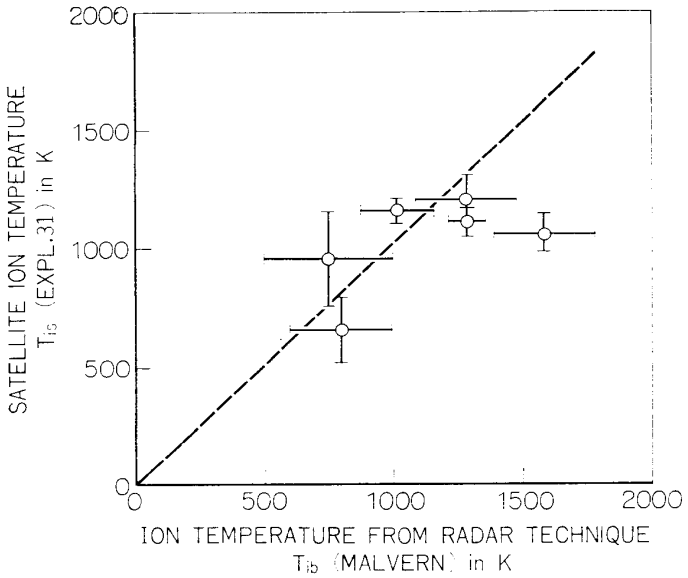

FIG. 83. Ion temperature from the ac mode ion probe T_{is} (Exp. 31) and the radar technique T_{ib} (Malvern). (Taylor et al. [*113*])

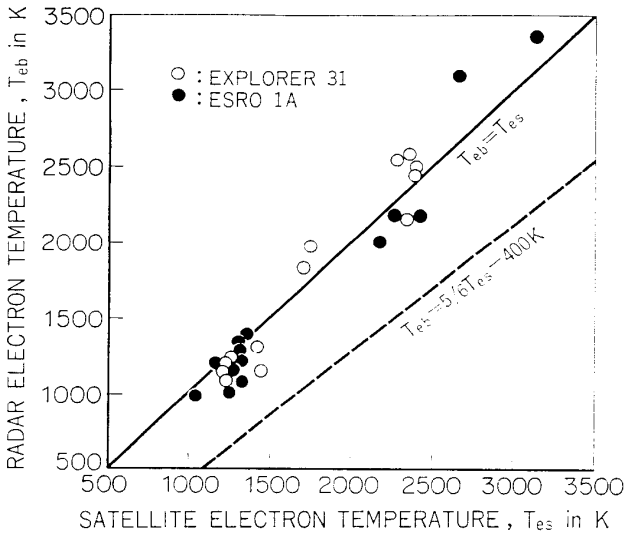

FIG. 84. Comparison of electron temperature measured simultaneously by modulation Langmuir probes and incoherent scatter radars (Wrenn et al. [*102*]).

temperature obtained from the Explorer 31 modulation probe was compared with radar measurements from Arecibo, Millstone Hill, St. Santin and Malvern. (Arecibo, Jicamarca and Millstone Hill were the stations where the systematic temperature discrepancy had been found for the slow sweep probe). The results of these new comparisons are shown in Fig. 84 together with the Explorer 31-Malvern data previously published. We can see that almost all the modulation probe temperature values show a fit of $T_{eb}=T_{es}$ within their errors.

When we look at these results described above under the assumption that the discrepancy is due to the contamination layer, we can easily understand that the

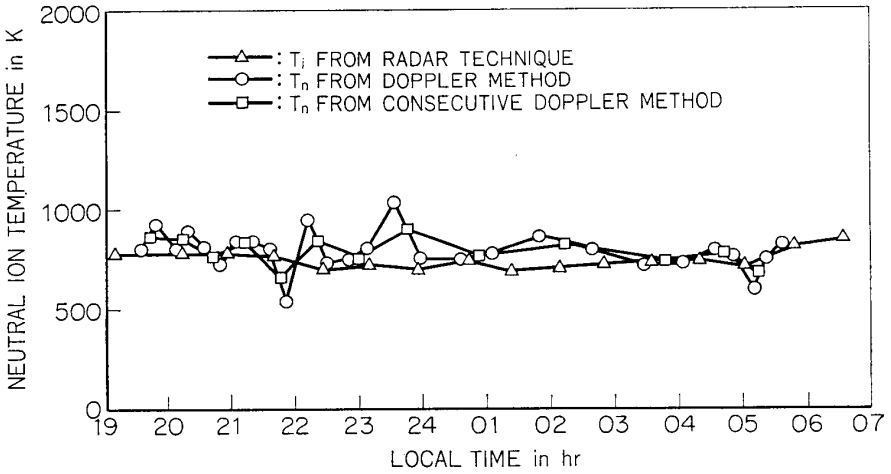

FIG. 85. Doppler and backscatter temperatures measured during the night of October 14–15, 1969. (Hays et al. [*117*]).
The triangles indicate the ion temperature measured at an altitude of 300 Km above Millstone Hill. The circles denote temperatures deduced from individual Doppler profiles. The squares correspond to temperatures obtained when two consecutive Doppler profiles are combined.

slow sweep Langmuir probe gives errors and higher temperatures than true values and the modulation Langmuir probe can give a correct electron or ion temperatures.

4. VALIDITY OF THE BACKSCATTER TECHNIQUE

In the present paper all discussions have been made by comparing with the value obtained by the backscatter technique, assuming that the backscatter technique gives a correct information. It will be useful to check this assumption in order to persuade that the ac mode Langmuir probe gives a correct ion and electron temperatures.

Hays et al. [*117*] compared the neutral temperature from the Doppler broadening of the 6300 A atomic oxygen emission observed at the Michigan Airglow Observatory (42°17′N 84°W) and the ion temperature measured by the Millstone Hill radar (42°30′N 72°W). The comparison seems useful and meaningful to check the validity of the incoherent backscatter data, for it is considered that near 300 Km at night there should little difference between the ion and neutral temperatures when there is no goemagnetic disturbance as well as travelling ionospheric disturbances. The general agreement between the above-mentioned two temperatures is complete as shown in Fig. 85. Averaging the temperature values over night leads to a mean Doppler temperature of 790°K, whereas the mean backscatter temperature of 740°K. This corresponds to a difference of 5.7% which is well within the limits of accuracy of these two experiments.

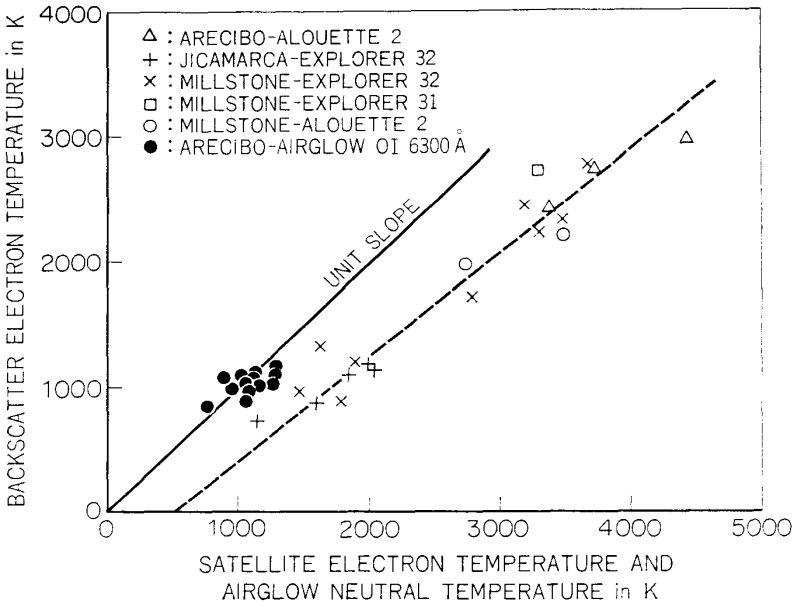

FIG. 86. Comparison of the airglow [0I] 6300-A neutral temperature with backscatter electron temperature (solid line) at night. $T_e=T_i=T_n$. Also shown are some results of satellite-radar backscatter electron temperature comparisons (dashed line) (Carlson et al. [*63*]).

One of the indirect evidences comes from the comparison of electron temperatures derived from the incoherent backscatter technique and the neutral temperature from Doppler broadening. In the same reason described above, when there is little or no energy input from protonosphere into the F region at night, the ion, electron and neutral temperatures at a given height should be equal. Thus the temperature by Doppler broadening of air glow can be directly compared with ion and electron temperatures obtained from the radar backscatter technique. Therefore the validity of the electron temperature obtained with the backscatter technique can be tested by the comparison with the neutral temperature by Doppler broadening.

Fig. 86 shows the result by Cogger et al. [*118*] obtained at Arecibo, Puerto Rico in 1969 and 1970, which shows a very good coincidence between the electron temperature from the incoherent backscatter technique and the neutral temperature from Doppler broadening of 6300 air glow; the 11% rms deviation is no greater than the expected scatter. However one point should be kept in mind. As described above on night time energetics, electrons and neutrals are generally considered to be in thermal equilibrium and this opinion is generally accepted. Nevertheless slight deviation of the electron temperature from the neutral temperature is found when the intensity of the solar radio flux is low as was described in chapter III. The deviation tends to increase according to the decrease of the solar radio flux intensity. Therefore strictly speaking, results obtained by Cogger et al. has a debatable point although the difference between two temperatures may be too small to discuss the validity of radar technique.

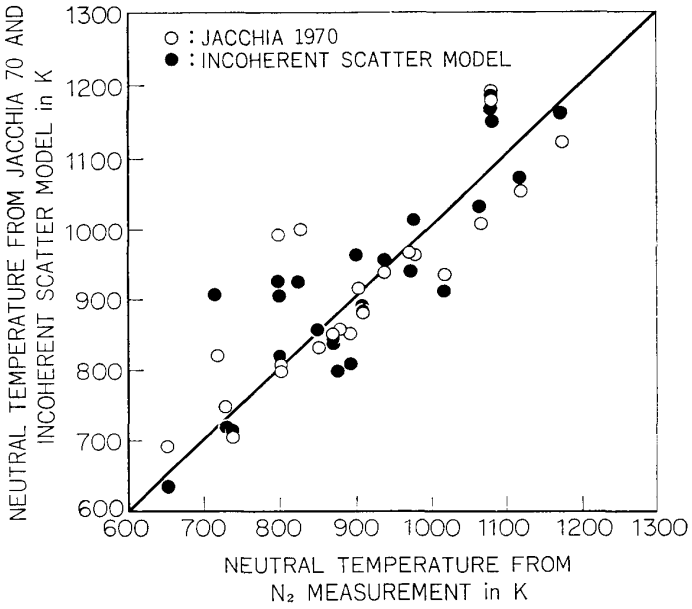

FIG. 87. A comparison of exospheric temperature from the incoherent scatter model and from the Jacchia 1970 model compared with the rocket measurement. (Waldteufel [*121*]).

Another results seems to show the validity of the backscatter technique from the neutral temperature measurement. The neutral temperature is indirectly obtained by measuring ion and electron temperatures with the backscatter technique by the use of the energy balance equation $L_{ei}=L_{in}$. Waldteufel and Cogger [*119*] examined the behaviour of the neutral temperature deduced from the data obtained at Arecibo from 1965 to 1970. The result was compared with Jacchia 70 (J70) and 65 model atmospheres which were summarized empirically from satellite air drag experiments. The comparison study of the data obtained in March 26/27, 1968 shows that observed temperature maximum and minimum of a diurnal variation are 1350°K at 1600 hrs and 850°K at 04 hrs, respectively, whilst J70 model shows 1250°K at 14 hrs and 1000°K at 02 hrs, respectively. Although the observed amplitude of the diurnal variation is definitely around 250°K larger than J70 model and the time of maximum temperature is different (for model temperature at 14 hrs and for incoherent backscatter at 16 hrs or later), the temperature deviation from the model atmosphere is too small to discuss the satellite discrepancy.

Waldteufle further constructed a global model based upon exospheric temperature measurements at St. Santin and Arecibo and compared the values predicted from this model with a series of thermospheric temperatures inferred from the scale height of in-situ nitrogen density measurements [*120*] obtained between 1962 and 1968. This comparison [*121*] is shown in Fig. 87. Finally atomic oxygen concentration values at 400 Km altitude were measured at St. Santin during a 5 day period in February 1969 by a technique developed by Bauer et al. [*122*] These values are compared with the atmospheric density deduced from the satellite orbit

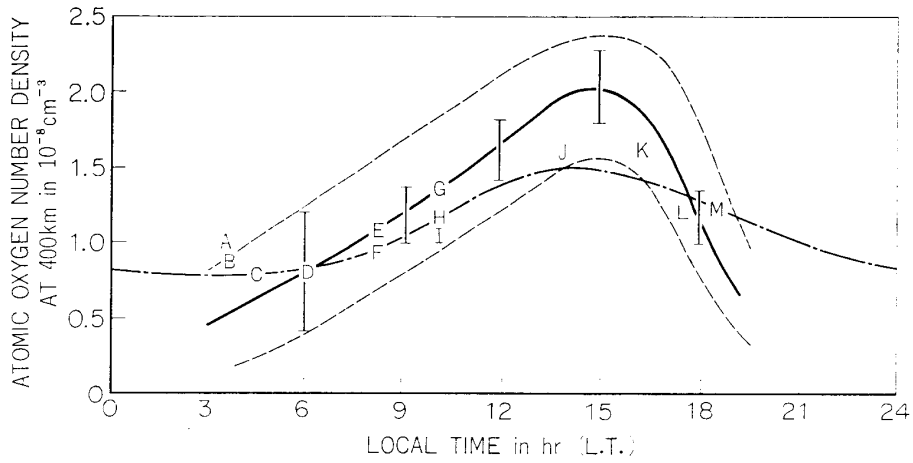

FIG. 88. A comparison of measured and model values of atomic oxygen number density at 400 Km. [*123*] The dashed line gives the range of $[0]_{400}$ inferred from incoherent scatter technique for 6–10 February 1969; the solid lines give the mean $[0]_{400}$, and typical error bars are shown. Mean satellite drag values for the 5-day period and the indication and perigee heights of the 13 satellites are presented. The quasi-sinusoidal curve is from the 1970 model of Jacchia.

Satellite	Inc (°)	Perigee (Km)	Satellite	Inc (°)	Perigee (Km)
A 68 41 A	28	330	I 68 43 B	10	225
C 68 38 B		195	K 66 44 C	18	305
B 66 34 B	−2.5	355	E 66 44 B	2	250
D 61 15	51.8	290	L 65 11 D	18	250
M 66 97 B	−27.5	305	H 68 84 A	58	265
G 68119 A	−40	250	J 64 06 C	44	405
F 68119 B	−40	250			

analysis in Fig. 88 [*123*]. Although there is a relatively large uncertainty in the [O] measurements and a number of corrections are necessary in order to make the comparison, the agreement is most satisfactory.

As was described above, it seems quite certain that the backscatter technique can give correct informations of ion and electron temperatures and therefore can be used as reference to check the validity of Langmuir probe and the retarding potential trap.

5. CONCLUDING REMARKS

The general conclusion drawn from the experimental results are as follows:

(2) In rocket experiments, the electron temperature obtained with Langmuir probe is 2 or 3 times higher than the theoretical value and the backscatter value in lower ionosphere.

(2) In satellite experiments, i.e. an intercomparison between one satellite and other satellite experiments, v-i curves of Langmuir probes agree very well. However the electron temperatures obtained from those Langmuir probes are about 1.4 times higher than that obtained by the backscatter technique, even though the semi-logarithmically plotted Langmuir curves are sufficiently straight ranging up to $7\,kT_e$.

(3) Langmuir probe and the ion trap operated in an ac mode give rather low electron temperature which agrees with the backscatter value.

(4) The ion temperature from the dc mode retarding potential trap approaches to the ion trap value which is operated in an ac mode as the decrease of ambient plasma density. The similar tendency is found in the electron temperature measurement with Langmuir probe.

Taking the above descriptions into account, we showed that these facts can be explained by the contamination effects of the electrode(s) of Langmuir probe or the retarding potential trap. At least in rocket observations, it is quite sure that the confusion has been caused mainly by the use of the contaminated DC Langmuir probe.

It should be strongly noted that the dc mode Langmuir probe and the retarding potential trap can not be applied to the space plasma without any procedure to avoid the contamination effect, such as a rapid sweep and a modulation technique.

For satellite experiments, unfortunately we have no direct experimental data in Japan, but some evidences do exist which suggest that the satellite discrepancy is also deduced by the contamination effects of Langmuir probe and the retarding potential trap.

Chapter VI General Conclusion

In this thesis the influence of a contaminated electrode on the plasma diagnostics was studied and its serious effects were emphasized, especially in case of Langmuir probe.

The contamination of the electrode surface was systematically and theoretically studied by introducing a new idea "Contamination layer model". The main predictions derived from the model were summarized as followings.

(1) The effect of contamination upon the probe characteristic curve decreases with the increase of the sheath impedance. Consequently it is expected that the electron temperature obtained from the contaminated Langmuir probe approaches to the true value as the density of ambient plasma becomes thinner.

(2) The increase of the sweep frequency of the probe bias can reduce the contamination effect. Therefore by choosing the frequency high enough to neglect the layer impedance, a correct information is expected to be obtained. One of the visualization of the principle is a rapid sweep Langmuir probe which sweeps the probe potential very quickly.

The two predictions described above were tested by means of the laboratory plasma and their validities were confirmed. By taking the above conclusions into account, we applied the contamination layer model to Langmuir probe and the retarding potential trap in the space plasma observation with an intention to solve the discrepancy of electron temperature in the ionosphere which has long been discussed. From the space experiments with rockets K-9M-28 and -29 we concluded that the erroneous result is mainly caused by the use of contaminated Langmuir probe up to the trajectory top of 350 Km.

Further we extended our study to satellite observations where the discrepancy has also been reported. We presented some evidences which indicate that the contamination of the probe surface could be one of the main causes of the discrepancy. Consequently suggested are the following three methods to get reliable information from Langmuir probe in the space plasma.

Firstly by using a rapid sweep Langmuir probe, nearly correct electron temperature can be obtained.

Secondly we can get a good information by using the resonance probe theory, that is, by applying small ac signal to the probe and picking up its distorted DC component at one bias point of the electron retarding region. The instruments which are grouped into this category are our E. T. probe and probe of University of London. The above two methods can be applied to the unclean probe in the space plasma in order to avoid the contamination effect.

Thirdly a glass sealed clean Langmuir probe can be used without any serious problems accompanied with the probe contamination. The probe can be used when high frequency response channel to accept a rapid sweep Langmuir probe is not available. Especially the probe may be useful for the measurement of electron temperature in the E_s layer. It is particularly noted that the glass sealed Langmuir probe is quite useful for the measurement of electron energy distribution by the second harmonic method, because it can give the correct original point, space potential, without the potential shift due to the ambiguity of the work function of the contaminated probe surface. Thus a glass sealed clean Langmuir probe is strongly recommended for the space plasma observation.

Department of Space Science
Institute of Space and Aeronautical Science
University of Tokyo
March, 20, 1975

References

[*1*] Appleton, E. V., and M. A. F. Farnett, On some direct evidence for downward atmospheric reflection of electric rays, Proc. Roy Soc., 109, 621–641, 1926.

[*2*] Breit, G., and M. Tube, A test of the existence of the conducting layer, Phys. Rev., 28, 554–573, 1926; also, A radio method for estimating the height of the ionosphere conducting layer, Nature, 116, 357, 1925.

[*3*] Chapman, S., The absorption and dissociative on ionizing effect of monochromatic radia-

tion in an atmosphere on a rotating earth, Proc. Roy. Soc., 43, 26–45, 1931.
[4] Reifman, A. F., and W. G. Dow, Dynamic probe measurements in the ionosphere, Phys. Rev., 76, 987–988, 1949.
[5] Bogges, R. L., L. H. Brace, and N. W. Spencer, Langmuir probe measurements in the ionosphere, J. Geophys. Res., 64, 1627–1630, 1959.
[6] Evans, J. V., Diurnal variation of the temperature of the F region, J. Geophys. Res., 67, 4914–4920, 1962.
[7] Pineo, V. C., and K. P. Hynek, Spectral widths and shapes and other characteristics of incoherent backscatter from the ionosphere observed at 440 megacycles per second during a 24 hour period in May, J. Geophys. Res., 67, 5119–5129, 1962.
[8] Hanson, W. B., Electron temperature in the upper atmosphere, Space Res., 3, 282–302, 1963.
[9] Dalgarno, A., B. McElroy, and R. J. Moffet, Electron temperatures in the ionosphere, Planet. Space Sci. 11, 463–484, 1963.
[10] McElroy, B., Excitation of atmospheric herium, Planet. Space Sci., 13, 403–433, 1965.
[11] Carlson, H. C., Ionospheric heating by magnetically conjugate point photoelectrons, J. Geophys. Res., 71, 195–199, 1966.
[12] Carru, H., M. Petit, and P. Waldteufel, Measures de temperatures electroniques et ioniques par diffusion incoherente, J. Atmosph. Terr. Phys., 29, 315–366, 1967.
[13] J. V. Evans, Midlatitude F-region densities and temperatures at sunspot minimum, Planet, Space Sci., 15, 1387–1406, 1967.
[14] Geisler, J. E., and S. A. Bowhill, Thermospheric temperatures at solar minimum, J. Atmosph. Terr. Phys., 27, 457–474, 1965.
[15] Da Rosa, A. V., The theoretical time dependent thermal behaviour of the ionospheric electron gas, J. Geophys., Res., 71, 4107–4120, 1966.
[16] Dalgarno, A., and I. C. Degges, Electron cooling in the upper atmosphere, Planet. Space Sci., 16, 125–129, 1968.
[17] Dalgarno, A., M. B. McElroy, M. H. Rees, and J. C. G. Walker, The effect of oxygen cooling on ionospheric electron temperatures, Planet. Space Sci., 16, 1371–1380, 1969.
[18] Nagy, A. F., E. G. Fontheim, R. S. Stolarski, and A. E. Beufler, Ionospheric electron temperature calculations including protonospheric and conjugate effect, J. Geophys. Res., 74, 4667–4676, 1969.
[19] Lejeune, G., and M. Petit, A study of the daytime electron temperature, Planet. Space Sci., 17, 1763–1780, 1969.
[20] Herman, J. R., and S. Chandra, The influence of varying solar flux on ionospheric temperatures and densities, A theoretical study, Planet. Space Sci., 17, 815–840, 1969.
[21] Herman, J. R., and S. Chandra, The role of atomic oxygen in the ionospheric F-region behavior, Planet. Space Sci., 17, 1247–1256, 1964.
[22] Bauer, P., G. Lejeune, and M. Petit, Thermal coupling between the upper F_2-region and the magnetosphere: Heat fluxes and energy production, Planet. Space Sci., 18, 1447–1470, 1970.
[23] Bowen, P. J., R. L. F. Boyd, C. L. Henderson, and A. P. Willmore, Electron temperature in the upper F-region, Proc. Roy. Soc., A 281, 526–538, 1964.
[24] Brace, L. H., B. M. Reddy, and H. G. Mayr, Global behavior of the ionosphere at 1000 Km altitudes, J. Geophys., Res., 72, 265–284, 1967.
[25] Willmore, A. P., Ionosphere heating in the F region, Proc. Roy. Soc., A 281, 140–145, 1964.
[26] Farley, D. T., J. P. McClure, D. L. Sterling, and J. L. Green, Temperature and composition of the equatorial ionosphere, J. Geophys. Res., 72, 5837–5851, 1967.
[27] Hirao, K., and K. Oyama, Profiles of electron temperature in the ionosphere observed with the electron temperature probe on rocket, Space Res., XII, 1335–1339, 1972.
[28] Mahajan, K. K., Extent of thermal non-equilibrium in the ionosphere, J. Atmosph. Terr. Phys., 29, 1137–1151, 1967.
[29] Evans, J. V., Millstone Hill Thomson scatter results for 1967, Technical Report 482,

Lincoln Laboratory, M.I.T., 1971.
[*30*] Misyura, V. A., Yu. G. Erokhin, G. N. Tkachev, V. I. Novozhilov, M. G. Trukhan, and V. YA. Bludov., Middle latitude ionosphere as obtained by iocoherent back scatter observations, Space Res., XI, 1033–1038, 1971.
[*31*] Clark, D. H., W. J. Raitt, and A. P. Willmore, The global morphology of electron temperature in the topside ionosphere as measured by ac Langmuir probe, J. Atmosph. Terr. Phys., 34, 1865–1880, 1972.
[*32*] Doupnik, J. R., and J. S. Nisbet, Fluctuations of electron density in the daytime F-region, J. Atmosph. Terr. Phys., 30, 931–961, 1968.
[*33*] Bourdeau, R. E., The temperatures of charged particles in the upper atmosphere, Space Res., V, 77–90, 1965.
[*34*] McClure, J. P., Thermospheric temperature variation inferred from incoherent scatter observations, J. Geophys., Res., 76, 3106–3115, 1971.
[*35*] Willmore, A. P., Electron and ion temperatures in the ionosphere, Space Sci., Rev., 11, 607–670, 1970.
[*36*] Dalgarno, A., and M. B. McElroy, Ionospheric electron temperatures near dawn, Planet. Space Sci., 13, 143–145, 1965.
[*37*] Evans, J. V., Cause of the midlatitude evening increase in F_0F_2, J. Geophys. Res., 70, 1175–1185, 1965.
[*38*] Maeda, K., Midlatitude electron density profile as revealed by rocket experiments, J. Geomag. Geoelect., 21, 557–567, 1969.
[*39*] Sonin, A. A., Theory of ion collection by a supersonic atmospheric sounding rocket, J. Geophys., Res., 72, 4547–4557, 1967.
[*40*] Hoult, D. P., D-region probe theory, J. Geophys., Res., 70, 3183–3187, 1965.
[*41*] Gleeson, L. J., and W. I. Axford, Electron and ion temperature variations in temperate zone sporadic E layers, Planet. Space Sci., 5, 123–136, 1967.
[*42*] Hooke, W. H., Electron, ion and neutral gas temperatures in temperate latitude sporadic E layer, Planet. Space Sci., 17, 737–748, 1969.
[*43*] Smith, L. G., A sequence of rocket observations of night-time sporadic E, J. Atmosph. Terr. Phys., 32, 1247–1257, 1970.
[*44*] Aubry, M., M. Blanc, R. Chauvel, C. Taieb, P. J. Bowen, K. Norman, A. P. Willmore, J. Sayers, and J. H. Wager, Some rocket results on sporadic E, Radio Sci., 1, 170–177, 1966.
[*45*] Timothy, A. F., J. G. Timothy, and A. P. Willmore, The ion chemistry and thermal balance of the E-region and lower F-regions of the daytime ionosphere; An experimental study, J. Atmosph. Terr. Phys., 34, 969–1035, 1972.
[*46*] Golomb, D., D. F. Kitrosser, and R. H. Johnson, Thermosphere structure over Churchill and Hawaii from chemical releases, Space Res., XII, 733–741, 1972.
[*47*] Hirao, K., and K. Oyama, Electron heating in the ionospheric dynamo region (preliminary study), Bulletin of ISAS, 8, 1026–1036, 1972.
[*48*] Sampath, S., T. S. G. Sastry, K. Oyama, and K. Hirao, Joule heating effect due to currents in the equatorial electrojet as observed by rocket borne probes, 16th COSPAR meeting, 1973.
[*49*] Wand, R. H., Radar Thomson scatter observations of temperature and ion neutral collision frequency in the E region, J. Geophys., Res., 73, 6370–6372, 1968.
[*50*] Hooke, W. H., Radar Thomson scatter observations of E-region temperatures interpreted as revealing reversible heating by atmospheric tides, J. Geophys. Res., 74, 1870–1872, 1969.
[*51*] Langmuir, I., and H. Mott-Smith, Studies of electrical discharges in gases at low pressure, Gen. Elec. Rev. 27, 449–455, 538–548, 616–623, 762–771, 810–820, 1924.
[*52*] Van Berkel, W. P. J., Einfluss von Änderungen des Sondenzustandes auf Sondencharakteristiken nach Langmuir, Physica, 5, 230–240, 1938.
[*53*] Anderson, T. A., Dynamic probe characteristics, Phyl. Mag., 38, 179–185, 1947.
[*54*] Easley, M. A., Probe techniques for the measurement of electron temperature, J. Appl. Phys., 22, 590–593, 1951.

[55] Wehner, G., and G. Medicus, Reliability of probe measurements in hot cathode diodes, J. Appl. Phys., 23, 1035–1046, 1952.
[56] Hirao, K., and K. Oyama, A critical study of the reliability of a Langmuir probe, J. Geomag. Geoelect., 24, 415–427, 1972.
[57a] Chen, S. L., J. S. Chang, and S. Matsumura, Electrostatic probe determination of electron density in medium pressure (0.2-28 Torr)(discharge plasma of argon), J. Appl. Phys., 41, 1711–1715, 1970.
[57b] Chen, S. L., J. S. Chang, and S. Matsumura, Studies of the large sheath concept for the continuum probe theory, J. Appl. Phys., 42, 499–501, 1971.
[58] Hirao, K., and K. Oyama, An improved type of electron temperature probe, J. Geomag. Geoelect., 22, 393–402, 1970.
[59] Thomas, T. L., and E. L. Battle, Effects of contamination on Langmuir probe measurements in glow discharge plasmas, J. Appl. Phys., 41, 3428–3432, 1970.
[60] Dote, T., Cleaning effect of the probe in chamber plasma, in Japanese, Memo in space plasma meeting, 40–44, 1972.
[61] Oyama, K., Evaluation of a charged particle temperature with contaminated Langmuir probe, in preparation.
[62] Waymouth, J. F., Pulse technique for probe measurements in gas discharges, J. Appl. Phys., 30, 1404–1411, 1959.
[63] Carlson, H. C., and J. Sayers, Discrepancy in electron temperatures deduced from Langmuir probes and from incoherent scatter radars, J. Geophys. Res., 75, 4883–4886, 1970.
[64] Smith, D., The application of Langumir probes to the measurement of very low electron temperatures, Planet. Space Sci., 20, 1717–1726, 1972.
[65] Smith, L. G., L. H. Weeks, and P. J. Mckinnon, Rocket observations of electron temperature in the E-region, J. Atmosph. Terr. Phys., 30, 1301-1312, 1968.
[66] Brace, L. H., H. G. Mayr, and J. A. Findlay, Electron measurements bearing on the energy and particle balance of the upper F region, J. Geophys. Res., 74, 2952–2961, 1969.
[67] Hirao, K., and K. Oyama, Electron temperature observed with the Langmuir probe and electron temperature probe, J. Geomag. Geoelect., 23, 161–167, 1971.
[68] Jacchia, L. G., Revised static models of the thermosphere and exosphere with empirical temperature profiles, Spec. Rep. 332, Smithson. Astrophys. Obs., 1971.
[69] Oyama, K., and K. Hirao, Possibility of the measurement of electron temperature by ac mode Langmuir probe, Symposium on Space Observation, in Japanese, 134–137, 1971.
[70] Hirao, K., and K. Oyama, Comparison of cleaned and uncleaned probes on board a rocket, Space Res., XIII, 489–492, 1973.
[71] CIRA, COSPAR International Reference Atmosphere 1965. North-Holland, Amsterdam.
[72] Blamont, J. E., M. L. Chanin, and G. Magie, Neutral temperature measurements between 80 Km and 100 Km by laser sounding from the ground, 16th COSPAR Meeting 1973.
[73] Wand, R. H., and J. E. Salah, Latitudinal and temporal variability of temperature in the lower thermosphere, 16th COSPAR Meeting 1973.
[74] Bettinger, R. T., A first order technique for the measurement of vehicle potential in the ionosphere, Technical Report 497, University of Maryland, 1965.
[75] Dote, T., T. Ichimiya, and K. Takayama, Some problems in use of a Langmuir probe on ionospheric sounding rocket, in Japanese, Internal report of chemical research institute, 75–86, March, 1964.
[76] Dote, T., H. Amemiya, and T. Ichimiya, Effect of the geomagnetic field on an ionospheric sounding probe, J. Geophs. Res., 70, 2258–2261, 1965.
[77] Sanmartin, J. R., Theory of a probe in a strong magnetic field, Phys. Fluids, 13, 103–116, 1970.
[78] Sanmartin, J. R., The determination of ionospheric charged particle temperatures from in-situ measurements, 16th COSPAR Meeting, 1973.
[79] Brace, L. H., G. R. Carignan, and J. A. Findlay, Evaluation of ionospheric electron temperature measurements by cylindrical electrostatic probes, Space Res., XI, 1079–1105, 1971.

[*80*] Hanson, W. B., D. R. Frame, and J. E. Midgley, Errors in retarding potential analyzers caused by nonuniformity of the grid-plane potential, J. Geophys. Res., 77, 1914–1922, 1972.
[*81*] Hanson, W. B., and D. D. Mckibbin, An ion-trap measurement of the ion concentration profile above the F_2 peak, J. Geophys., Res., 66, 1667–1671, 1961.
[*82*] Goldan, P. D., E. J. Yadlowsky, and E. C. Whipple, Errors in ion and electron temperature measurements due to grid plane potential nonuniformities in retarding potential analyzers, J. Geophys. Res., 78, 2907–2919, 1973.
[*83*] Knudsen, W. C., Evaluation and demonstration of the use of retarding potential analyzers for measuring several ionospheric quantities, J. Geophys. Res., 71, 4669–4678, 1966.
[*84*] Whipple, E. C., The equilibrium electric potential of a body in the upper atmosphere and in interplanetary space, NASA X-615-65-296, 1965.
[*85*] Kimura, I., Comparison of the electron density measured by Doppler and impedance probe methods, The 51st annual meeting of Geomagnetism and Geoelectricity of Japan, 1972.
[*86*] Deforest, S. E., Spacecraft charging at synchronous orbit, J. Geophys. Res., 77, 651–659, 1972.
[*87*] Oyama, K., and K. Hirao, Design parameter of an electron temperature probe, Internal Report of ISAS, in Japanese, 1972.
[*88*] Hoegy, W. R., Probe and radar electron temperatures in an isotropic nonequilibrium plasma, J. Geophys. Res., 76, 8333–8340, 1971.
[*89*] Evans, J. V., Theory and practice of ionosphere study by Thomson scatter radar, Proc. IEEE., 57, 496–528, 1969.
[*90*] Wrenn, G. L., The Langmuir plate and spherical ion probe experiments aboard Explorer 31, Proc. IEEE., 57, 1072–1075, 1969.
[*91*] Shkarofsky, I. P., Accuracy of Langmuir probe measurements and skin potential on satellites, J. Geophys. Res., 76, 3746–3754, 1971.
[*92*] Donley, J. L., The thermal ion and electron trap experiments on the Explorer 31 satellite, Proc. IEEE, 57, 1061–1069, 1969.
[*93*] Lunc, M., A criterion for the degree of departure from equilibrium and its application to rarefied gases, Rarefied Gas Dyn. Proc. Int. Symp. I, 94, 1963.
[*94*] Spencer, N. W., L. H. Brace, and G. R. Carignan, Electron temperature evidence for nonthermal equilibrium in the ionosphere, J. Geophys. Res., 67, 157–175, 1962.
[*95*] Brace, L. H., N. W. Spencer, and G. R. Carignan, Ionospheric electron temperature measurements and their implications, J. Geophys., Res., 68, 5397–5412, 1963.
[*96*] Spencer, N. W., L. H. Brace, G. R. Carignan, D. R. Taeusch, and H. Niemann, Electron and molecular nitrogen temperature and density in the thermosphere, J. Geophys. Res., 70, 2665–2698, 1965.
[*97*] Carru, R., M. Petit, and P. Waldteufel, Measures de temperatures electroniques et ioniques par diffusion incoherente, J. Atmosph. Terr. Phys., 29, 351–366, 1967.
[*98*] Schlapp, D. M., Some measurements of collision frequency in the E-region of the ionosphere, J. Atmosph. Terr. Phys., 16, 340–343, 1959.
[*99*] Beynon, W. J. G., and E. S. Owen Jones, Seasonal variations in the lower and upper atmosphere, Nature, 206, 1243–1245, 1965.
[*100*] Thrane, E. V., and W. R. Piggot, The collison frequency in the E-region and D-regions of the ionosphere, J. Atmosph. Terr. Phys., 28, 721–737, 1966.
[*101*] Walker, J. C. G., Electron and nitrogen vibrational temperature in the E-region of the ionosphere, Planet. Space Sci., 16, 321–327, 1968.
[*102*] Wrenn, G. L., D. H. Clark, W. J. Raitt, and H. C. Carlson, Modulation Langmuir probe and incoherent scatter radar measurements of ionospheric electron temperature J. Atmosph. Terr. Phys., 35, 405–413, 1973.
[*103*] Brace, L. H., H. C. Carlson, and K. K. Mahajan, Radar back scatter and rocket probe measurements of electron temperature above Arecibo, J. Geophys. Res., 74, 1883–1885, 1969.
[*104*] Evans, J. V., A comparison of rocket, satellite and radar determinations of electron

temperature at midlatitude, J. Geophys. Res., 70, 4365–4374, 1965.
[105] Willmore, A. P., Electron and ion temperatures in the ionosphere, Space Sci. Rev., 11, 607–670, 1970.
[106] Hanson, W. B., L. H. Brace, P. L. Dyson, and J. P. McClure, Conflicting electron temperature measurements in the upper F region, J. Geophys. Res., 74, 400–401, 1969.
[107] Booker, H. G., and E. K. Smith, A comparative study of ionospheric measurement techniques, J. Atmosph. Terr. Phys., 32, 467–497, 1970.
[108] McClure, J. P., and B. E. Troy, Equatorial ion temperature; a comparison of conflicting incoherent scatter and Ogo 4 retarding potential analyzer values, J. Geophys. Res., 76, 4534–4540, 1971.
[109] Brace, L. H., G. R. Carignan, and J. A. Findlay, Evaluation of ionospheric electron temperature measurements by cylindrical electrostatic probes, Space Res., XI, 1079–1105, 1971.
[110] Donley, J. L., L. H. Brace, J. A. Findlay, J. H. Hoffman, and G. L. Wrenn, Comparison of results of Explorer 31 direct measurement probes, Proc. IEEE, 57, 1078–1084, 1969.
[111] Oya, H., and R. F. Benson, A new method for in-situ electron temperature determination from plasma wave phenomena, GSFC Report X-621,72,112, 1972.
[112] Benson, R. F., and W. R. Hoegy, Effect of an isotropic nonequilibrium plasma on electron temperature measurements, J. Geophys. Res., 78, 4702–4706, 1973.
[113] Taylor, G. H., and G. L. Wrenn, Comparison of simultaneous satellite and ground-based measurements of ionospheric parameters, Planet. Space Sci., 8, 1663–1666, 1970.
[114] Sagalyn, R. C., and R. H. Wand, Daytime rocket and Thomson scatter studies of the lower ionosphere, J. Geophys. Res., 76, 3783–3799, 1971.
[115] Chandra, S., B. E. Troy, J. L. Donley, and R. E. Bourdeau, Ogo 4 observations of ion composition and temperatures in the top side ionosphere, J. Geophys. Res., 75, 3867–3878, 1970.
[116] McClure, J. P., Comparison of T_e and T_i from Ogo 6 and from various incoherent scatter radars, J. Geophys. Res., 78, 197–205, 1973.
[117] Hays, P. B., A. F. Nagy, and K. D. McWatters, Comparisons of radar and optical temperature measurements in the F region, J. Geophys. Res., 75, 4881–4882, 1970.
[118] Cogger, L., and G. L. Nelson, Coincident F-region temperature determination from incoherent backcatter and doppler broadening of (01) 6300A, J. Geophys. Res., 75 4887–4889, 1970.
[119] Waldteufel, P., and L. Cogger, Measurements of the neutral temperature at Arecibo, J. Geophys. Res., 76, 5332–5336, 1971.
[120] Spencer, N. W., G. P. Newton, G. R. Carignan, and D. R. Taeusch, Thermospheric temperature and density variations with increasing solar activity, Space Res., X, 389–412, 1970.
[121] Waldteufel, P., Exospheric temperatures from rockets and incoherent scatter measurements, J. Geophys. Res., 76, 6970–1994, 1971.
[122] Bauer, P., P. Waldteufel, and D. Alcayde, Diurnal variation of the atomic oxygen density and temperature determined from incoherent scatter measurements in the ionospheric F region, J. Geophys. Res., 75, 4825–4832, 1970.
[123] Alcayde, D., P. Bauer, C. Jeack, and J. Falin, Diurnal variation of atmospheric density at 400 Kilometers, J. Geophys. Res., 76, 7814–1816, 1971.